Novel Processing, Microstructure and Properties of a Cobalt-Chromium-Molybdenum Orthopaedic Alloy

A thesis submitted in partial fulfilment of the requirements for the degree of

Doctor of Philosophy

By

Bhairav Patel

Department of Mechanical Engineering

University College London

Torrington Place, London WC1E 7JE

U.K.

2012

Declaration

I, Bhairav Patel, hereby confirm that the work presented in this thesis is my own. Where information has been derived from other sources, I confirm that this has been indicated in the thesis.

……..

Bhairav Patel

Abstract

The annual rise of hip procedures occurring year upon year is a major concern, especially with revision rates increasing. There is need for improvements for orthopaedic materials to compensate for this problem with higher success rates in the long term. The main failure of current metallic materials used in hip replacement devices is due to wear and the metallic ions being leached out. Cobalt-based alloys are one of the best bearing surface materials used in hip replacement, however, a better understanding of the microstructure and mechanical properties is required to enhance its properties and also the need for new fabrication techniques to be explored to develop materials that can reduce the number of revision surgeries. The most common cobalt based alloy (F75) used in orthopaedics is investigated and a novel route to manufacture the alloy is conducted. Heat treatments via annealing and normalising are analysed. In the annealed alloy up to 1100°C there is an increase in hardness and carbide content. Above this temperature, there is a significant decrease in both properties due to carbide dissolution. XRD analysis identifies the phases present and how they varied with temperature. The production of the F75 alloy via spark plasma sintering has yielded an alloy with carbide free microstructures. The grains are finer than the conventional methods of fabrication (cast and wrought) and the hardness is significantly higher even in the absence of the carbides. The hardness has been attributed to the formation of oxide phases within the microstructure and chromium and molybdenum rich phases that act as solid solution hardeners. The oxide in the microstructure is identified as chromium oxide formed by a redox reaction between cobalt oxide found on the surface of cobalt particles and chromium. Tribological performance has been investigated upon this newly manufactured alloy (SPS alloy) against two commercial medical grade cobalt based alloys (F75 and F1537) used in hip replacement devices. The SPS alloy had higher hardness, which resulted in the lowest wear rate and friction coefficient, with lower amounts of chromium and molybdenum detected from the wear debris compared to the F75 and F1537 alloys. The wear debris size and size distribution generated from the SPS alloy were very small and the shape was more spherical. The element leaching is conducted upon these alloys, with the SPS alloy forming an oxide layer upon the surface that could be beneficial for limiting ion leaching and for tribological performance.

Publications and Conference Presentations

Publications

Bhairav Patel, Fawad Inam, Mike Reece, Mohan Edirisinghe, William Bonfield, Jie Huang and Arash Angadji. A novel route for processing cobalt-chromium-molybdenum orthopaedic alloys, *Journal of the Royal Society Interface.* 7 (2010) 1641-1645

Bhairav Patel, Fawad Inam, Mike Reece, Mohan Edirisinghe, William Bonfield, Jie Huang and Arash Angadji. Mechanism of chromium oxide formation in Cobalt-Chromium-Molybdenum (F75) alloys prepared using Spark Plasma Sintering, *Advanced Engineering Materials.* 13 **(**2011) 411-417

Bhairav Patel, Gregory Favaro, Fawad Inam, Michael J. Reece, Arash Angadji, William Bonfield, Jie Huang, Mohan Edirisinghe. Cobalt-based orthopaedic alloys: relationship between forming route, microstructure and tribological performance, *submitted to Materials Science and Engineering C: Materials for Biological Applications.* (2011)

Conference Presentations

Bhairav Patel, Fawad Inam, Mike Reece, Mohan Edirisinghe, William Bonfield, Jie Huang and Arash Angadj A novel route for processing cobalt-chromium- molybdenum orthopaedic alloys, International Society For Technology in Arthroplasty, 23rd Annual Congress, Dubai, UAE (2010)

Bhairav Patel, Fawad Inam, Mike Reece, Mohan Edirisinghe, William Bonfield, Jie Huang and Arash Angadj, A novel technique to produce Co-Cr-Mo Orthopaedic alloys, PhD Forum, Department of Mechanical Engineering, UCL, London, UK (2010)

Acknowledgements

I would like to thank my supervisor, Professor Mohan Edirisinghe for this opportunity to do this PhD and his guidance and support for this project and also like to thank Dr. Jie Huang for her academic support.

I would like to thank the Orthopaedic Research UK (fromerly the Furlong Research Charitable Foundation) for their funding for this work and especially Dr. Arash Angadji for his advice throughout this project.

I would like to thank Professor Michael Reece from Queen Mary, University of London and Dr. Fawad Inam from Glyndŵr University for their assistance and expertise for this project. The advice given by Professor William Bonfield FRS at project review meeting is greatly appreciated.

Also, would like to thank Gregory Favaro (CSM Instruments SA, Switzerland), Ben Owen (Nanosight, UK) and Dr. Barry Sampson (Imperial College London) for their assistance in parts of this project. The continuous support provided by my colleagues are unforgettable and many thanks to them.

I would like to thank EPSRC (UK) for funding some parts of this project through the platform grant (EP/ E04539).

I would like to thank my parents, Mr Rajnikant Patel and Mrs Kokila Patel for their love and support throughout my life, especially during this project and I hope this PhD thesis will bring some joy to them as an achievement fulfilled by me.

DEDICATION

To

My Parents

Rajnikant and Kokila Patel

for their sacrifices and support during the time of this research

Table of Contents

List of Figures

List of Tables

Glossary of Abbreviations

AC – alternating current

ASR – articular surface replacement

CAD – computer aided design

CCD – charged coupled device

Co – cobalt

Cr – chromium

DC – direct current

DLC – diamond-like carbon

DLS – dynamic light scattering

ECAS – electrical current assisted sintering

EDS – electric discharge sintering

EDX – electron dispersive x-ray

FCC – face centred cubic

HA – hydroxyapatite

HC – high carbon

HCP – hexagonal close packed

HIP – hot isostatic pressing

ICP – inductively coupled plasma

LC – low carbon

Mo – molybdenum

MoM – metal-on-metal

MS – mass spectroscopy

NTA – nanosight tracking analysis

O – oxygen

PE – polyethylene

PMMA - polymethylmethacrylate

RS – resistance sintering

SEM – scanning electron microscopy

SPS – spark plasma sintering

UHMWPE – ultra high molecular weight polyethylene

Chapter 1
Introduction and Background

1.1 Background

Hip replacement devices are one of the most implanted devices in the human system. The first ever total hip replacement device was implanted by Philip Wiles in 1937 using stainless steel [Wiles 1957]. McKee and Watson-Farrar modified a Thompson stem with a metal-on-metal (MoM) articulation in the 1950s and Ring also used the same concept for his designs [Mckee & Watson-Farrar 1966; Ring 1971]. In 1960, the MoM combinations were rejected in favour of a metal-on-plastic device by John Charnley [Charnley 1960]. He successfully implanted a stainless steel cemented stem with a Teflon acetabular cup fixed via screw and cement, which was a low friction artroplasty for the hip [Charnley 1969]. Due to the major failure of the plastic components due to their particles leading to osteolysis, the metal-on-metal combinations were reintroduced and have been used ever since, with excellent success rates. However, due to the concerns of metallic ions being leached from the implants, ceramic materials were introduced as an alternative. These ceramic materials, have very low wear rates and excellent friction coefficients however, their brittle property is still a major concern as sudden fractures can be very problematic, especially in the hip area.

Over the last year (2010/2011), there have been about 180,000 operations for joint replacement reported in England and Wales [NJR 2011]. For the previous years (2008-2010), the number of operations were 159,003 (2008/09) and 163,219 (2009/10), indicating that the number of joint replacement operations are still on the rise. Of those 180,000 operations, 87,038 were hip operations and this has increased from 79,036 operations the previous year (2009/10). The number of revisions is also on the rise, previous

year (2009/10) there were 8,285 revisions and this year (2010/11) there were 9200 revisions. This shows that hip replacement devices are still being needed and used extensively. Over the next three decades, the number of hip replacement is set to rise by 40% [Birrell et al. 1999].

As the statistics show the number of hip replacement devices is on the rise year upon year. There seems to be an overwhelming problem with the region of the hip and/or having these devices being revised (meaning secondary operations are being required to fix the problems of failed primary devices). The cost of hip replacement operations nowadays is between £7,500 and £13,450 [Private Healthcare UK, 2011]. In 1995, the estimated cost of the operation was between £200 and £2000 [Murray et al. 1995]. This major rise can be seen as a major burden upon the National Health Service. With the cost of hip replacement surgery being so high and the devices not lasting as long, there seems a fundamental problem that needs assessing for long term satisfaction from patients and surgeons for these devices. With the industry estimated to be worth US$5.7 billion per annum worldwide, it can be seen as a very lucrative medical market [Philipson et al. 2005].

Market leaders: Zimmer, Depuy, Stryker, Biomet and Smith & Nephew show a larger interest in financial attributes as indicated by their large revenues and profits rather than providing the patients with suitable hip replacement devices, for example Depuy, a subsidiary of Johnson and Johnson, had a major recall of their articular surface replacement (ASR) systems in August 2010 [Athavaley 2012]. The company denied that the product used in the market since 2003 were showing signs in patients of pain and disability. The product was causing various problems, the metallic debris led to tissue reactions near the hip joint. The ions released from the product were found in the blood and cerebral spinal fluid [FDA 2011]. Depuy had sold more than 93,000 products across many countries and has cost them dearly to clean up the mess. However, this is not the first recall, in the late 1990s, 3M Capital

Hip had a major recall, causing the European device regulation to act, and an investigation was conducted by Lord Hunt, the health minister [Muirhead-Allwood 1998; MHRA 2001]. But it seems the same mistakes have happened again.

The ASR resurfacing system was approved for the European market, however the US denied approval. For the European market, the products were only really tested through hip simulators, not via clinical trials, due to the products classing as a IIb device, which does not require patient testing for market approval. The simulator tests evaluated the wear over time, the materials used in the device and device strength. These results seemed adequate for the European Union standards. But studies upon the ASR, had showed problems early in implanted patients within two years [Langton et al. 2010]. In the US, the FDA, asked for clinical studies called an investigational device exception. The fracture rate of the devices in the study was higher than the recommend rate of 1% per year [Shimmin 2005]. One study of a two year follow up had a fracture rate of 4.9% and a low success rate in women [Haute Authorite de Sante 2008]. This promoted the FDA to ban the use however some surgeons were using the product regardless of the dangers. The recall of this devices was based a upon the higher failure rates of 12% within the first 4 years [Cohen 2011]. However, revision of this device is more difficult as the joint is completely destroyed and the risks involved to the patient of undergoing operation and the success rate of the new implant are very high [Grammatopolous et al. 2009].

There is also another problem that is causing major concern to the industry, the use of large head MoM implants. The use of large heads has been proposed as a method of combating dislocation of the device. However, this causes corrosion at the interface between the head and stem. A study, of 144 patients with a two year follow-up showed an increase in the metallic ion levels in the large head range manufactured by Zimmer, Biomet, DePuy, and

Smith and Nephew [Lavigne et al. 2011]. The use of these larger heads have shown to increase the failure rates with 21% revision rates in 4 years to 49% revision rates in 6 years [Cohen 2011]. This is a major concern as the design developments in the industry seem to cause more problems rather than solve issues.

The hip joint is used for both mobility and stability, therefore is essential for functioning for the patient. The need for the function to be restored is a necessity and to provide better long term solutions for the various hip diseases is becoming more serious. The most common bone disease is arthritis and with older generation having this disease causing pain and discomfort the only solution at the present time is the hip joint being replaced with artificial material.

There has been a revived interest in MoM hip replacements over the past 20 years [Dumbleton & Manley 2005]. The materials used in the hip replacement devices, first and foremost need to be classified as a biomaterial and fulfil the criteria, to ensure there are no foreign body reactions taking place within the body that causes further problems. They also need to replicate the original function of the intended replacement, i.e. the hip. The hip's main function is for stability and providing motion to the body.

Hip replacement devices, as pointed out predominantly consist of traditional metallic materials. Nowadays, the materials used in hip replacement devices have grown and now all classes of materials are used in various sections of the implant [Davis 2003]. These materials in the initial stages showed much promise, but as history has passed the materials are showing signs of failure and need revaluating, assessing and critically innovating. The statistics are showing that an urgent need is required to make significant improvements to the current materials being used in the human body.

The materials used as mentioned began with stainless steel, with polymer liners. As the polymer debris was causing major problems to the surrounding tissues, materials reverted back to a MoM approach to eliminate the polymer. The bearing surface area, which is the region between the actebular cup and femoral head, showed the most amounts of failures and/or the reasons of other failures were linked with debris formed from this area. Therefore, isolating and improving the failure in this region was the most important factor for improvements in longevity of the devices. As history continued, titanium and its alloys were developed to be used as bearing surface materials, as there were known to have a lower Young's modulus, which limited stress shielding and also that had excellent osteointergration ability. However, due to its low shear modulus these alloys were deemed to be problem in areas of high wear. The next material used was cobalt-based alloys, imported from aerospace engineering, where they were used in high temperature resistance, corrosion resistance and wear resistance environments with successful effects [Morral 1966; Scales 1971]. Within the hip replacement environment they seemed an excellent choice and have remained an excellent choice ever since, even when ceramic materials were introduced as an alternative [Sieber et al. 1999].

As with all metals, the properties of the alloy are related to their microstructure and this is related to their processing techniques. For cobalt based alloys two processing techniques have been used to manufacture the alloy, these are cast and wrought. An alternative method to fabrication of the alloys is powder processing. This technique uses powders to be fused together via sintering and has shown to significantly improve the properties of the alloys.

The powder processing technique has significant advantages over conventional manufacturing:

- The whole production can be controlled: The manufacturing process can be controlled at each step, enabling more reproducibility

- Competitive characteristics can be regulated: certain characteristics from certain phases can be produced as the various parameters are controllable increasing the opportunity of these characteristics to form regularly.

- Any desirable shape can be produced: the powder is compacted into a set die; the die can be made into the desired shape or close to the shape. This reduces the costs of machining and finishing and enables complex shapes to be produced.

- Wider range of products can be made: as the die set can be reused, more products can be made and using different materials a range of products can be made increasing the scope of the technique.

- Fabrication of components that would otherwise decompose or disintegrate: some materials have distinctive decomposition temperatures and some induce phase changes through the cooling or heating process. By regulating the process, these components will remain or can be formed which can lead to enhanced properties.

The other major concern in the hip replacement industry is the release of metallic ions from the MoM hip replacement devices. As with all metals over time, metal ions get leached out depending upon the environment they are placed in.

For cobalt based orthopaedic alloys, there has been an increase in attention in the metallic ions being leached out during function as it has been suggested that they cause adverse effects to the surrounding areas in the hip. Compared to other combinations, the MoM bearings usually generate relatively low

wear. In the early metallic materials, studies of hip replacement devices implanted and followed up with serum and urine metal levels showed that chromium and cobalt levels very up to 9 times higher than normal levels in serum [Jacobs et al. 1996]. In the urine minute levels of chromium above normal were obtained. Since the evaluated levels, the next generation hip replacement devices had serum, blood and urine level monitored constantly, but still similar levels were being generated [Schaffer et al. 1999; Bronder et al. 1997, Lhotka et al. 2003]. The metal levels were measured using atomic absorption spectroscopy or inductively coupled plasma mass spectroscopy.

Metal particles produced from the MoM debris are very small, typically <0.05µm [Doorn et al. 1998]. This is much smaller than the polyethylene particles and so below the highest macrophage activation level (0.2-0.81µm), however osteolytic response have been known to occur [Ingham & Fisher 2000; Schmalzried 1999]. As the particles are small they have a tendency to travel into tissues nearby and have also been found in the liver, spleen and lymph nodes [Urban et al. 2000]. Cobalt based alloy particles have been known to be toxic to macrophages, effect osteoblast cells which cause bone formation and corrosion products such as chromium orthophosphate cause bone resorption leading to osteolysis [Haynes et al. 1993; Allen et al. 1997; Urban 1994; Lee et al. 1997].

Metallic materials have been known to be sensitive in certain people, with around 15% of the population being dermal hypersensitive to metals [Jacobs et al. 2000]. In the MoM devices there has been sensitivity to some of the alloy constituents, however testing for this sensitivity has been difficult [Evans et al. 1974; Hallab et al. 2001]. The issue of hypersensitivity has not shown significant evidence to indicate that it has effects on the longevity or performance of these implants [Willert 2005].

The risk of metallic ions or particles inducing the formation of cancerous tissue is a major problem. Even though no significant proof has been shown, suggestion have been made that the metallic ions cause cancer and other adverse effects to surrounding tissues. Cobalt and nickel are classified as carcinogens by the International Agency for Research into Cancer, however orthopaedic implants are not classified [IRAC 1999]. Some studies have indicated that cancerous tissues have formed as a result of having hip replacement devices in place, however many of these implants fail due to other various factors [Tharani et al. 2001; Visuri 1996; Visuri 1987].

New routes to manufacture cobalt based alloys with desirable properties need to be investigated. Objectives need to be formulated to be able to achieve this aim.

1.2 Objectives of Research

This section outlines the objectives of the research devised for the aims of the project.

1.2.1 Processing, Microstructure and Phase Analysis

1.2.1.1 Currently used cobalt based alloys in hip replacement devices

The first objective is to analyse the current cobalt based alloys used in hip replacement devices. As all cobalt-based alloys are different and with different compositions of elements used, this results in different properties exhibited. Therefore, analysing a current cobalt orthopaedic alloy for its microstructure and phase analysis will enable an understanding of the structures in the microstructure and phases present which can establish the behaviour of the alloy. These cobalt based alloys are known to be affected by heat treatment and a study to determine the effects of the treatment under different cooling conditions could enable an improved understanding of the alloys. Annealing and Normalising are two treatments that can be investigated to determine its effects on the microstructure, phases and carbide content.

1.2.1.2 Sintering of powders using Spark Plasma Sintering

The second objective is to investigate a new method of manufacturing the cobalt based alloys. Many different techniques have been suggested, but electric assisted current sintering, especially Spark Plasma Sintering (SPS) has shown to significant improve properties in alloys over other conventional sintering techniques. The most common form of the cobalt-based alloy is the ASTM F75, and has widespread approval as a composition for orthopaedic alloys. Therefore, the F75 composition will be chosen to be fabricated via SPS to determine its properties for hip replacement devices. The feasibility of sintering technique in terms of producing a fully dense alloy needs to be assessed, as many sintering technique produce materials with some porosity present which requires additional processing to remove. The resultant microstructure and phase analysis of the spark plasma sintering needs to be evaluated, as this can give an indication of the behaviour of the alloy in terms of its properties.

1.2.1.3 Evolution of the SPS microstructure

The development of microstructure from the processing point of view is very critical to determine how the alloy is produced and the resultant properties. Therefore, analysing how the microstructure has developed through the processing route of SPS will enable a greater understanding of this alloy and its relationship to its properties.

1.2.1.4 Commercial grade orthopaedic alloys

Conventional manufactured orthopaedics alloys via cast (ASTM F75) and wrought (ASTM F1537) methods are investigated for their microstructure and phase analysis. Cobalt based alloys are usually only manufactured via these two routes for orthopaedics and determining what structures and phases are present will enable an understanding of the properties of the alloys.

1.2.2 Properties

The third objective is to evaluate the properties of these alloys modified by heat treatment and the different processing routes adopted to fabricate the cobalt based orthopaedic alloys.

1.2.2.1 Heat Treatment

The hardness of the two heat treated alloys are investigated to determine the effects of the cooling methods. Hardness will give an indication of the wear resistant of the alloy and how it can be improved by heat treatment.

1.2.2.2 SPS alloy

The hardness and grain size of the SPS compacts are evaluated to determine the strengths of the newly formed alloy. The chromium oxide content has also been measured as this is known to be the hardest phase in the alloy and its influence on the hardness of the SPS alloy is determined.

1.2.2.3 Tribological Performance

The tribological performance of the SPS alloy, F75 and F1537 alloys are evaluated to determine the strengths of the powder processed alloys against the conventional manufactured alloys. The initial hardness, micro- and nano-, will be tested to give an indication of the strength of the alloys in terms of wear. The amount of material loss, wear rate, friction coefficient, wear track and wear track profiles of the three alloys will be determined to assess the performance of the alloy. The tribological performance is a major factor for hip replacement devices, as having the ability to increase the wear resistance enables a more successful implant in the long term.

1.2.2.4 Wear Particles

The wear particles generated from the tribological performance testing are gathered and analysed for their size, size distribution, shape and elemental content. Particles generated during wear form in different sizes and shapes

and this determines how the body may react to the particles. The composition of the particles is a key factor in the reactions of biological molecules as certain ions are known to leach out and cause major problems to surrounding tissues.

1.2.2.5 Metal element leaching

The fourth objective will be to assess the metal elements that leach out of the alloy. These cobalt based alloys have been known to leach metal ions out of the alloy into the human body, assessing the three alloys used in the tribological performance tests for metal elemental leaching will determine what elements are being leached out. The microstructure of the alloys will be assessed to determine the effects of the metal element leaching study.

1.3 Structure of thesis

This section outlines the structure of the thesis and what is being presented within each chapter.

Chapter 1: the debriefing of the project, an introduction and background of the work and the purpose of the project being undertaken are outlined. Objectives drawn up to evaluate how the aim of the project can be achieved. Finally a detailed description of the structure of the thesis.

Chapter 2: An extensive review of the literature is conducted. The aim of the research is to investigate new methods of fabricating cobalt based alloys for orthopaedics, a collection of literature has been surveyed to understand the powder processing and the methods that can be used to sinter alloys. A relevant literature on the topic of orthopaedics and hip replacement devices has been constructed focusing upon the hip, the related diseases in the joint, treatment of those diseases, the materials used in hip replacement devices, specifically focusing on cobalt based alloys and their current manufacturing methods, alternative manufacturing techniques, coupling of materials used in

bearing surfaces, failure of the devices, the mechanism of ions leached from the alloys and research carried out to improve the properties of cobalt based orthopaedic alloys.

Chapter 3: describes the materials used and their characteristics, the equipment used and their capabilities and the experimental methods used to obtain results to evaluate the objectives.

Chapter 4: describes results obtained to evaluate the first and second objective. The Chapter is split into four sections: **Section 4.1:** describes the current cobalt based alloy used in hip replacement devices. The microstructure of the alloy and the compositional analysis is undertaken to determine which grade of alloy is used. Heat treatment is performed upon the alloy to determine how the microstructure and phases present react to the addition of heat with two different cooling methods. **Section 4.2:** describes an alternative powder processing technique to produce orthopaedic alloys. A superior manufacturing technique, namely spark plasma sintering is used to fabricate the ASTM F75 composition into a fully dense alloy. The resultant microstructure and phase analysis are evaluated. **Section 4.3:** describes how the microstructure has formed using SPS and how the phases present benefit the alloy it terms of its application. Chromium oxide rich phases have formed within the microstructure and the formation of this phase and other phases are explained through a mechanism produced via the SPS system. **Section 4.4:** describes the microstructure and phase analysis of two conventional manufactured orthopaedic alloys which will be used in tribological performance testing.

Chapter 5: describes results obtained to evaluate the third and fourth objectives. This Chapter is split into five sections. **Section 5.1:** describes the effects of heat treatment on the hardness of the orthopaedic alloys. Annealed and Normalised heat treatment methods investigated in Section 4.2 are

evaluated for their hardness property to determine its effects. **Section 5.2:** describes the hardness and grain size properties of the powder processed alloy formed in Chapter 4. The properties of the newly formed alloy are evaluated and compared to the conventionally manufactured orthopaedic alloys. **Section 5.3:** describes the tribological performance of commercial used orthopaedic alloys and the powder processed alloy developed in Chapter 4. The three alloys are evaluated for their initial hardness, material loss, wear rates and friction coefficient, wear track and wear track profile. **Section 5.4:** describes the wear particle generated from Section 5.3. The wear particles are analysed for their size, size distribution, shape and elemental analysis. **Section 5.5:** describes the metal element leaching studies conducted to determine the elements that leach out of the three alloys used in Section 5.3. The alloys are evaluated for their metal leached elemental content, their microstructure after leaching and their microstructural element composition after leaching.

Chapter 6: describes the conclusions drawn up for the results obtained from Chapter 4 and Chapter 5 and the future scope of this work is detailed here.

References used throughout the thesis are detailed at the end of the thesis.

Chapter 2
Literature Review

2.1 Introduction

The objective of this research is to attempt to manufacture cobalt based alloys using an alternative fabrication method to produce materials with significant improvements for use in hip replacement devices. To fulfil this objective, first a review of the literature relevant to this subject needs to be prepared:

Understanding the joint being replaced and its function to the human body and the diseases that occur in this region: the joint in question is the "hip joint", this is an important joint to the human body, both in terms of the stability and motion. There are many diseases associated to the hip joint and many that develop over time.

How to treat the hip diseases non-operatively and operatively and the different types of products that can be used: treatment of the hip diseases requires different methods, some require operations while others can be treated using an administration of drugs. The operative solutions come in two forms, total hip replacement or hip resurfacing.

The conditions required for materials used in the body and the materials used in hip replacement devices: there are criteria that need to be satisfied for artificial materials to be used in the human body, as not all materials are suitable. The materials used in various parts of the hip replacement devices are explained and the method of manufacturing cobalt based alloys and the different types of alloys are described.

Combinations: these hip replacement devices are found in many different coupling of materials from metal-on-plastic to ceramic-on-ceramic. All combinations are described here.

Powder processing and other rapid prototyping techniques have been used to make metallic alloys: powder processing techniques and electric current assisted sintering are described here as methods to form alloys.

Hip replacement devices have been known to fail with the most prominent method resulting from wear: these devices fail due to many different reasons, the various methods are described and special attention is given to wear and how it occurs due it being a major factor in terms of failure.

Mechanisms of the leaching of ions: metallic ions leaching of the cobalt based alloys is a major concern and the mechanism of the ions being leached out is described.

Advances in cobalt based orthopaedic alloys: evaluated are various techniques to improve the properties of cobalt based orthopaedic alloys.

2.2 What is the hip?

The hip is a joint made of a connection between the femur and acetabulum (Figure 2.1). The joint is a ball and socket joint whereby the femur head rotates within the acetabulum surface. This provides the body with a support to withstand the body's weight in both static and dynamic motion.

As this joint sustains large number of forces, the bones within this area become worn and the ligaments and tendons become weak. Diseases begin to develop and occur that cause pain and problems.

2.3 Hip Diseases

There are many diseases that occur in the hip region. The main three are osteoarthritis, rheumatoid arthritis and hip fractures. There are other rare diseases such as lupus, femoral head necrosis, dysplasia, dislocation, impingment, infection and ankylosing spondylitis that can occur.

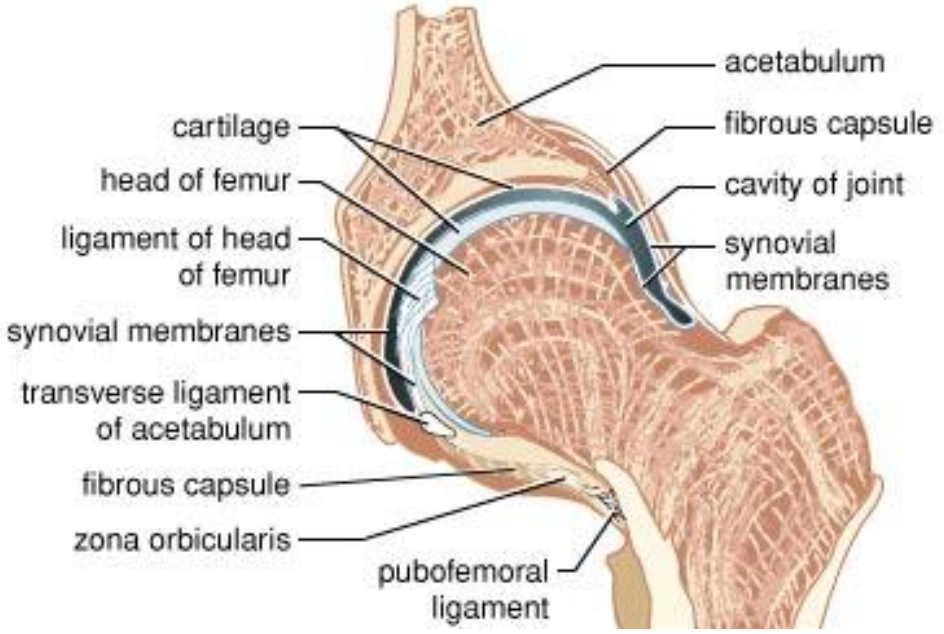

Figure 2.1: A diagram of the hip joint with features labelled [Britannica 2010]

Arthritis is the most common bone disease that occurs in the joint region, whereby the joint becomes inflamed and/or damaged. Osteoarthritis and rheumatoid arthritis are specific types, where the former affects the local region of one or two joint without inflammation and the latter describes joint and organs being damaged with inflammation. Pain usually occurs in the hip as the synovial lining becomes inflamed or the cartilage becomes worn away resulting in the bones rubbing against each other. Treatments include taking painkillers to ease the pain, steroid injections into the affected joint, disease modifying anti-rheumatic drugs can be taken that slow and limit further damage, non-steroidal anti-inflammatory drugs which reduce the inflammation in the joint and total hip replacement in severe cases.

Lupus or Systemic Lupus Erythematosus is an inflammatory disease that usually attacks soft tissues that consist of collagen fibres. As it is a systemic disease it damages organs and the patient needs a thorough check-up if this disease is present. Treatment for the disease requires cortisone injections, but secondary problems such as osteonecrosis can form in both hip joints. Therefore, if one hip has osteonecrosis it is essential to examine the subsequent hip for signs.

Femoral head necrosis is a disease whereby the loss of blood supply in the femur head causes the bone to die. It is caused by either traumatic femoral head necrosis or non-traumatic asvascular necrosis. In the former, fracture or dislocation of the femoral head causes the blood vessels in the head to be damaged; resulting in the head dying and the hip cannot support the body's weight. In the latter, causes are not understood fully, but related to alcohol, excess cortisone doses, blood disorders and/or tumours [Mont et al. 2006)]. However, to treat the disease large doses of cortisone injections are administer to the affected joint. Also, has been suggested that blood clots in the vessels cause the bone to receive no oxygen and nutrients and eventually dies out. Total hip replacements and resurfacing are some of the successful treatments for the disease.

Dysplasia or Congenital Hip Dysplasia is a condition where the hip joint has change shaped from birth. The femoral head does not sit in the acetabulum comfortably and the dysphasia term indicates that both the head and cup are irregular shape. This can cause pain and result in secondary arthritis. Usually, early operations may have occurred at a young age to correct the defect. Treatment is difficult due to the changes in the skeletal structure but total hip replacement can work with use of bone grafts and modifying the bones in the area to accept the prosthesis.

Dislocation is when the ball has completely removed itself out of the socket. Total hip replacement are very difficult to perform and high risk. The skeleton is small in the hip region, therefore small femoral head are required and the socket needs to remodeled to accept a new cup and the femur needs to be moved downwards to accommodate the stem, risking damage to surrounding tissues, nerves and blood vessels.

Impingement results from damage to the labrum. The labrum is at either ends of the cartilage and provides a soft protection. It is made from a fibrous structure and prevents the femur head from rubbing against the cartilage and the acetabulum. The impingement usually occurs in extreme movement of the hip, during exiting of the car or removal of shoes. A lot of pain occurs in the groin area and some may require walking aids. Usually, keyhole surgery is sufficient whereby torn labrum and/or damaged cartilage is removed. In severe cases, the femur neck, the section between the femur head and the femur shaft is planed down to prevent more impingement taking place. Results show that 75% have less pain and no other damage to the femoral head occurs [Stephen et al. 2006**]**.

Bacterial infections of the joint can cause secondary effects such as osteoarthritis and sometimes total hip replacement is required. However, before replacement can occur the infection needs to be inactive and the area needs to be healed. But, often the replacement can cause the infection to become active again and cause further problems than before. Usually the patients are put on a long course of antibiotics, but bacteria can form resistance to the drugs.

Ankylosing spondylitis is a rare inflammatory disease whereby the joints, especially the spine and hip, become fused. It usually starts with the fusion of smaller bones in the pelvis and works its way through to force the whole hip joint to be fused. It can then travel upwards to force the spine to fuse all the

way up to the neck. The fused spine does not cause a lot of problems, but the fused hip causes major problems with stiffness and breaking of bones. Both hips can become fused and usually younger people are affected by this disease. The treatment is the total hip replacement, but it was considered that in young patients loosening rates were high, however the results have been successful to 85% after 15 to 25 years and after 20 years 80% were functional. Two thirds of the patients had both hips replaced and the average age of the patients was 40 years [Joshi et al. 2002; Sweeney 2001].

2.4 Treatments of diseases and fractures

As mentioned throughout section 2.3, most treatments require total hip replacements. There are also other non-operative and operative solutions.

2.4.1 Operative Solution

The operative solution requires the introduction of a prosthetic implant. There are two types of implants most commonly used, either total hip replacement or hip surfacing.

2.4.1.1 Total Hip Replacement

The most common procedure attached to hip diseases is the total hip replacements and has had a successful outcome to relieve pain and increase mobility with 95% of patients [Johnsson and Thorngren 1989]. As the hip joint has degenerated away due to diseases suffered the joint needs to be replaced with an artificial device.

Total hip replacements involve the total replacement of the hip joint with an implant. There are three components to the prosthesis (Figure 2.2):

1. A metallic femoral stem component
2. An acetabular cup, sometimes with a liner added for further lubrication
3. A femoral head component, that connects to the top of the femoral stem

The femur cavity is drilled out and replaced with a long stem. The stem is fixed either with bone cement (polymethyl methacrylate or PMMA) or cementless. The stem can be coated to increase integration between the implant and the bone. This coating is made of bioactive ceramic, usually hydroxyapatite. The acetabulum is reamed to provide a stable area for the acetabular cup to be fixed via screws or bone cement. At the end of the femoral stem is a femoral head which connects to the acetabular cup to create the ball and socket joint.

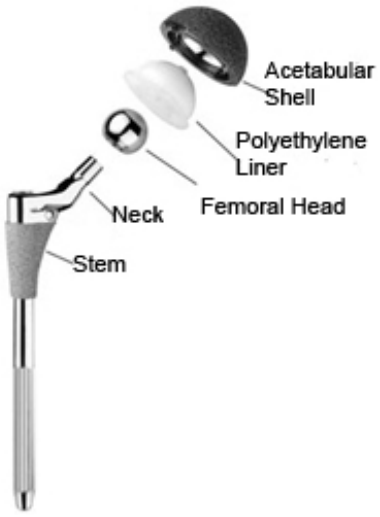

Figure 2.2: Components of the total hip replacement device with features labelled [Zimmer 2003]

Most of the credit for the total hip replacement should go to Sir John Charnley. In the 1950s, he successful implanted a stainless steel cemented stem with a teflon acetabular cup fixed via screws and cement [Charnley 1960]. Nowadays, there are different materials being used for different components of the device with high success rates.

2.4.1.2 Hip resurfacing

Hip resurfacing is a simpler procedure and an advantageous operation as bone loss is keep to a minimum. However it is only used in patients where bone

stock is plentiful. Again, Sir John Charnley developed the idea in the 1950s to produce an implant for the younger active patients. His use of polytetrafluroethylene had good results early on, however due to the high wear rates, failures occurred. Other materials were used and considered with different combinations of metals, ceramics and polymers. But for the high wear rates, the concept was shelved. Until, Derek McMinn redeveloped the product, in 1997 in Birmingham, UK and formed the Birmingham Hip Resurfacing system [McMinn 2003]. The system is a MoM implant (Figure 2.3) and requires the femur to be reshaped to allow the cap to fit, compared to the total hip replacement, where the femur is drilled into to allow the stem to sit. The acetabular cup is fitted as usual. This reduction of bone loss also helps when revision is required as there is sufficient bone for the stem to be accepted. Whereas, in the total hip replacements the revision requires the femur bone to be broken for removal of the original stem and reset with wires to stabilise the bone and the new stem for healing to occur.

In young patients, the Birmingham Hip Resurfacing has shown that when revision is required is it simpler to convert to the total hip replacement device [Ball et al. 2007]. The survivorship of the Birmingham Hip Resurfacing system after 11years has been successful up to 99.5% [Daniel et al. 2004]. The failures resulted from a deep infection and a collapsed femoral head. The most common failures occur from metal wear, femoral neck fractures and aseptic loosening.

Hip resurfacing has allowed patients to return to their normal everyday activities without problems and has been seen as a major advantage over total hip replacements [Naal et al. 2007; Zhan et al. 2007].

Figure 2.3: The Birmingham hip resurfacing device [Walter 2006]

2.4.2 Non-operative Solution

As the operative solution may not be life saving, the non-operative solution should also be considered. This is usually a temporary measure before surgery or used in controlling the suffering of pain and to increase mobility. There are many suggestions that the general practitioner or consultant surgeon may recommend, some are as follows: to reduce weight if overweight to relieve stress of the damaged hip, using a walking stick in the opposite side to the diseased hip to reduce the force impacted on the hip, taking joint supplements to provide the damaged cartilage the ingredients for regrowth and most commonly to take pain killing and/or anti-inflammatory drugs.

Tipton et al. has suggested another non-operative alternative, by injecting sodium morrhuate a drug which has shown to grow ligaments and tendons up to 40% stronger than natural growth [Tipton et al. 1983; Maynard et al. 1985]. The ligaments and tendons are essential in restabilising the joint which has become slack as the cartilage is worn away via arthritis.

2.5 What is a biomaterial?

A biomaterial is “a nonviable material used in a medical device, intended to interact with biological systems” [Williams 1987].

Many different materials have been used as biomaterials in biological system for total replacement and in medical devices. For materials in orthopaedics two important criteria need to be met. The material should have adequate mechanical properties for functional and biological use and be biocompatible with the environment it is placed in. Biocompatibility relates to the body's interaction with the material in question with its purpose and the site it is located.

The material selection criteria required for orthopaedics are [Taylor & Francis 1999]:

- Has to be biocompatible resulting in limited or no inflammatory or toxic reactions
- Adequate mechanical properties, close to or mimic bone
- Processing of the material should be cost effective
- The implant should be able to carry out the function it is required to perform, i.e. provide the stability and mobility of the hip

It has been known that any foreign material inserted into the body is not 100% compatible. However, materials can be classified as bioactive, bioinert and/or biodegradable. Bioactive materials represent materials that have the ability to interact with their chosen environment to form a response, e.g. hydroxyapatite. Bioinert materials form limited or minimal responses from the body, e.g. stainless steel. Biodegradable materials become resorbed and replaced with new tissue or degrade over time within the body, e.g. tricalcium phosphate.

In terms of the hip joint, the force impacted on the hip while standing is about three times the body weight, while at maximum activity is about 10 times the body weight and while moving creates a cyclic loading of about 10^6 cycles in 1 year [Black 1992]. Therefore, the materials selected need to also meet these criteria for function and mechanical stability.

2.6 Materials

The materials that have been used and are being currently used in hip joints are metals, ceramics, polymers and composites, all for different areas in the hip joint for different reasons. One of the first types of materials used were metals.

2.6.1 Metals

2.6.1.1 Stainless Steel

As explained Section 1.1, Sir John Charnley first developed both hip replacement devices [Charnley 1960]. The first device was a total hip replacement made out of stainless steel. This was the first metallic material used for hip joint replacement. Stainless steel has excellent corrosion resistance due to its high chromium content. The chromium combines with any oxygen to form a coating layer of chromium oxide. There are different grades of stainless steel available for orthopaedic use, but for implant usage austenitic stainless steel is widely used. To remain in the austenitic phase the stainless steel requires a certain amount of stabilisers such as nickel or manganese, which enable the phase to be held at room temperature. The most common clinical austenitic stainless steel used in orthopaedics is the AISI 316L (Table 2.1).

As the mechanical properties of austenitic stainless steel, especially the wear resistance were not adequate for MoM joints such as the hip, they were shelved. The high wear debris and loosening of the implant caused many failures. Other metals were considered and two showed superior mechanical and corrosion properties, these were cobalt-based alloys and titanium and its alloys. Stainless steel is usually used as screws, plates, nails and in other devices it is easy to process, readily available and has a low cost.

New austenitic stainless steel are being developed and used as joint replacements with higher chromium content, manganese used as a substitute for nickel and higher nitrogen content **[**Sumita et al. 2004]. The nitrogen

increases corrosion resistance and yield stress while stabilising the austenitic phase.

2.6.1.2 Titanium and its alloys

Titanium and its alloys, were chosen due to its excellent mechanical properties, especially its Young's modulus of 110GPa, which was closer to bone compared to stainless steel, excellent corrosion resistance and lower density (Table 2.1). But in 1964, Branemark made a discovery that made titanium even more popular for use as implant material [Branemark et al. 1964]. He established that titanium formed an integration with bone and called it osteointegration. This enabled the failure of the implant to be significantly reduced as there was less risk of loosening.

Table 2.1: The metallic materials currently used in hip replacements [Navarro & Michiardi 2008]

Material	Alloying element (wt %)	Elastic Modulus (GPa)	Yield Strength (MPa)	Ultimate Tensile Strength (MPa)
Stainless steel 316L	Balance Fe, Cr 17-20, 12-14 Ni, 2-3 Mo, 0.03 C	205-210	170-750	465-950
CoCrMo F75	Balance Co, Cr 27-30, Mo 5-7, Ni 2.5	220-230	275-1585	600-1785
Ti4Al6V	Balance Ti, Al 5.5-6.5, V 3.5-4.5	110	850-900	960-970

The most common types of titanium alloys used are commercially pure titanium, grade 4 and Ti6Al4V. Commercial pure titanium's mechanical

properties can be varied depending on the oxygen content in the material with a maximum of 0.4 per cent (grade 4), giving it higher strengths [Ratner et al. 2004]. The high corrosion resistance of titanium and its alloys is due to the TiO_2 oxide layer that forms at the surface.

Commercial pure titanium is usually used in as dental implants, which is a single-phase alpha microstructure whereas the biphasic alpha-beta microstructure of Ti6Al4V is usually used in orthopaedics. The aluminium and vanadium elements act as alpha-beta stabilisers and enhance the mechanical properties compared to commercial pure titanium.

However, limitations in the material are due its low shear resistance and high wear, cost is high as a result titanium is usually only used as the stem implanted into the femur. In bearing surfaces it was popular however, due to high number of failures and loosening they became less popular. Also, it was found during removal of the devices that surrounding tissues had become black and metallosis had occurred [Nasser et al. 1990; Clarke et al. 1992]. This was created by debris particles which resulted from inadequate integration of the surface oxide layer to the titanium. As a result for bearing surfaces cobalt-based alloys have been more widely used.

Titanium and its alloys have excellent properties, but the ability for processing (machining, forging and heat treating) is relatively difficult due to the vanadium present. Studies have shown that this element is cytotoxic and limits its processibility [Friberg et al. 1979; Thompson & Puleo 1996]. As a result of this, other titanium alloys were developed; these were Ti6Al7Nb, Ti5Al2.5Fe, Ti35Nb5Ta7Zr and Ti35Nb5Ta7Zr0.4O [Long et al. 1998]. The first two alloys were developed as they were vanadium free and exhibit similar properties to Ti4Al6V. The latter two alloys were subsequently developed with lower elastic moduli (55 and 65 GPa respectively) closer to bone and

excellent biocompatibility. These alloys are still being developed for commercialisation.

2.6.1.3 Cobalt-based alloys

These alloys were chosen due to the inadequate wear properties of the other two materials. Cobalt was discovered by Brandt in 1735 [Wang 2006]. Cobalt based alloys were first used in turbine blades and gas turbines due to their ability to withstand high temperatures. However, their other properties, corrosion resistance and wear resistant is what brought them to the forefront for orthopaedics [Donachie 2002]. These properties are due to the microstructure of the alloy, the cobalt has two crystalline structures, hexagonal closed packed (HCP), and face-centred cubic (FCC), each exhibit different strengths, the chromium improves oxidation and hot corrosion resistance as well as producing carbides M_7C_3 and $M_{23}C_6$, the molybdenum acts a solid solution hardener with the formation of intermetallic compounds and carbides M_6C. Carbon within the structure forms carbides MC, M_7C_3, $M_{23}C_6$ and M_6C. The M denotes either cobalt, chromium or molybdenum [Sims 1969]. There are different grades of cobalt based alloys in orthopaedics: (Table 2.2)

2.6.1.3.1 F75

This is the most common cobalt based alloy used in hip replacements. The high corrosion resistance due to the formation of chromium oxide is its unique characteristic. The chemical composition is 28 wt% Cr, 6 wt% Mo, and balance wt% of Co [ASTM Standard F75 1998]. The as-cast version consists of a Co-rich matrix, secondary phases and carbides randomly distributed throughout the structure.

Table 2.2: The grades of cobalt based alloys with their mechanical properties [Davis 2001]

Specification	Alloy System	Condition	Yield Strength (MPa)	Tensile strength (MPa)	Elastic Modulus (GPa)
F75	Co-Cr-Mo	Cast	450	655	248
F799	Co-Cr-Mo	Thermo mechanically processed	827	1172	
F90	Co-Cr-W-Ni	Wrought	379	896	242
F562	Co-Ni-Cr-Mo	Annealed	241-448	793-1000	228
		Cold-worked and aged	1586	1793	

2.6.1.3.2 F799

This alloy is hot forged after it has been cast. This process of working plastically deforms the structure and exhibits higher mechanical properties, especially fatigue, yield and ultimate tensile strength compared to F75.

2.6.1.3.3 F90

This alloy has additions of tungsten and nickel to improve fabrication. Has similar properties to F75 but can be enhanced if cold worked.

2.6.1.3.4 F562

This is one of the strongest available alloys used and can be significantly improved by cold working and aging it. Below 419°C, the HCP structure forms and above the FCC structure forms. The HCP structure exhibits higher strength as there are less slip systems and limits the dislocation movement.

2.6.1.3.5 Ways of Manufacturing

As it can be seen from the enhancement of properties, processing of the cobalt-based alloys is essential. This produces different microstructures with variable properties. There are three ways of manufacturing the alloy: cast, wrought and powder processing.

2.6.1.3.6 Cast

Casting of materials is the simplest form of fabrication of alloys for various shapes. The metals are melted above their melting point to form a molten mixture. The desired shape is produced into a mould and the molten mixture is poured in and allowed to solidify. Even though it is easy, the material tends to have voids of porosity in the structure. These voids affect the mechanical properties and if porosity is very high the material is subsequent hot isostatic pressed to close the pores and improve the mechanical properties. This process requires, heating the material near its solidus temperature and with the addition of pressure, around 100MPa, forces the pores to close up. Casting of cobalt based alloys for surgical use goes back over 60 years, and such improvements have been made to enhance the mechanical properties of the alloy using this technique [Disegi et al. 1999].

2.6.1.3.7 Wrought

The performance of the cast cobalt based alloys were adequate, however the mechanical properties were not suitable for the function. To limit this problem, wroughting of the cast version was suggested as it had been shown in other materials to improve properties [North et al. 1976]. Wrought processing can be done hot or cold. It is the forging of the cast ingot into the desired shape or into another ingot to be machined into a desired shape. This enables the grain structure to be modified, voids to be closed and increases the strength of the metallic alloy [Cawley et al. 2003]. However, due to the increased strengths machining of the product into the desired shape was difficult and only simple shapes could be formed.

2.6.1.3.8 Powder Processing

Powder processing or powder metallurgy has been very effective for processing of alloys for surgical use. Powder processing is the sintering of powders to produce a product. In powder processing, the whole production can be control, competitive characteristics can be regulated, any desirable shape can be produced, wider range of products can be made and components can be fabricated that would otherwise decompose or disintegrate.

In the 1960s, the first powder processed alloy for surgical use was manufactured; it was a Co-Cr-Mo femoral stem via isostatic pressing [Deidar et al. 2006]. The outer layer was porous, this enabled bone tissue ingrowth for stability and fixation of the implant without cement. Powder processing of cobalt based alloys has been performed using many different methods from atomising, such as gas, plasma rotating electrode process, and water [Dowson, 1990; Eisen, 1984]. Plasma rotating electrode process has been used to produce femoral stems that have superior mechanical and corrosion resistance compared to the cast versions [Eric et al. 2002; Thomas et al. 1996].

Currently, powder processing has shown improved biocompatibility, mechanical properties, corrosion resistance, precise chemical compositions and waste free-net shape products. The porosity can be controlled and composite materials can be made depending on the function [Leszek et al. 2001; Becker et al. 1995]. However, there are limitations, whereby powders are expensive and require expensive special sintering processes to produce a product that can have unwanted porosity that reduces corrosion resistance [German 1984].

2.6.2 Polymers

Most common polymers used in hip joint replacement are polyethylene (PE) and polymethylmethacrylate (PMMA).

PMMA or bone cement as explained previously, was used by Charnley for the fixation of the stainless steel stem into the femur cavity. Bone cement is formed by self-polymerising of a powder consisting of prepolymerized PMMA, an intiator and a radiopacifier and liquid phase consisting of MMA monomer, an accelerator reagent and a stabiliser. A paste is formed of the two parts that solidifies after polymerisation. The materials create an excellent fixation, however it is not bioactive. There are problems, the monomer may leak into the blood causing an embolism, the exothermic reaction produced during polymerisation can cause necrosis of blood vessels, nerves or bone tissue, as the cement sets it shrinks slightly causing a loss of contact between bone, cement and prosthesis, stress shielding of the bone can cause the cement to fracture and crack and wearing of cement particles can cause foreign body reactions and accelerated wear in the bearing surfaces.

New organic iodine opacifiers are being developed as the old ceramic radiopacifiers reduce the mechanical properties as they do not proper mix in the paste [Artola et al. 2003]. Even though there are risks involved bone cement is still successfully used as a fixation medium and improvements have been made to administer the cement effectively using monomer cooling, vacuum mixing and injecting devices, which increase stability and mechanical properties of the cement.

PE and more specifically Ultra High Molecular Weight Polyethylene (UHMWPE) has been used as a liner for the acetabular cups. It is the ideal liner material due to its low friction, high abrasion resistance and low density with excellent toughness, biocompatibility and biostability [Fisher & Dowson 1991; Sutula et al. 1995]. However, the most important concern is the wear particles that are produced. These particles have shown to produce an inflammatory response called osteolysis [Maloney & Smith 1995]**.** Osteolysis is the disease whereby bone resorbing cells (osteoclasts) are activated to perform the resorption of bone. Modifications are being made to reduce the

low molecular weight chains, the orientation and compaction of the polymer chains and to produce harder surfaces to reduce wear.

2.6.3 Ceramics

Some of the first ceramics used and are still being used in joint replacement were alumina and zirconia. Their material properties are determined by their microstructure, which is dependent upon the fabrication method. One of the main reasons for their use in hip replacements was due to their high strengths, biocompatibility, corrosion resistance and especially their excellent wear rates [Hench & Wilson 1993]**.** The failure of the ceramic materials is due to their low fracture toughness.

Alumina has been used in orthopaedics for 20 years due to its low friction and wear coefficient. Alumina components must be highly spherical; therefore surface finish is very important to reduce wear and friction. There is always a problem with stress shielding due to the high elastic modulus (380GPa) of the material and can cause loosening and risk of failure. Therefore, alumina heads are used in conjunction with UHMWPE acetabular cups.

Zirconia is the highest strength material available for surgical use and has excellent mechanical properties for hip replacements. It has the lowest wear rates of all the materials [Villermaux 2000].

The most common bioactive ceramic used in hip replacements is Hydroxyapatite (HA – $Ca_{10}(PO_4)_6(OH)_2$). It has been used as a coating material on the surface of the implant to increase bonding strength between implant surface and adjacent bone, also limits the reaction to foreign material in the body as it is highly biocompatible.

Currently, work is being conducted on other derivatives of HA, such as β-tricalcium phosphate (β-TCP, $Ca_3(PO_4)_2$). These fall in the calcium phosphate

family and have shown the ability to completely resorb away and be replaced with bone. HA even though it is in the same family cannot fully resorb due to its chemical stability that reduces its solubility rate ensuring that it remains intact at its site [Takahashi et al. 2005; Ginebra et al. 2006]. Calcium phosphates have also been developed into bone fillers that can be injected in the damaged bone tissues that can self-harden and produce low exothermic reactions limiting damage to its surrounding area [Ginebra et al. 1997; Takagi et al. 1998].

2.7 Combinations

2.7.1 Metal-on-plastic

These were one of the first combinations used, by Charnley with the use of Teflon with stainless steel. However, the wear rates of these devices when compared to the MoM combinations are significantly higher [Black 1996]. Advances in polymer science development, saw the formation of UHMWPE and was first used in 1962, by Charnley [Kyomot et al. 2007]. The UHMWPE was susceptible to oxidative attacks due to the process of sterilisation, which used gamma rays, leaving it vulnerable [Kurtz 2004]. The modification of this material into cross-linked UHMWPE saw enhancement in properties, especially higher wear resistance, reduction in wear debris and higher oxidative degradation resistance [Chiesa et al. 2000; Chiesa et al 2004; Ferroni & Quaglini 2010]. However, the wear debris formed from this combination was the main issue with the devices. The particle sizes were larger than metal debris and the chemistry of the particles caused major problems, called osteolysis, which increases the risk of loosening of the implants and failure of the devices. The osteolysis mechanism is due to three points, the creation of the particles, migration of those particles and the cellular response to the particles [Harris 1994]. During wear of this combination, polyethylene particles are formed which are large in diameter (~10μm) and macrophages find it difficult to ingest. Submicron particles form from abrasive wear, as this wear causes crystalline stretches of the

polyethylene which extends the polymer chains and causes rupture into smaller particles [Jasty et al. 1997]. These smaller particles have the opportunity to interact with the surrounding areas, especially the bone in the joint space [Schmalsried et al. 1992]. The cellular response of the particles is from the macrophages and the fibroblasts. Usually, macrophages ingest the material, when they are unable to perform their function; the fibroblasts have to then ingest the particles. The fibroblasts synthesize the material and release cytokines and growth factors, which cause an adverse reaction. This reaction is quite complex but results in bone resorption, through osteoclasts or monocytes [Athanasou et al. 1992]. With this osteolysis being a major problem, plastic materials have not readily been introduced in the bearing surfaces area of hip replacement devices since.

2.7.2 Metal-on-metal

As the alternative to metal-on-plastic, MoM was revisited and has been around ever since. MoM developed through the cobalt based alloys to stainless steel to titanium and back to cobalt based alloys. This was mainly due to the higher wear resistance of the cobalt based alloys [Donachie 2002]. This combination has been used throughout the whole history of hip replacement devices and has been highly successful. However the MoM devices are failing due to various reasons, predominantly due to wear and metal ion leaching [Konttinen et al. 2005; Langton et al. 2010; Merrit & Brown 1996].

2.7.3 Ceramic-on-ceramic

The lowest wear rates are associated with these combinations due to the extreme hardness of the materials used [Willmann 1998]. But the same problems are associated, the ceramic-on-ceramic shapes need to be very complimentary of each other, otherwise large sections can be worn away. The ceramic-on-ceramic has been known to make a lot of noise during articulation [Restrepo et al. 2008]. And the brittle nature of ceramic material is still a

major concern of sudden breakage during function [Park et al. 2006]. This combination is of recent usage and follow-up studies over 20 years need to be investigated to have a better assessment for long term viability of this material [Hamadouche et al. 2002; Jazrawi et al. 1999].

2.7.4 Ceramic-on-plastic

Ceramic against plastic was the new combination developed and had good success rates early on [Skinner 1999]. The plastic was used as the liner material, between two ceramic materials or between ceramic and metal. This was due to the shaping of the ceramic materials and the associated problems detailed above.

2.7.5 Ceramic-on-metal

Ceramic on metal is a new combination developed by John Fisher [Fisher 2005]. This was suggested as an alternative to the ceramic on plastics, due to the plastic still being a major concern over osteolysis and also due to ceramic-on-ceramics having the concerns over sudden fractures. The metal with the ceramic was seen to give the best of both worlds, with the loss of the plastic and reduction in the number of metallic particles and the reduction in sudden fracture.

Having a mismatch of materials, as it the case here of the ceramic and metal, this has been known in history to lead to major problem [Affatato et al. 2010]. Mismatch of properties of the two materials in contact with one another has known to never be very successful. The ceramic being harder, due damage the surface of the metal, the metal is deformable various the ceramic is brittle. The ceramic is tougher, whereas the metal is malleable. Initial the combination may seem to have a high success rate, however over a longer period of time the results could be very different. Materials in combination with similar properties or with similar chemistries have been known to survive longer as the materials are the same in nature and complement each other.

2.8 Powder Processing of alloys

The powder is compacted and consolidated into a set die of a specific shape. With the application of heat through diffusion processes, called sintering and often external pressure a solid material can be formed. The material is never really molten, however sometimes liquid can be present in elements in the die that have low melting temperatures. Sintering is regarded as the fusion of the particles. It is known that increase mechanical and physical properties are improved as the density of the material increases. Some materials are produced with porosity in mind, but for hip replacement devices, especially bearing surface materials should be fully dense.

Compaction of powder can be done using different methods:

Cold Uniaxial Pressing: elemental metal or compound powders are mixed with lubricant and pressed with pressures of 600MPa in metal dies [Fleck 1995]. The compaction forms a "green "compact of the component and takes the shape of the die. Having non-uniform shaped particles enables a higher green compact strength to form as the particles deform one another and take up less space in the die [James 1977]. The pressing of the powder may not be uniform through the green compact due to the frictional effects between particles and the die wall. If higher as-pressed densities are required the compaction pressures need to be increases, this requires larger and stronger presses and tools that can become very expensive.

Cold Isostatic Pressing: powders are loaded into a rubber membrane or metallic die. Uniform pressure is applied to the die from all directions; this is known as isostatic external pressure [Kennard 1991]. The isostatic pressure ensures the as pressed density will be more uniform. Again, non-uniformed shaped particle enhance the green compact strength. This technique of compaction is usually used for semi-fabricated products such as bars, billets, sheets or shapely objects, where extensive finishing of the products is required. The products formed are not fully dense and require additional

working of the products to increase density, usually through, hot forging, rolling or extrusion [Greetham 2001]. Sintering of the powder is the next step.

Once compacted, the die can be placed in a furnace to heat the powders up. First the heating removes the lubricants involved and then at a higher temperature diffusion and fusion of particle occurs. A vacuum or a range of atmospheres during sintering can be used, as some materials depending upon the chemistry, require specific environments [Greetham 2001]. The density of the material can be manipulated through the sintering parameters and the components produced will have very little finishing required. Therefore, most of the powder used at the beginning is not wasted and reduces the costs.

Some sintering techniques:
Hot Isostatic Pressing: powders are consolidated in a metallic die or possibly glass. The die is vacuumised and so no gases can contaminate the material. It is heated up and simultaneously isostatically pressed to deform the powder and die [Widmer 1982]. The densification depends upon the yield strengths of the powders; higher yield strengths require more pressure [Boncoeur & Palacio 1983]. However, having very high temperatures enable low pressures to be used. This technique can be costly as the pressure vessel needs to be able to withstand the high temperatures and the internal pressure that form. Similar to cold-isostatic pressing, finishing is required to form the desired product.

Hot Forging (Powder Forging): the cold pressed and sintered components are very close to the final product shape, however may not be fully dense. Therefore, the porosity needs to be reduce to have adequate mechanical properties [Cocen & Onel 2002].

Cold pressed and sintered components have the great advantage of being close to final shape (near-net shape), but are not fully dense. Where densification is

essential to provide adequate mechanical properties, the technique of hot forging, or powder forging, can be used.

In powder forging an as-pressed component is usually heated to a forging temperature significantly below the usual sintering temperature of the material and then forged in a closed die. This produces a fully dense component with the shape of the forging die and appropriate mechanical properties. Powder forged parts generally are not as close to final size or shape as cold pressed and sintered parts. This results from the allowances made for thermal expansion effects and the need for draft angles on the forging tools [Greetham 2001]. Further, minimal machining is required but when all things are considered this route is often very cost effective.

2.9 Electric Current Sintering

As a powder processing tool electrical current assisted sintering (ECAS) has increased greatly due to its ability to form sintered compact of much enhanced properties compared to the other more conventional powder processing techniques [Munir & Quach 2011].

ECAS is a system where electric current and pressure are applied simultaneously to consolidate and sinter the powders to achieve densification rapidly. The powders can be conductive or non-conductive. Conductive powders are heated via the Joule effect and non-conductive powders are heated through the use of a conductive die, usually made of graphite. The principle of sintering is similar to hot isostatic pressing, where heat and pressure are applied simultaneously, but the main difference being the heat generate in ECAS is through the electrical current. Having high power supplies can lead to rapid and efficient heating enabling heating rates of 1000°C/min [Orru et al. 2009]. The applied pressure is via uniaxial pressing, however some system can do isostatic or quasi-isostatic [Saito & Sawaoka

1973; Song et al. 2004]. The pressure achieved can be as great as 8GPa [Zhou & Kwon 2005].

2.9.1 Developments of the ECAS processes

The use of ECAS to form materials from powders has grown significantly due to the availability of commercial machines, the origin of this process is very old [Munir et al. 2006]. Sereval different processes that apply electric current or have an electric field present to assist powder material fabrication have been developed in the past. The first patent filed was in 1922, of the invention to produce dense compacts from oxide powders using electric current flows through the specimen to achieve appropriate sintering temperature [Duval d'Adrian 1922]. In 1927, Hoyt developed the idea to simultaneously apply uniaxial pressure and electric current to metallic powders [Hoyt 1932]. Hoyt system used mechanical pressure through electrodes to the metallic powder (mixed WC/Co) and applied electric current from an external electric circuit to the electrodes, therefore heating the powders sufficiently to cause sintering. The processing time was in the range of minutes. Gilson, in 1927, used this same technique to perform reactive sintering using individual powders assisted with electric current [Gilson 1930].

In 1933, Taylor processed the mixed WC/Co powder into a fully dense body in one second or fraction of a second, by modifying Hoyt design [Taylor 1933]. The short processing time was due to the ability to subject the powder to a discharge of pulsed direct current, followed by applying alternating current (AC). The discharge was produced using a condenser coupled to 2500V of direct current (DC). The use of discharge was due to the difficultly of initially allowing electric current to flow through the powders when using a low voltage AC source, as the powders have an initial resistance. In 1944, Cramer developed apparatus to sinter metallic powders in fractions of seconds using simultaneously applied mechanical pressure and AC or DC current of around 20kA, resulting in about 620MA/m^2 of current density [Cramer 1944].

This high current density enabled the powder particles that were in direct contact with one another to become fused due to the high point temperatures achieved and in a cold state which reduced the porosity further with the applied pressure.

Ross modified the apparatus further to have the application of electric current applied in pulses, with varying durations, by varying the current density and manipulating the number, intensity and duration of pulses dependent on the material being sintered [Ross 1945]. The short duration of pulsed current caused the powder to be heated and sintered, but the die remained cold.

Rensselaer Polytechnic Institute (USA) studied a process called resistance sintering under pressure [Lenel 1955]. The apparatus used for resistance sintering were similar to spot welding machines and used a low voltage high current power supplied by a welding transformer and a current motor generator. Sintering was considered to be efficient using two current pulses, as powders usually have oxides present upon the surface and therefore the first pulse breaks down the resistance of the oxide and the second sinters the powders.

In 1965, Japax Scientific Corp. Menlo Park, CA (USA) association with Japax Inc. of Kanegawa (Japan) developed a method to combine pressing and sintering in one process by “spark energy” an unspecified impulsive force [Degroat 1965]. But large scale of components was very difficult. In spark sintering, the idea of using a vacuum and removing the oxides of the powder would cause self-bonding of the particles [Jones 1940]. The use of a capacitor bank produced high energy electrical discharge and produced a spark between the particles. The spark causes ionisation and allows the current to flow through the compacts to cause heating of the particles for sintering.

In 1966, Inoue developed an ECAS technique using electric current and low mechanical pressure, below 10MPa [Inoue 1966]. The lighter applied pressure and the pulse current formed the spark discharge for sintering. The discharge has so much high energy that this caused the particles to fuse together. The use of higher pressure in earlier ECAS machines was thought to reduce the contact resistance and equalise it to the internal resistance of the particles so current could pass through the particles to allow heating. However, Inoue said that the contact resistance needs to be greater than the internal resistance during the initial stage of sintering, to enable the spark discharge energy to remain high and not dissipated during resistive heating of the particles [Inoue 1966].

The innovation of Inoue was questioned, as Hoyt and Gilson were able to produce dense compacts using 6.9MPa of pressure, without spark discharges forming [Hoyt 1932; Gilson 1930]. However, Inoue described his invention in a patent filed in 1966, where is said that the spark discharge causes partial ionisation of the particles surfaces that are in contact and they apply impulsive pressure on one another, including the external pressure applied to cause fusion of particles [Inoue 1966a]. He continued to say that the high temperatures generated from the spark discharge was sufficient to cause initial bonding of the particles and the subsequent flow of current causes heating of the powders through resistive or joule heating, he named the technique electric discharge sintering [Inoue 1966a].

In another Inoue patent, he stated that metallic particles form a film on the surface which impeded fusion of the particles [Inoue 1970]. He continued to say that the high temperature formed in the initial stages of sintering and the reducing atmospheres employed caused breakage of these films to allow bonding. The spark discharge generated in between the particles travel through the whole powder bed and cause discharges to occur in various powder gaps, enabling the films to be destroyed through shock wave or

dynamic pressure. The discharge also forms conductive bridges to allow the subsequent current to flow through the powder efficiently.

In 1967, Lockheed Aircraft Corp. obtained the license rights to Inoue process and produced apparatus, they changed the name to spark sintering, due to the ability to press and sinter in one shot [Boesel et al. 1969]. The spark sintering process was modified by Lockheed and that it consisted of two stages [Goetzel & Marchi 1971]. The first was an initial activation under low pressure using a pulsed or high frequency AC current combined with a DC current to generate the spark discharge to form bonds between the particles. The second stage involved resistance heating using electrical energy under higher pressure to cause densification of the compact.

Around the 1970s, spark sintering had become a practical and economical process for the sintering of materials worldwide. There were still some problems, the graphite dies used in the process were wearing away and therefore alumina high wear resistance dies were used [Weissler 1978]. The short high current pulses adopted by Taylor to produce compact in a non-conducting die was unsuccessful as the current flow was inefficient, therefore Lockheed Missiles and Space Co. developed the use of AC and DC current simultaneously, to reduce the film effect on the surface of the powders and make current flow more efficient [Saito & Sawaoka 1973].

The number of scientific articles based on ECAS has increased dramatically, due to the commercial availability of the apparatus. Various elements, compounds and alloys have been processed using ECAS, however the mechanisms that take place to form the compact has not been discussed or investigated.

The electric current activation sintering can be divided into two different methods for sintering: Resistance Sintering (RS) and Electric Discharge Sintering (EDS)

RS uses a sinusoidal form of low voltage and high current. EDS utilises a bank of capacitors to storage electrical energy and release it suddenly to produce a high energy discharge. This uses higher voltages and higher current than RS. The EDS method uses electromagnetic techniques for compaction through the effects of change of current/time. The processing time of the RS (10^{-5} to 10^{-2}s) is much higher than EDS (10^{0} to 10^{3}s).

2.9.2 Resistance Sintering

Over 80 years of research have been performed using RS method and many apparatus have been produced to use this technique. Different sinusoidal forms have been adopted to achieve sintering and as a result different names and acronyms have been created. Most common ones are Spark Plasma Sintering, Pulsed Electric Current Sintering, Pulse Discharge Sintering and Plasma Activated Sintering. The main feature of the RS system is the electrical current and therefore the waveform of the current is a fundamental characteristic. There are different versions of the waveform with square, sinusoidal and seesaw, some of the ones used, but the most common are shown in Figure 2.4.

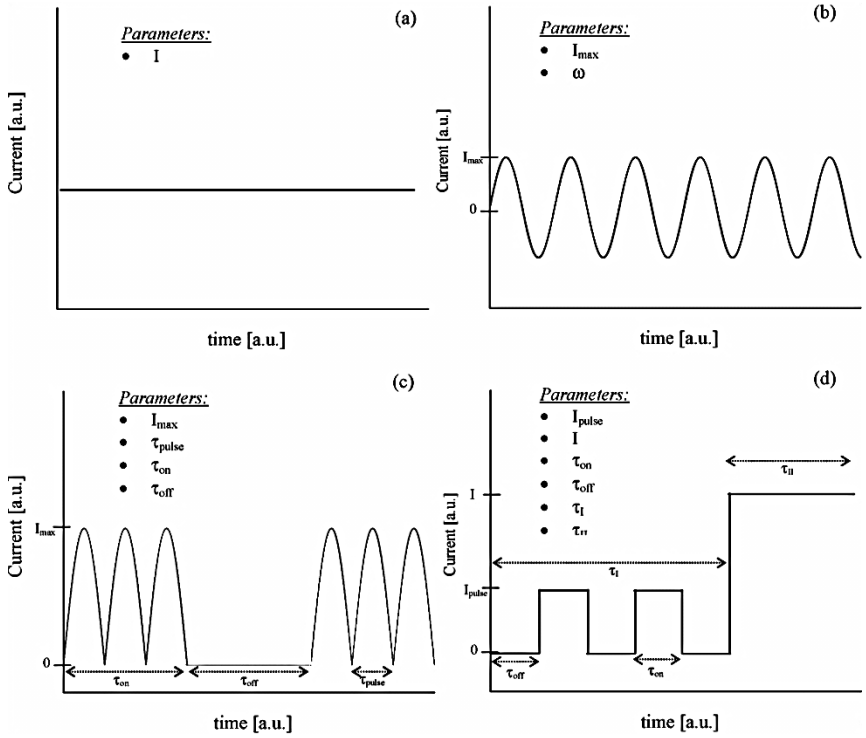

Figure 2.4: Typical electric current waveforms applied in the RS processes: (a) constant DC, (b) AC, (c) pulsed DC and (d) pulsed DC + DC. a.u. indicates arbitrary units [Orru et al. 2009]

The most simple waveform is the constant DC which has a current intensity I and AC which has a maximum current intensity, I_{max}, with a frequency, v. Figure 2.4c is the pulsed DC waveform which has a, I_{max}, the pulse duration, τ_{pulse}, and the on- and off-time, τ_{ON} and τ_{OFF}. The Figure 2.4c shows the waveform of a two stage pulsed DC+DC method, where a pulsed DC is first formed and then a constant DC is applied. The stages are split into a τ_I and τ_{II}. There are still many different waveforms, however not much investigation on these versions have been made and experimental measurements of the electric current feature are also very low [Matsugi et al. 1996; Kimua 1997; Anselmi-Tamburini et al. 2005]. The most common used in RS apparatus is the Pulsed DC, due to the extensive use of the Sumitomo Coal Mining Co. Ltd. (Japan), which utilises this waveform in its commercial RS experiments. This apparatus was patented in 1960s and commercial machinery was made in late 1980s by Sumitomo and Sodick Co. Ltd [Omori et al. 1997]. These machines

adopted the SPS process, which used electrical sources similar to electric discharge machines [Omori et al. 1997]. These were low-voltage high current powder systems, with a pulse interval of 1ms, while some other versions produced by Sumitomo had a pulse duration of 2.7ms [Omori et al. 1997].

For constant DC or AC waveforms, custom-built machines were requried, however, there are some machines that adopt the waveform of Figure 2.4c and 2.4d. FCT Systeme GmBH (Germany) produces machines that apply waveforms varying in pulse shape and pulse frequency [Xie et al. 2003]. The FCT Systeme machine can have a pulsed DC with on/off cycles of 0-225ms [Vanmeensel et al. 2005; Sastry et al. 2004]. The waveform of Figure 2.4d has been commerical by Sodick Co. Ltd, Materials Modification Inc., USA and Eltek Co., Korea. The waveform is achieved by, first applying the pulsed electric current under low pressure and the DC is followed in the second stage [Groza et al. 1992; Kalyanaraman et al. 1998; Kim et al. 2006].

Superior Graphite Co. Ltd. (USA) have a commerical RS apparatus that is slightly different to the tranditional ECAS systems, where powders for sintering are placed in a free-flowing particle die [Gopalsami 2002]. The free flowing particles are electrically conductive and act as pressure transmitter and resistive heat source under a low voltage and high DC current application, therefore pseudo-isostatic pressure is applied [Zhang 2003].

Due to the short time the current heats the powder, between the successive impulses; the actual average temperature of the powders is lower than the instantaneous temperature achieved during normal current flow [Michalski 2003]. The energy supplied from each pulse is up to 8.1kJ and the pulse frequency is between 0.5-2Hz [Jaroszewicz & Michalski 2006; Michalski 2006]. The heating rates and temperature is controlled by the pulse discharge energy ($E = CV_2/2$ where V is the charge voltage and C the capacitance of the capacitor battery) [Michalski & Siemiaszko 2007]. Due to the high energy

supplied from the pulses this technique has been claimed to be more efficient for sintering than other electrical assisted processing techniques [Michalski & Siemiaszko 2007].

2.9.3 Electric Discharge Sintering

This method uses a capacitor bank to storage electrical energy and discharge it suddenly through a non-conducting container filled with powder. The high energy discharge of current through the powders allows heating and sintering of the individual particles. The powder particles can be compacted using the magnetic field which causes them to radially collapse inward. After the discharge, the solid compact can move freely into its container and removal is achieved with processing [Clyens et al. 1976; Johnson et al 1976]. The advantage of this method of compaction, is ease of removal capability from the container, the low costs and the reusability of the containers [Al-Hassani 1979; Shakery et al. 1979].

One of the first electrical discharge machines was developed as a magnetic forming machine [Williams 1977]. The capacitor bank consists of a total capacitance up to 25mF and a charging voltage up to 30kV can be achieved [Rajagopalan et al. 2000; Grigoriev & Rosliakov 2007]. The charging of the capacitor bank is through a variable transformer and a rectification and smoothing unit [Williams & Johnson 1982]. The applied discharge current density can reach up to 2800MA/m^2 and the intensity up to around 90kA [Wu & Guo 2007; Wu et al. 2007]. The current down the length of the sample decreases monotonically, however it can be increased by adjusting the sample diameter [Clyens et al. 1976]. During the processing the current flowing through the powder exhibits a waveform typically of that shown in Figure 2.5 [Alp et al. 1985].

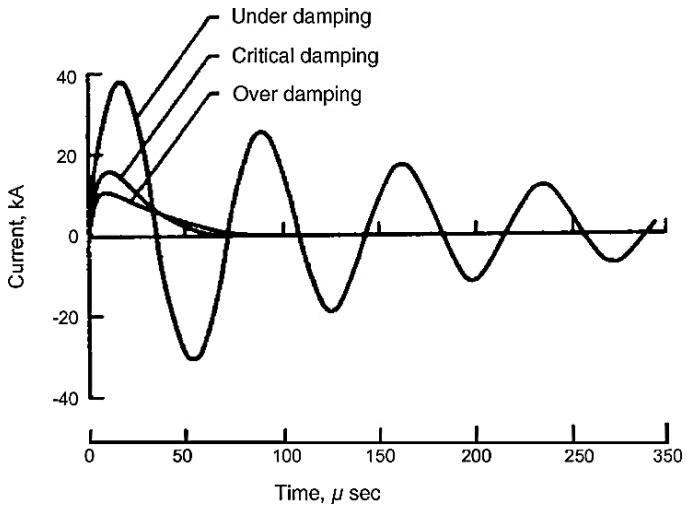

Figure 2.5 Typical waveform of current flowing through powder during EDS process. [Alp et al. 1985]

Some investigations carried out using this method of compact, suggest that the EDS process is in two stages [Zavodov et al. 1999]. In the first stage the powder is subjected to the high-voltage pulse, while in the second stage the sintering of the compact occurs through the applied current density which can be in the order of 10^2 to 10^3 A/cm^2. The two-stages have been considered of as it is thought that during processing the electrical current decreases from one stage to the each.

Pressure or pressureless EDS can be performed [Alp et al. 1987]. With pressure EDS, it can be static or dynamic and the pressure with the electrical discharge aids the ability to achieve higher densities [Okazaki 2000]. The pressure also aids the discharge process by making it more effective in the initial stages of sintering [Rajagopalan et al. 2000].

Various metallic powders have been sintered using EDS, some not so successfully, but the ferrous materials have been [Williams & Johnson 1982]. Many shapes and even complicated products can be processed using EDS processing, but the particles size and packing help the current flow and produce homogenous density and mechanical properties [Alp et al. 1987].

Many factors such as powder properties, electrical parameters and container dimensions affect the energy produced for compaction [Shakery et al. 1979]. However, pressureless EDS produces low relative densities and additional sintering is required to produce denser specimens [Alp et al. 1987; Johnson et al. 1976].

Powder particles of a small size sometimes cannot achieve homogenised structure due to the very short sintering time, even when the temperatures are close to the liquid phase. Therefore, to increase homogenisation or reaction between the powders the compact has to be heated to form liquid phase sintering [Lenel 1955]. With the high temperatures densification at the centre of compact can be achieved, however the higher density is usually found at the ends of the compact [Shakery et al. 1979; Clyens 1976].

The discharge energy produced through the powder column is proportional to the current flowing [Johnson et al. 1976]. The current is governed by the capacitance, resistance and inductance of the circuit [Shakery et al. 1979]. The higher the current flowing through the circuits the increased strength and density of the green compact produced from the magnetic body forces, making the current density very important [Shakery et al. 1979]. The sintering of the powder occurs in a certain range of discharge energies, which is dependent upon the powder column and powder chemistry [Clyens et al. 1976; Johnson et al. 1976]. Too high discharge energy applied causes melting or even rapture of the container [Al-Hassani 1979]. With too low discharge energy the powder diameter cannot be reduced by the magnetic field and removing the compact from the container would be difficult [Clyens et al. 1976; Johnson et al. 1976]. This is due to the electrical resistance, too high resistance, not sufficient current, too low resistance and the current cannot pass through the powder compact efficiently and the compact may not be fully sintered [Lenel 1955].

Another EDS technique is High Energy High Rate consolidation which uses stored rotational kinetic energy that can be converted into electrical energy using the Faraday effect [Elkabir et al. 1986]. It is a low voltage, high current device that uses a pulse mode to provide resistive heating at interparticle interfaces [Ervin et al. 1988; Elkabir et al. 1986]. The high current pulse can be up to 250kA in a few hundred milliseconds, while the current density achieved is 100-500MA/m^2 and the process lasts around 3s, with most energy produced in the first 0.5s [Ervin et al. 1988; Persad et al. 1989]. During the pulse phase, pressure is applied and held for between 3-5mins and the specific energy produced is in the range of 400-14250J/g [Raghunathan et al. 1991].

One of the most common types of ECAS is spark plasma sintering, which will be explained in Chapter 3 and used in Chapter 4.

2.10 Modes of failure and methods of treatment

Even though success rates of total hip replacement and hip resurfacing has increased dramatically over the years, however, there are still some problems that cause fails that need addressing.

Failures are as follows:

- Complications during surgery
- Wear of the bearing surfaces
- Infection
- Dislocation
- Prosthetic Fracture
- Loosening
- Joint stiffening

Rarely are there complications during surgery. However, there can be problems with the surrounding area as nerves and blood vessels can become damaged and need immediate restoration. These can be repaired during the

procedure, but delay the overall time and recuperation. Also, fractures of the implant or the bones can occur causing more problems.

As with any operation, blood clotting can be problem. However, there are measures that are in place if this ever happens. As explained before, dormant infections can become active and new infections can occur due to the implant or due to the conditions in the theatre.

Dislocation of the replacement device can occur. When the ball moves out of the socket, it can be easily put in place by the orthopaedic surgeon. The surgeon may then advise the patient that certain activities are prohibited to limit recurrence of the problem.

Prosthetic fracture is a major concern, as wear and tear of the implant over its life cycle can cause breakage. The older material implants are more likely to break, but newer ones with higher strengths and increased durability are likely to last longer.

Loosening of the implant is usually related to the wear or the adhesion between the adjacent surfaces. This can also occur due to stress shielding. As bone is a dynamic material, it requires stress for it to grow and therefore, the implant takes the stresses impacted on the joint, resulting in the bone to resorb away. This leaves the adhesion between the bone and the implant surface weak. The loosened implant then moves around the open cavity and could break.

Joint stiffening is a problem whereby soft tissues within the joint area become bone by a process called heterotopic ossification. This is the formation of extra bone in non-bone tissues.

2.10.1 Wear

As it can be seen the common denominator in the other failures is due to wear of the bearing surfaces. This is also the most common failure method [Wilches et al. 2008]. There are two types of wear failures: Abrasive Wear and Sliding Wear

2.10.1.1 Abrasive Wear

Hard particles force themselves between the two bearing surfaces and move relative to the direction of motion [Bhatt & Goswami 2008]. They cause scratches and material to be gouge out from the surface **[**Zum Gahr 1998]. High stresses can occur when the particles become lodged between the surfaces.

In alloys with hard phases, the abrasion resistance is determined by the size and shape of the both the abrading species and hard phases. Therefore, the resistance will increase as the volume fraction of the hard phase increases.

2.10.1.2 Sliding Wear

This form of wear is complex. It occurs when two surfaces are in contact and motion with one another. The risk of damage is determined by the material used and if there is any lubrication to assist motion.

There are three mechanism by which sliding wear generally occurs: [Davis 2001]

First mechanism is due to the oxide layers on surface of the material. These layers are controlled by temperature or frictional heating. As they grow due to increased heat, glazes form that are highly reflective, smooth, peaks of randomly distributed oxide debris. These glazes become lodged between sliding surfaces and cause abrasion. The combination of sliding and abrading is known as fretting.

The second mechanism is due to high contact stresses forcing the oxide layers to be grinded or broken away. This leaves the materials to rub against each other. In terms of metals, cold welding can occur between the metallic surfaces and as motion occurs fracture, transfer or deformation of material is exhibited. In terms of ceramics, the motion of the surface can cause fracture due to the high brittleness of the material.

Third mechanism is due to cyclic stresses caused by the adjacent materials forcing themselves on another periodically. Fractures and cracks can develop due to the forces exerted.

2.11 Mechanism of release of metallic ions

The mechanism of release of metal ions from the metallic implants is also very important; as this could indicate a way of preventing the metal ions leaching in the first place. The release of these ions is dependent upon the electrochemical rule. Most of these metallic materials form a corrosion resistance film upon the surface to prevent the metal ions leaching away. However, not all ions released are toxic and/or induce toxic reactions.

The human body can be a hostile environment for these implants. The chloride ion concentration in serum is 113 mEq L^{-1}, which is very corrosive. The blood consists of proteins and amino acids that act as electrolytes and interact with the metallic material effecting the corrosion resistance [Merritt and Brown 1988; Williams et al. 1988]. The oxygen level in the blood is much lower than in air, therefore the oxidic film that forms on the surface of the metal cannot be regenerated, resulting in the release of metallic ions [Jack 1984]. The body fluid has a pH of between 7.0 and 7.4, however bone tissue where the implant is fixed initially has a pH of ~5.2 before rising to 7.4, this acidic condition can have a drastic effect on the material [Hench & Ethridge 1975; Bruesch et al. 1985].

As indicated, the corrosion resistance of the metal is dependent upon the surface oxide that forms as a passivity layer. The film is dependent upon the constituents of the alloy, in the cobalt based alloys, the film consists of oxides of cobalt and chromium [Smith et al. 1991]. Chromium and molybdenum are found at the inner layers and surface consists of large amounts of OH^- ions [Hanawa et al. 2001].

The oxide film, in different solution environments have both active and passive surfaces when in contact with an electrolyte [Kelly 1982]. Therefore, the surface oxide film undergoes a process of partial dissolution and reprecipitation when in an aqueous solution as shown in Figure 2.6.

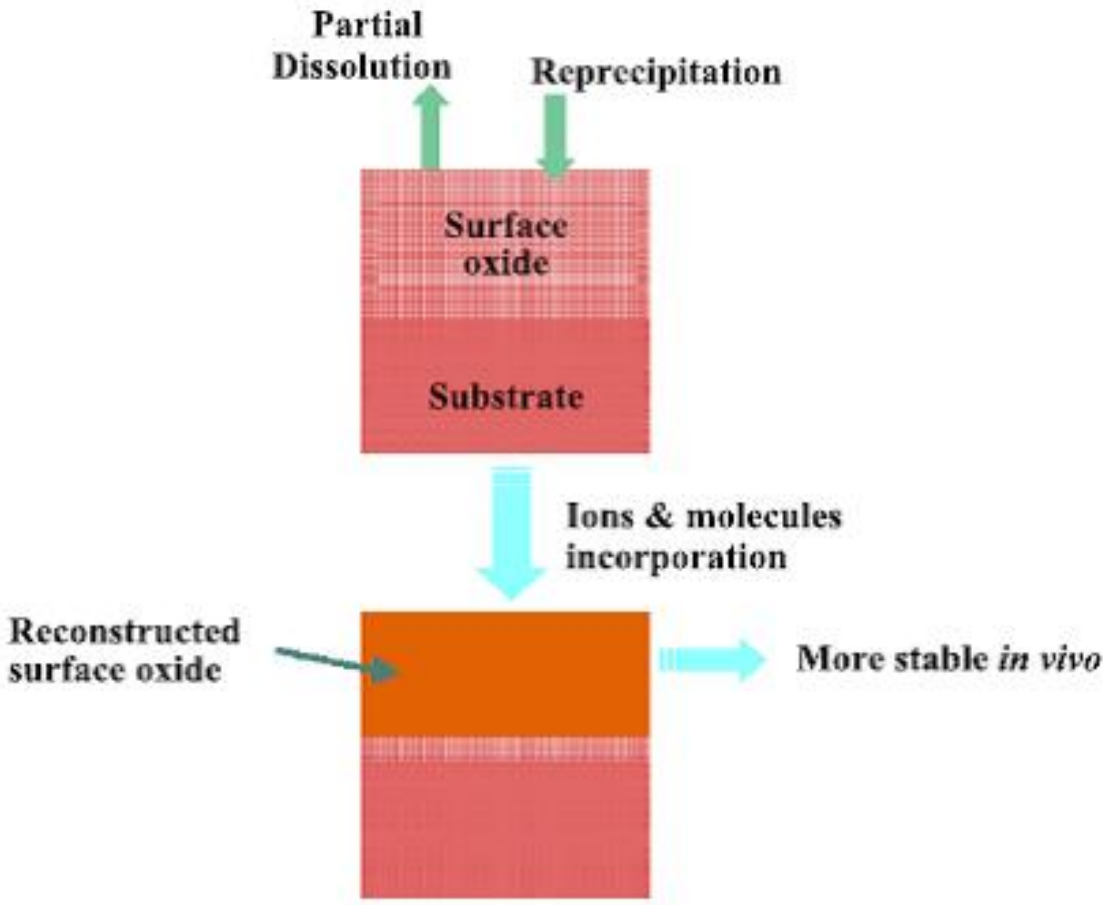

Figure 2.6: The process of partial dissolution and reprecipitation of the surface oxide film [Hanawa 2004]

If the rate of dissolution is greater than the rate of reprecipitation, then the gradual release of metal ions will occur. As the metal ion leaching surface oxide is slow to regenerate, the dissolution rate of the film can be accelerated by the proteins and amino acids [Merritt & Brown 1988; Williams et al. 1988]. Another theory on how the metal ions are released is due to the interaction with macrophages. When the implant is introduced in the body, it is treated as a foreign body and macrophages and other immunological cells attach to the surface of the new material [Tang & Eaton 1993]. The macrophages produce oxygen species when they phagocytosis particles, these oxygen species are catalysed by superoxide dismutase and produces H_2O_2 [Johnston et al. 1978; Ward 1983; Hansen 1987]. This molecule interacts with the surface of the metallic material and causes the release of metallic ions from the surface [Edwards et al. 1988; Behl et al. 1994].

Once the surface oxide film is constructed it can be altered depending upon the environment it is placed in. In the cobalt based alloys, the initial surface consists of oxides of chromium and cobalt when exposed to air, once submerged in cell culture, the cobalt in the oxide becomes dissolved and only chromium oxide and oxides of molybdenum are identified, above which calcium phosphate forms as indicated in Figure 2.7.

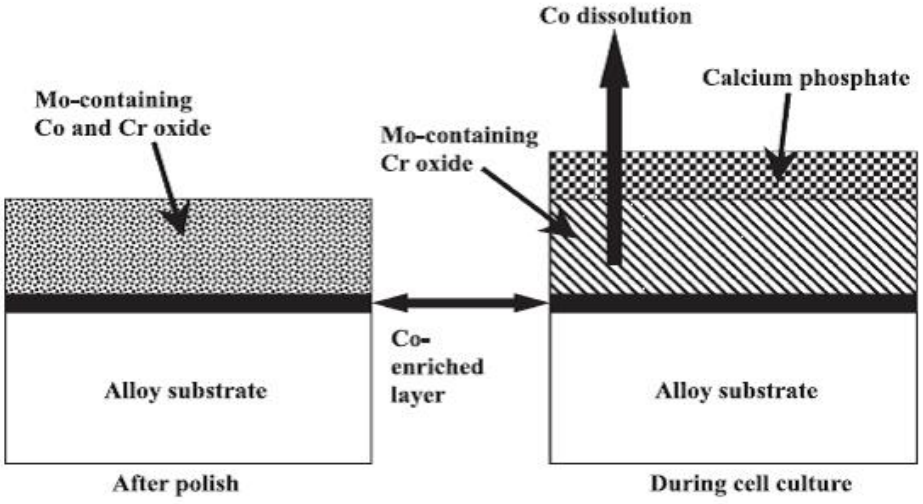

Figure 2.7: Regeneration of oxide surface after polishing and submerged in cell culture [Hanawa 2004]

With the hip replacement devices, the main function is from the wear and fretting of the surfaces. As the surface oxide layers are damaged during function of the device the exposed surface gives a larger opportunity of the metal ions being leached out and the wear debris also leaching ions in the body. In the cobalt based alloys, the most preferential element to be released from the alloys is cobalt [Storp & Holm 1977]. This exposure increase the corrosion of the metal, however, if the film is regenerated the metal ion leaching can be reduced. Therefore, the leaching can be managed if the film can be regenerated rapidly.

The metal ions leached from the metallic implant do not always cause damage. It depends upon the ion being leached and the chance of interaction with a biomolecule or how its reacts with water and anions (Figure 2.8). All molecules in the body can combine with the metal ion. The ion is highly reactive and can react with water or anion and reduces its opportunity to react with the biomolecule (Figure 2.8A). There are some ions that are inactive, nickel and copper, which remain for a longer period, but these are more susceptible to reactions with biomolecules and causing toxicity (Figure 2.8B).

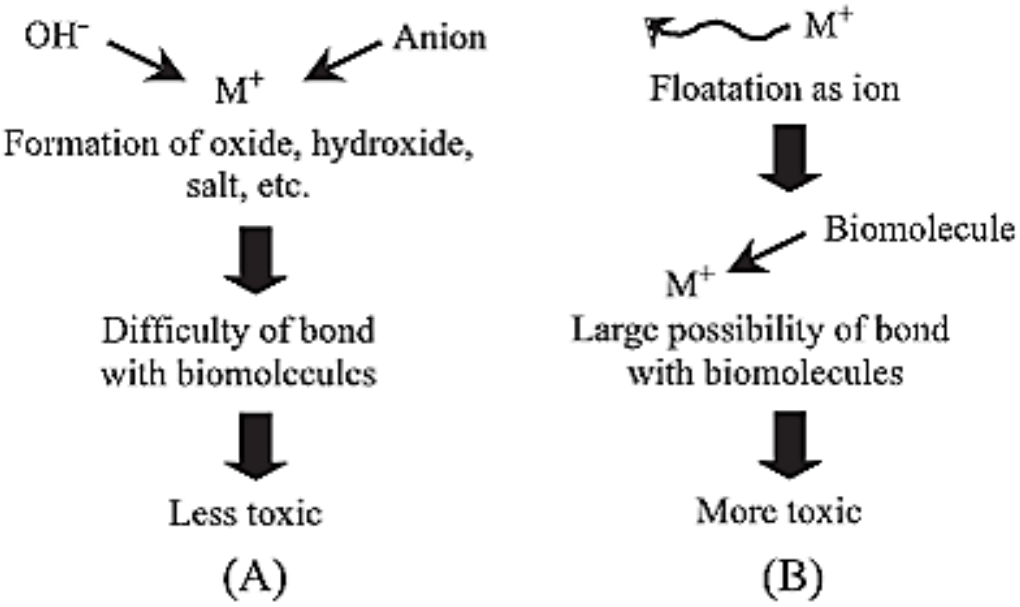

Figure 2.8: Metal ion reacting with water and anion or biomolecule and the possibility of toxicity [Hanawa 2004]

Therefore, the toxicity of the metallic materials is dependent upon the corrosion resistance of the material, the specific ions that are released, and the activity of the ion and the toxicity of the ion.

2.12 Advances in cobalt based alloys for orthopaedics

The advances in the cobalt based alloys used in orthopaedics have been very limited. The main work conducted in the hip replacement industry with these alloys is for analysis of wear using hip simulator testing to determine the performance of the alloy and for new designs of the implant to allow improvement in the fitting between cup and head to reduce wear. Not much work is being done to investigate new methods of fabrication or improvements of the alloys for its application. Some of the advances investigated are detailed below:

Processing of alloys has shown to produce significant improvements in the properties. In the cobalt based alloys used in orthopaedics not much processing has been attempted to improve the alloy. But there are some investigations that have taken place to attempt improvements.

Kircher et al. used electron beam melting manufacturing of the Co-Cr-Mo (similar composition to F75) alloy [Kircher et al. 2009]. Electron beam manufacturing is a rapid manufacturing technique that uses computer aided design software to build up layers of the component. A fine layer of the powder is placed on a steel platform and the electron beam generated using electric current to pass through a tungsten filament melts the layer of powder. Subsequently, another layer of powder is placed on top of the melted powder and the process of melting is repeated. By placing layer upon layer of powder the component is built up. A vacuum is used due to the electron beams involved and a temperature of 800°C is maintained. Once the component is built up, the chamber is flooded with helium gas for rapid cooling. Comparing the properties of the electron beam melting produced alloy against the

commercial grade alloys, exhibited an alloy whose mechanical performance exceeded or meet the requirements of the F75 and F1537 alloys.

Bardos investigated hot isostatic pressing (HIP) of powder to form higher strength Co-Cr-Mo alloys [Bardos 1979]. HIP as stated in Section 2.8 is one of the basic powder processing technique. In this investigation high pressure and a high-temperature autoclave with argon gas was used to sinter the powder. The HIP compact produced grains of 0.8µm compared to the commercial manufactured alloys of 8µm, the mechanical strengths of the HIP alloy was significant higher than the conventional fabricated cobalt based orthopaedic alloys, especially the fatigue strength. Biocompatibility and corrosion behaviour showed similar results to the cast Co-Cr-Mo alloys.

Dourandish et al. has used a simple pressureless powder processing technique to sinter Co-Cr-Mo (F75) powders to prove the ability of powder metallurgy to produce an orthopaedic device [Dourandish et al. 2008]. The investigation used powders packed in an alumina die and sintered via liquid phase sintering in an argon atmosphere furnace. The compact produced were dense however not fully with around 5% porosity in the structure and 34% porosity at the surface edges, this contributed to the hardness of the alloy which were similar to the current manufactured cobalt based orthopaedic alloys.

Janaki Ram et al. investigated the use of laser engineered net shaping to manufacture CoCrMo alloys for improvement in wear resistance [Janaki Ram et al. 2008]. Laser engineered net shaping is a novel additive manufacturing process developed by Sandia National Laboratories (USA). This process uses a computer aided design model to generate a computer component and slices the model into layers. The deposition process to form the component required is built up of the computer generated layers. A laser beam generates a pool of molten melt and subsequently powder is injected into the melt pool and rapidly solidified, the laser beam moves to the next coordinate and over time a

layer is built and the process is repeated until all the layers are built up forming the required component. This process occurs in an enclosed chamber filled with argon. The laser engineered net shaping alloy is compared against conventional manufactured Co-Cr-Mo orthopaedic alloys for their hardness and tribological performance using a dry sand/rubber wheel wear test. The hardness of the laser engineered net shaping alloy and the Co-Cr-Mo alloy shows no significant improvements and the wear resistance of is significantly lower.

Zhuang and Langer have investigated ways to improve the properties of cast Co-Cr-Mo alloys by controlling the casting conditions during the solidification process [Zhuang & Langer 1989]. The current used medical grade alloy (F75) is cast using a sand mould and cooled in air. This investigation used a metallic mould with cooling water. The microstructure produced is of equiaxial grains compared to the dendritic structure in the medical grade alloy. The new microstructure has produced a slight increase in the hardness of the alloy, but the main improvement made with the effects of cooling is the significant enhancement in the fatigue strength.

Modifications to the current commercial manufactured alloys have also been investigated to improve properties.

Saldivar-Garcia and Lopez have investigated heat treatment techniques to improve the wear resistance of the alloys [Saldivar-Garcia & Lopez 2005]. They have tried to increase the HCP over the FCC content within the microstructure. Within an alloy a single HCP phase has been shown to improve the crystal structure and wear resistance [Buckley 1968]. They used conventional heat treatment techniques, where wrought and as-cast commercial alloys were subjected to homogenised heating followed by quenching to produce full FCC content and then rehomogenised to increase the HCP fraction to near full HCP content. Tribological performance of the

alloys were tested using pin-on-disk apparatus and the results showed that the higher HCP content alloys exhibited high wear resistance compared to the higher FCC content alloys.

Zhuang and Langer have investigated the effects of alloy additions on the fatigue behaviour of Co-Cr-Mo surgical implant alloys [Zhuang & Langer 1989]. They used commercial as-cast Co-Cr-Mo alloy with different additions of nickel, aluminium, titanium and boron. The alloys were produced by vacuum induction melting and cast in sand moulds with air cooling. The addition of elements did not make improvements to the cast alloy. The grain size has been shown to be reduced by the additions of aluminium, titanium and boron but by 5%. The nickel addition reduces the tensile strength and hardness, but improves the elongation of the alloy.

Gradzka-Dahlke et al. investigated the addition of biocompatible materials to the Co-Cr-Mo alloy to improve the mechanical properties [Gradzka-Dahlke et al. 2008]. The materials selected were calcium phosphate, boron carbide and silicon nitride. The alloys were produced by water atomisation method with 10% of the biocompatible materials added to the powders. The Co-Cr-Mo powders were annealed first, subsequently the modifiers were added and then processed under an argon atmosphere. The calcium phosphate filler material improved the compression strengths and yield point and aided frictional process during wear testing. The other two fillers increased the brittleness of the alloys. But the tribological performance of the additional materials increased the wear as their particles acted as abrasives, increasing wear.

Lee et al. investigated the addition of nitrogen and chromium to the current Co-Cr-Mo orthopaedic alloys to improve their mechanical properties [Lee et al. 2007]. The nitrogen and chromium were added to the Co-Cr-Mo alloy by melting the existing alloy using a vacuum induction method and pouring the melt into a metallic mould in a nitrogen atmosphere and subsequently adding

chromium nitride powder into the melt. The additional powder contributed to an increase in content of nitrogen up to 0.61wt.% from 0.25wt.% and the chromium up to 34wt.% from 30 wt.%. The additional content significantly improves the yield and tensile strength compared to Cr-Cr-Mo alloys. The main improvement made is the significant increase in elongations to approximately 40%.

Spriano et al. investigated modification of the surface of the Co-Cr-Mo orthopaedic alloy for improved wear resistance [Spriano et al. 2005]. The surface of the Co-Cr-Mo alloy is modified with Tantalum. The Co-Cr-Mo alloy undergoes thermal treatment in molten salts (compounds of cobalt and tantalum) under argon flux and is tested for tribological performance against non-treated alloy using a pin-on-disk wear apparatus. The wear performance of the modified surface shows significant improvements in wear resistance.

Dobbs and Robertson have investigated heat treatment of cast Co-Cr-Mo orthopaedic alloys to improve the mechanical properties [Dobbs & Robertson 1983]. The heat treatments were administered to the cast Co-Cr-Mo alloys via solution treatments using an electrical resistance tube furnace in high purity argon and quenching with cold water. The resultant tensile properties showed no significant increases in the yield point, but the tensile strength increased significantly and the elongation almost doubled. The most improvements made were in the fatigue resistance, where the improvements were up to 28 times the cast Co-Cr-Mo alloy.

Montero-Ocampo et al. have investigated the effects of alloy preheating on the mechanical properties of as-cast Co-Cr-Mo-C alloys [Montero-Ocampo et al. 1999]. As-cast Co-Cr-Mo alloy was induction melted under vacuum and cast under an argon atmosphere in a preheated mould. The preheated alloy exhibited improved mechanical strength and increased ductility than that of

as-cast Co-Cr-Mo alloy. The ultimate tensile strength and the elongation properties had the most improvement.

Coating the surface of the commercial medical grade alloys has also become common to improve the wear resistance of the alloy.

Sheeja et al. in 2001 investigated the using of diamond-like carbon (DLC) coatings on the Co-Cr-Mo (BioDur CCM Plus, Carpenter Technology) alloy [Sheeja et al. 2001]. The DLC coatings have gained attention for wear resistance applications and for with its biocompatibility and chemical inertness. The coatings are deposited using a filtered cathodic vacuum arc. This technique uses a vacuum chamber, a graphite cathode to form carbon plasma and a negative bias on the substrate cobalt based alloy, to produce films of multi-layer carbon. The films were 420nm thick and tribological testing was conducted using a pin-on-disk apparatus. An uncoated Co-Cr-Mo alloy and a coated DLC were tested, however the coated substrate showed no significant improvements in the wear resistance or the coefficient of friction to suggest that DLC coatings improve wear resistance in cobalt based orthopaedics alloys.

Fisher et al. have investigated the use of different coatings on the Co-Cr-Mo and their tribological performance [Fisher et al. 2004]. They have used titanium nitride, chromium nitride and chromium carbonitride coatings deposited using evaporative physical vapour deposition and DLC coated using plasma assisted chemical vapour deposition. The DLC coating thickness is 2μm and other coatings are 8-12μm. The wear performance of the coatings and commercial grade orthopaedic alloys is tested using a hip simulator. The chromium nitride coated combination showed the most reduction in the wear rate, whereas the others coating materials did not show significant improvements in wear rates. The hardness of the alloys with the coatings (20-

25GPa) deposited had a significant increase over the current medical grade alloys (4.2-4.5GPa).

Koseki et al. investigated the use of carbon ion implantation to improve the tribological properties of Co-Cr-Mo alloys [Koseki et al 2008]. Coatings of carbon ion implantation and DLC were deposited using plasma-source ion implantation method and tested for their tribological performance using the pin-on-disk method. The coating of the carbon ion implantation and DLC increased the hardness by 1.37 and 1.87 times of the substrate Co-Cr-Mo orthopaedic alloy. The tribological performance of the coated materials showed that the DLC had increased wear and the carbon ion implantation had lower wear than the uncoated Co-Cr-Mo alloy.

Vandamme et al. investigated the effects of carbide coated Co-Cr-Mo implant alloys for their wear behaviour [Vandamme et al. 2003]. An unnamed metal carbide was deposited on the surface of the Co-Cr-Mo alloy by microwave plasma-assisted reaction using a microwave plasma-assisted chemical vapour deposition system equipped with a tubular fused quartz reaction chamber and tested for tribological performance using a ball-on-disk wear test apparatus. The wear factor of the carbide Co-Cr-Mo alloy compared to an uncoated Co-Cr-Mo alloy showed a small reduction in the wear.

Yen and Hsu investigated electrolytic Al_2O_3 coating on Co-Cr-Mo implant alloys to improve the wear resistance [Yen & Hsu 2001]. The electrolytic coating is deposited using a naturally aerate solution of $Al(NO_3)_2$ and a potentiostat. The alloy was the cathode, graphite was used as the anode and saturated AgCl/Ag was the reference electrode. The Al_2O_3 coating was deposited on the surface of the alloy and subsequently annealed to improve adhesion. The coated alloys and uncoated Co-Cr-Mo alloys were wear tested using a pin-on-disk wear apparatus. The coated Al_2O_3 alloy showed an eight times reduction in wear compared to uncoated Co-Cr-Mo alloy.

From the investigations carried out by various researchers on the cobalt based alloys some have shown improvements in the properties for orthopaedic applications. However the improvements have not been significant to cause changes in the current manufacturing techniques used for hip replacement devices. Modifying the conventional fabricated alloys to cause changes in the microstructure has yielded some improvements but there has not been significant improvements in the properties. The use of new processing techniques for cobalt based alloys show that solid alloys can be fabricated, however the mechanical properties produced are similar to the current orthopaedic alloys and therefore changing manufacturing techniques may not be so efficient. The use of coatings on the surface of the cobalt based alloys have shown some interesting results in terms of tribological performance. The results indicate that some coatings increase wear resistance of the material, however coating materials that are under constant wear will over its functional time period wear away and the substrate underneath is the original Co-Cr-Mo alloy. When this is left exposed and the wear will accelerate, as the hard coating particles can act as abrasives.

Therefore to conclude, the current research in the cobalt based alloys has shown some improvements, however novel processing route seems the most interesting way forward as this will enable the opportunity to produce dense alloys with microstructures and properties that can make significant improvements over the current conventional manufacturing techniques.

Chapter 3
Experimental Details

3.1 Introduction

In this chapter, the materials, equipment and the procedures used for the experiments are described. The materials used, their corresponding suppliers and the product details are provided. The experiments designed to evaluate the objectives are described. The characterising of the subsequent samples is described. All systems were calibrated and measurements were checked against references or literature values.

3.2 Materials

Three elemental powders were used to form the alloy: Cobalt (Co), Chromium (Cr) and Molybdenum (Mo). Two commercial alloys were purchased for comparison for tribological performance. One hip replacement device was given for initial characterisation of the currently used materials. Ethanol, hydrochloric acid, copper chloride and distilled water were used for etching and ethanol used for balling milling. Bovine Serum was used for the wear testing of the alloys. Nylon pot and zirconia slenders were used for ball milling. Distilled water was used as the medium for metal elemental leaching experiments. Epoxy resin and silicon carbide grinding paper were used to mount and polish the samples respectively.

3.2.1 Powders

3.2.1.1 Cobalt

Cobalt is a chemical element, indicated with the symbol Co and an atomic number 27. It has ferromagnetic properties. Cobalt is found as compounds within most rocks, soil, plants and animals. It usually is combined with nickel and found in meteoric iron. It has two crystallographic structure, face centred

cubic (FCC) and hexagonal close packed (HCP). There is transition of the structures at around 450°C, but as this transition has a small energy difference, both structures are known to be found simultaneously in cobalt alloys [Lee et al. 1978].

To protect against oxidation, cobalt forms passive oxide layers, but it can be attacked by halogens and sulphur. There are several oxides of cobalt: cobalt (II) oxide, cobalt (II, III) oxide and cobalt (III) oxide. The common oxidation states are +2 and +3, but there are others ranging from -3 to +4.

The discovery of cobalt is attributed to Georg Brandt in 1735 [Wang 2006]. Cobalt was mainly used to add blue colour to glass, glazes and ceramics. Nowadays, cobalt is used to make superalloys for gas turbines and aircraft engines, due to the high temperature stability. It is also used due to its corrosion and wear resistant, therefore implemented in medical field for orthopaedics and combined with other elements to improve wear resistance [Michel et al. 1991]. Also, used in dental prostheses, as an alternative to nickel alloys, due its sensitivity and for high speed steels to increase heat and wear resistance.

Cobalt has been used in batteries in the lithium cathodes, and in nickel-cadmium and nickel metal hydride batteries to improve oxidation [Hawkins 2001; Armstrong et al. 1988; Zhang 1999]. It has been used as an oxidation catalyst in the chemical reaction [Hebrard et al 2009]. The isotope of cobalt Co^{60} is used in radiography, as a gamma ray source it can produce specific quantity and high activity when bombarded with neutrons [Audi 2003].

Cobalt can be found and is essential to the human body. Cobalamin, also known as Vitamin B_{12} consists of cobalt, and this vitamin is essential for the blood, brain and nervous system for maintaining function.

3.2.1.2 Chromium

Chromium is a chemical element, indicated with the symbol Cr and an atomic number of 24. It is antiferromagnetic at room temperature, but above 38°C it can be paramagnetic. It is found in the Earth's crust and the environment, produced due to erosion of chromium rich rocks [Emsley 2001].

In a high oxygenated environment the surface of the metal forms a thin layer due to passivation. The layer is not like rust, which penetrates into the surface; this layer remains fairly stable upon the surface. It has a wide range of oxidation states, with +3 and +6 being the most common and +1, +4 and +5 being rare.

Chromium was first discovered by Johann Gottlob Lehmann in 1761, however he misidentified the compound basing it on lead [Guertin 2005]. In 1797, Louis Nicholas Vauquelin had crocoite ore and using hydrochloric acid and a charcoal oven to form metallic chromium [Vauquelin 1798]. Chromium can also be found in gemstones of ruby and emerald.

Chromium is used as a strengthening element in alloys, where it can form carbides and for its corrosion resistance. In steel, the main corrosion property is dependent upon the concentration of chromium added in the iron alloy. It is a very hard material and so is used as coating upon substrates to make them more resistant [Dennis & Such 1993]. It is also used in dyeing, as it can form the yellow, red and green colours depending upon the compound. It has been used in wood preservation, as chromium (IV) salts are toxic and destroy fungi and insects that attack the wood [Hingston 2001]. Due to the high heat resistance and high melting point of chromium compounds, the material has been used in high temperature refractory purposes, however this in declining due to toxicity of chromium(IV) [Papp 2006].

Chromium has no uses in the biological environment [Di Bona et al. 2011].

3.2.1.3 Molybdenum

Molybdenum is a chemical element, indicated with the symbol Mo and atomic number 42. It can be found in minerals such as wulfenite and powellite, with most it from molydenite. It has many oxidation states, with +4 and +6 being the most common.

In 1752, Bengt Andersson Qvist came across molydenite but dismissed it as nothing new. In 1778, Carl Wilhelm Scheele realised that the mineral found was a new entity and in 1781, Peter Jacob Hjelm successfully isolated molybdenum from carbon and linseed oil [Van der Krogt 2006; Gagnon 2007; Scheele 1779; Hjelm 1788].

As molybdenum can withstand high temperatures making it less malleable, it is mainly used are for armour, aircraft parts, electrical contacts, industrial motors and filaments [Emsley 2001]. It is also used in alloys to increase high temperature corrosion resistance and weldability [Glenn 2005].

3.2.1.4 Nanopowders of Co, Cr, Mo

Powders of Co, Cr and Mo were obtained from American Elements, USA. The average particle size of the powders is shown in the Table 3.1. The Co powder was pre-oxidised with 10% oxygen (O) by the supplier to enable safe handling.

Table 3.1: The average particle size of the as supplied powder

Powder	Co	Cr	Mo
Average Particle Size /nm	28	100	85
Product Number	CO-M-O2-NP	CR-M-O2-NP	MO-M-O2-NP

3.2.2 Alloys

3.2.2.1 As-received hip replacement device

The as received hip replacement devices was supplied by JRI through Orthopaedic Research UK. A bearing surface hip replacement device consisting of a metallic femoral head and actebular cup, used in the initial investigation to gather an understanding of hip replacement devices.

3.2.2.2 F75 alloy

The F75 alloy was supplied by WearTech, UK. The most commonly used cobalt based alloy in orthopaedics, formed via the casting method. The elemental content of the alloy is shown in Table 3.2.

3.2.2.3 F1537

The F1537 alloy was supplied by Lamineries Matthey SA, Switzerland. Another conventional method of manufacturing of alloys is by wroughting. This F1537 is the wrought version of the F75. It comes in two different types: low carbon (LC) and high carbon (HC) and can come in different worked conditions, from hot anneal to warm anneal to warm forged. The elemental content of the alloy is shown in Table 3.2.

Table 3.2: Elemental content of F75 and F1537 alloys

Alloy	Cobalt (Co)	Chromium (Cr)	Molybdenum (Mo)	Carbon (C)	Other elements
F75	Balance	30%	6%	0.20%	0.80%
F1537	Balance	27%	6%	0.04%	1.8%

3.2.3 Etching solution

To determine grain characteristics, some alloys require etching to reveal the grains in the microstructure. The etching solution contained: ethanol (C_2H_5OH), hydrochloric acid (HCL), and copper chloride ($CuCl_2$). This was used to be able to identify the grains in the cobalt based alloys, as usually the

grains are very difficult to visualise without etching. There are different methods in etching the grains. The simplest method is using just solution as used in this experiment. There are methods that use electrolytes and other electrical devices to charge the liquid and to electrolytically corrode the surface.

3.2.4 Ethanol

General purpose research grade ethanol (C_2H_5OH) supplied by Sigma Aldrich, UK was used in this research for the reduction of agglomerations of the powders and as the lubricant during the ball milling process. The use of ethanol has been known to reduce agglomeration so that particles are smaller in size [Tang et al. 2008].

3.2.5 Grinding paper and epoxy resin

Silicon carbide paper and epoxy resin were purchased from MetPrep, UK. Circular silicon carbide grinding paper, used with a grinding machine is crucial for the grinding and polishing of the surfaces of the alloys for microstructure examination and alloys for the wear testing and surface roughness measurements. Silicon carbide is one of the hardest materials and so from a high 120 grit paper down to a polishing 4000 grit paper was used to polish the surface of the alloys to mirror finish. Optical microscopy was used to examine the surface after polishing and ensure a limited number of scratches were present before commencing with other analysis. Tap water was used as a lubricant during the polishing process to allow frictionless motion between the alloy and the paper and to remove excess debris away from the polishing area, to avoid abrading the alloy surface.

Epoxy resin was used to mount the metallographic pieces for ease of grinding and polishing and for the hardness test of non-flat surface pieces. The epoxy resin comes in two parts: one part hardener and one part resin. Four parts resin to one part hardener are combined together in a 40mm die set and the sample

piece is placed in the centre. The resin is allowed to set for a minimum of 10hours.

3.2.6 Ball milling pot and slenders

The milling pot was made of nylon. This is a strong material to withstand the impact of the slenders present and has a high expansion coefficient, which can withstand the energy released during milling. In some processes of ball milling, energy can be released from either the reactions of powders with one another or from reactions of the powders with the lubricating medium. If the encompassing material does not have a high enough expansion coefficient the material can swell up and burst open or when removing the lid, the contents could burst everywhere as the energy releases into the atmosphere and byproducts can be toxic.

The slenders were made from zirconia, a very hard material with higher hardness and wear resistance, to break down agglomerates and ensure thorough mixing of the powders, to increase homogeneity.

3.2.7 Bovine Serum

Bovine serum was supplied through Sigma Aldrich, UK (Product Code: B9433, Batch number: 120M8410). It is a USA origin, sterile-filtered medium and suitable for cell culturing. The serum is from the blood of a bovine species, in the USA slaughtered at less than 12 months. Table 3.3 details the constituents of the serum.

Bovine serum is extensively used as a blood substitute medium, as it has similar liquid properties and constituent materials, such as proteins, amino acids and other molecules. For this study the medium was used as a lubricating fluid to mimic the liquid properties for the wear test. It is mixed with water as the bovine serum has very low viscosity and hardly any water content, whereas in the body blood consists of 80% water content and the rest

is made up of the cells, plasmids and minerals. Using pure serum, due to its low viscosity will not allow ease of movement of the bearing surfaces, causing limited movement and a failed tested in terms of achieving results.

Table 3.3: Adult Bovine Serum content, USA origin, sterile filtered (product number: B9433)

Sodium	315 mg/dl
Glucose	100 mg/dl
Total protein	7.5 g%
Albumin	3150 mg/dl
Globulins: Alpha	1.09 g/dl
Globulins: Beta	0.94 g/dl
Globulins: Gamma	2.32 g/dl
Triglyceride	14 mg/dl
Cholesterol	172 mg/dl
Iron	178 µg/dl

Many researchers use other solutions such as sodium chloride, phosphate buffer solution and simulated body fluid. Those solutions are good for the cell culturing as they have good mineral content, but for wear testing analysis, the fluid properties are more critical than the biological content as this will affect the friction of wear and affect the tribological performance.

3.2.8 Distilled water

Distilled water is used as experimental water (pH: ~7). Normal tap water, contains ions and particles, which can affect the results, therefore distilled water is used. The water is heated and then allowed to cool, to produce a liquid which is purer, in terms of it being H_2O. In some regions the tap water is very hard due to it containing a higher mineral content. This type of water has been considered to be more beneficial for the cardiovascular system. However, for the experimental use and for the use for this thesis, distilled

water is more appropriate, as the metal ion leaching studies require less mineral content, to reduce the content of those mineral and the formation of compounds or the ions can cause an increase in corrosion and leaching.

3.3 Equipment

This section details the equipment used to conduct the experiments and characterise the compacts. A description of each equipment is given.

3.3.1 Equipment used for processing and forming the compacts

3.3.1.1 Spark Plasma sintering

Powder processing has many advantages over conventional sintering techniques. Usually conventional powder metallurgy sintering methods adopt a system whereby external heat from a filament or an arc, heats the die from the outside and therefore the diffusion of heat is assumed to heat the powder up. The process of heating can be inefficient. The powders closest to the die may become heated sufficiently, however the powder in the centre of the die may not get enough heat to cause fusion. This inefficiency causes the major problem of voids in the case of fully solid materials. Materials that have voids when they are supposed to be dense have lower strength properties for structural uses. Porosity of the material can be an advantage when it comes to ingrowth of tissues, however for bearing surfaces in hip replacement devices no porosity should be present. Electric current assisted sintering has been one of most advantageous powder processing techniques to achieve enhanced properties, with the most common method being SPS.

SPS produces highly dense materials with minimum grain growth. This is achieved by a pulsed electrical current heating the material while applying a pressure to compact the powdered material [Shen et al. 2003; Yan et al. 2005]. The powder is heated via the Joule effect, as the electrical discharge from the spark in the gap causes the powder to deform and fuse together [Tokita 1993]. This process has the ability to densify nanopowders, in order to produce

microstructures with finer grains and superior mechanical properties [Johnson 1991; Gao et al. 1999]. It has been used to produce various metallic alloys, ceramics and composites for functional and structural uses [Yoritoshi et al. 2005; Munir et al. 2006; Inam et al. 2008; Dusza et al. 2009].

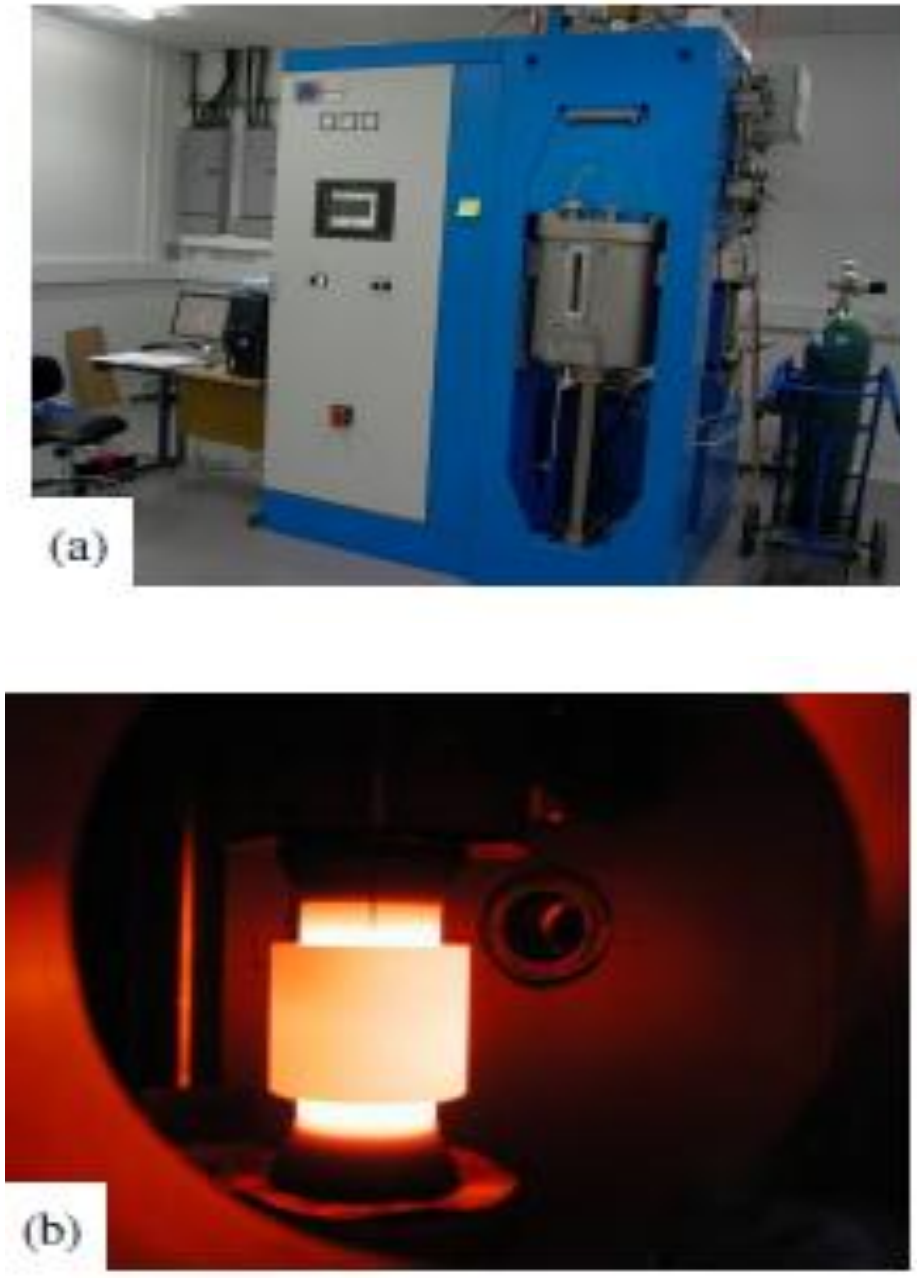

Figure 3.1: SPS facility by FCT Systeme, Germany, (a) SPS facility at Queen Mary, University of London, UK and (b) SPS at 1800°C [Inam 2009]

In this study, all the samples were SPSed in a HPD 25/1 furnace by FCT Systeme, Germany (Figure 3.1). The current set up at Queen Mary, University of London allows samples of up to about 80 mm to be produced with sintering temperatures up to 2200°C. Details of the graphite parts and their assembly are shown in Figure 3.2. The furnace has an optical pyrometer above the furnace and focussed inside a hole in the top graphite punch (Figure 3.2). Typically, the voltage applied between the upper and lower punches is in the order of a few voltages and the current can be as high as a few thousand amperes. Graphite dies were lined with graphite paper (Le Carbone, UK, thickness: 0.38 mm) before pouring powder in them. It was used to prevent direct contact between graphite parts and the powder and to guarantee electrical contacts between all parts. Graphite dies were covered with carbon insulation (SGL, UK, thickness: 7mm) to avoid heat loss during SPS operation.

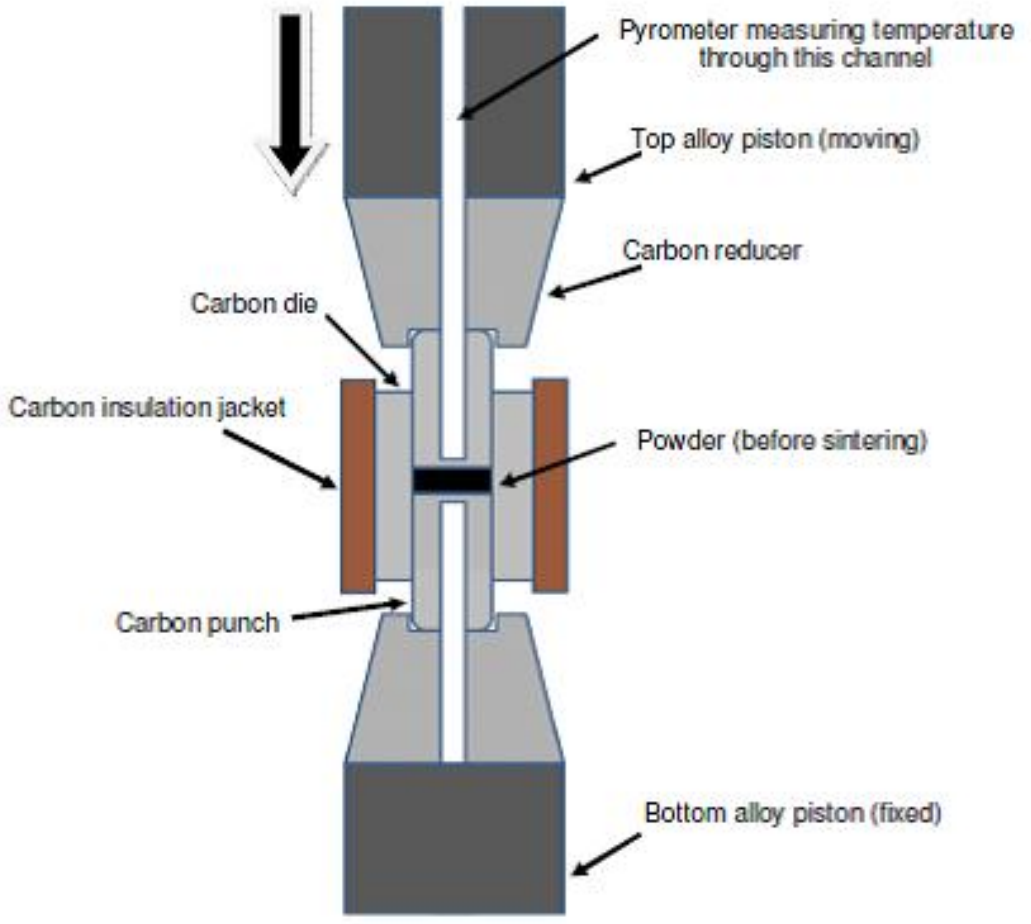

Figure 3.2: Cross sectional view of carbon die set [Inam 2009]

3.3.1.2 Furnace

The furnace used to conduct the heat treatment testing was a UAF 16/5 Lenton Themal Design Ltd, UK furnace. The furnace has an output power of 5kW and a maximum operating temperature of 1600°C. The furnace is equipped with a temperature/programme controller (Eurotherm 2216) that can set specific temperature dwell times and heating ramps. These furnaces are equipped with a low thermal mass ceramic fibre insulation and silicon carbide elements. The element enables heat to be radiated into the sample piece.

3.3.1.3 Incubator

Memmert D91126 (Memmert GmbH, Germany) incubator was used to keep the temperature at 37°C for the metal element leaching experiments.

3.3.2 Equipment used for characterisation of the compacts

3.3.2.1 Optical microscopy

The Nikon Eclipse ME300 microscopy is an optical microscopy that utilises light to reflect upon the surface of the samples to be captured by the charged couple device (CCD) camera (JVC, Japan) and converted into a digital image, using image processing software .

3.3.2.2 Scanning electron microscopy

Different scanning electron microscopes (SEM) have been used in this project. They are:

- FE-SEM; FEI Inspect F
- Hitachi S-3400N
- JEOL JSM-6301F

The SEM is a high powerful microscopy intended for use to produce high resolution images at higher magnifications. This uses electrons to interact with the surface of the sample and then be scattered off, captured by a detector and converted into a digital image.

The SEM consists of seven components: a vacuum, beam generation, beam manipulation, beam interaction, detection, signal processing, and display and record system.

A vacuum is essential to the system as the electron beam produces electrons, these will interact with other molecules and disperse in random directions. The vacuum creates an environment where as many gas molecules present are removed; therefore the electrons have limited number of molecules to interact with before reaching the sample. The electron beam generates the electrons required to interact with the surface of the sample. The electrons are formed from an electron gun, which consists of a filament of tungsten wire, lanthanum crystal or cerium hexaboride, a grid cap (Wehnelt Cylinder), which control the flow of electrons and a positively charged anode plate that pulls and accelerates the electrons down to the sample. The beam manipulation is a system that consists of electromagnetic lenses and coil that control the size, shape and position of the electrons towards the sample surface. The beam interaction is the interaction of the electrons with the sample and the signals generated after interaction. The electrons travel into the sample and interact with particles within the sample or upon the sample surface. The electron once interacted will scatter into a random direction. The interacted electron may also scatter out other events, such as back-scattered electrons (original electron), secondary electrons (electron excited from the specimen), X-rays (electron dislodges an electron of the sample from its orbit and X-rays are released due to the energy change), cathode luminescence (light scattered out), specimen current (electron absorb) and transmitted electrons (electron passes through). The detection system consists of many detectors attempting to capture the electrons that have interacted with the sample. Different detectors pick up different signals. The signal processing system, converts the signals received from the detectors into a digital image. Display and recording system, enables the user to view the processed signals as an image and using software can save the image.

It can be seen, that the sample preparation is key to the achieving a good quality image. For conductive materials the samples are ready to be visualised by the SEM, for non-conductive materials, coating is required to make the surface conductive. For liquid samples adequate drying is required to ensure no water molecules remains which will reduce the resolution of the image.

3.3.2.3 Electron dispersive X-ray analysis

This is coupled to the SEM for analysis of elements or chemical characterisation. The electron dispersive X-ray analysis (EDX) relies on the fact that each element has a different atomic structure and so X-rays that are given off from each element are identities specific to that element, therefore analysing the X-rays that are given off from the element would enable the ability to distinguish which element is present.

As mentioned before, the electrons that enter the sample can also emit X-rays once it has interacted with the sample. The electrons enter the atom of the element present within the sample. The electron then dislodges an electron from an inner shell of the elemental atom. Once that electron has created a space, an electron from a higher shell with higher energy replaces the inner shell lower energy electron and emits a beam of the difference in energy in the form of an X-ray. The X-ray now carrying the difference of energy of the two shells, once captured in a detector can be analysed through the energy to identify which element it came from, therefore characterising that element existing in the sample.

3.3.2.4 Philips defractometer

X-Ray diffraction (XRD) analysis of phases in the powders and the alloys were conducted using a X'PERT PRO (Philips) defractometer. Around 95% of solid materials have a crystalline structure. When X-Rays are fired at the material, phases interact with the rays and produce a diffraction pattern identifying the phase present. Hull, explained that "each crystalline substance

gives a pattern; that the same substance always gives the same pattern; and that in a mixture of substances each produces its pattern independently of the others" [Hull 1919]. The X-ray patterns can be classified as the "fingerprint" of the crystalline materials [Snider 1992].

The theory behind this system is explained:

When an X-ray is fired at an atom, the electrons surrounding the atom begin to oscillate at the same frequency as the X-ray beam. The resultant is the distribution of waves which interfere with each other and so no energy is released. Atoms in a crystal are orientated into a regular pattern and as the X-ray interacts with the atoms, beams are produced that exist in different directions, with some in very specific directions. The crystal unit cell is made up of interplanar spacing made up of h, k, l indices. These indices give the order of atoms in the unit cell. As the X-rays with a specific wavelength reflects off the plane of atoms in the unit cell, the X-rays are diffracted with the same wavelength into a specific path depending upon the d spacing of the atoms and the angle of the incident rays . This relationship was defined as a mathematical model by Bragg in 1913, known as Bragg's Law.

Bragg's Law is defined as:

$$2d \sin\theta = n\lambda$$

d is the spacing between diffracting planes, θ is the incident angle, n is any integer and λ is the wavelength of the beam.

These rays scattered in specific directions appear upon the diffraction pattern as spots. Moseley in 1913 explained that there is a relationship between the wavelength of the X-ray emissions and the identity of the element emitting the X-rays [Heimann 1968]. This correlated with the amount of an element

present in the mixture and the intensity of the spectral lines of that element. This was the beginnings of the X-ray spectroscopy.

The setup of the sample holder, the detector and the gearing system is known as the goniometer. The distance between the X-ray focal spot and the sample holder is equal to that of the sample holder and the detector. If the detector and sample holder were in a 2:1 ratio, the detector moves in a circle with a constant radius. For a Theta: 2-Theta goniometer, the X-ray tube remains stationary, the sample holder and detector move in the Theta and 2-Theta range respectively. For the Theta: Theta goniometer, the sample remains stationary in horizontal position, the X-ray tube and the detector both move simultaneously over the angular range Theta. The diffraction spectrum consists of a plot of the intensities and the Theta or 2-Theta detector angles, depending upon configuration of the goniometer.

The peaks of the spectra of the diffraction pattern are identified using the International Center Diffraction Data which maintains the database of inorganic and organic spectra. Two database (PDF I and PDF II) are distributed yearly that provide updated information upon d-spacing, chemical formula, relative intensity, particular phases, cell parameters, etc.
This powder diffraction method is ideal for characterisation and identification of crystalline phases in materials. The phases are identified through a search and matching system.

3.3.2.5 Leco and CSM Nanoindentator

The measurement of hardness is usually via the indentation method. For all scale of hardness from macro- to nano- the most efficient technique is the Vickers indentation method.

3.3.2.5.1 Leco microhardness tester

The microhardness measurements were conducted upon a Leco-M400G microhardness tester. In the 1920s, Vickers, Ltd formed the ability to measure hardness of a material using an indenter to deform the surface of a material. A diamond pyramid hardness test was developed, which used a comparable list of numbers that represent the hardness of steel. The indenter was a square-based pyramid that formed an angle of 136° from its opposite sides at the apex. The diamond was used to indent into the surface of the material at a specific load ranging up to 120 kg.f and the imprint left was measured using a calibrated microscope. The diameters of the impression at 90° to one another are measured and using the formula, the Vickers number can be calculated:

$$HV = 1.854\ (F/D1 \text{ x } D2)$$

Where F is the applied load, D1 and D2 are the horizontal and vertical diameters of the indentation.

3.3.2.5.2 CSM Nanoindenter tester

Nanohardness measurements were conducted upon a CSM Instruments Nanoindentor. Nanoindentation measurement is similar to microindentation, where an indenter tip with a known geometry is forced in the surface of material. That is the only similarities. The indenter is driven in with increasing load up to a pre-set maximum value and then the load is reduced to partial or complete relaxation. This process is repeated at different positions upon the material and indenter penetration of the material is examined using a differential capacitive sensor. A graph is plotted of the applied load against indenter penetration for each loading/unloading curve. The load/displacement curve can provide data upon hardness and elastic modulus.

To calculate the Indentation testing hardness, using the curves the Oliver & Pharr power law method and the following formulae is used [Oliver & Pharr 1992]:

$$H_{IT} = \frac{F_{max}}{A_p(h_c)}$$

Where h_c is the depth of the contact of the indenter with the test piece at F_{max}. A_p (h_c) is the projected area of contact of the indenter at distance h_c from the tip. A_p is a function of the contact depth h_c and is determined by a calibration of the indenter tip.

The Vickers Hardness, HV is defined as:

$$HV = \frac{F_{max}}{9.81\ A_c(h_c)}$$

Where A_c is the developed contact area and can be calculated from the projected contact area A_p and the indenter geometry as:

$$A_c = \frac{A_p}{\sin \alpha}$$

Where sinα is the angle between the axis of the diamond pyramid and its faces.

α= 68° for a Vickers indenter and α = 65.27° for a modified Berkovich indenter.

Finally, for a Vickers indenter: $HV = 0.0945.\ H_{IT}$

And for a modified Berkovich indenter : $HV = 0.0926.\ H_{IT}$

3.3.2.6 Tribometer

The wear test was conducted upon a CSM Instruments Tribometer (CSM Instruments SA, Switzerland). It tests the material to obtain friction and wear data. The objective of the machine is the testing of material to simulate the real frictional conditions under functional use. The tribometers range from macro to nano. The frictional coefficient is directly measured through the

machine, whereas the other data is calculated after the test. There are various controllable parameters, the applied load, the speed, the static partner and the environmental conditions. i.e. humidity, temperature, lubricant, vacuum.

The most conventional wear testing configuration is the pin-on-disk, where a cylindrical pin is rubbing against a flat sample disc. The pin can be replaced with a ball that changes the configuration into a ball-on-disc, but the measurement is exactly the same. During the wear testing, there is a running in phase at the beginning of the test due to the uneven nature of the sample, after a period of time, a steady state phase develops which indicates the actual frictional activity of the test. In the running in phase, the uneven sample surface has a low number of asperities, as the surface becomes broken down by the pin or ball resulting in a more asperities in contact, the test runs smoothly.

The wear rate of the sample is measured using a profile of the wear track. The wear track will indicate the amount of material loss, through that the wear rate can be calculated using the formula:

$$V_i = k_i F \ s \text{ [Archard 1993]} \qquad \text{Equation 1}$$

Where is Vi the wear volume, F is the Normal load, s is the sliding distance and k_i is the specific wear rate coefficient.

The wear rate of the partner (in this case was a ball), is calculated using a wear profile of the surface ball and using the formula:

$$h = R - \sqrt{R^2 - \frac{d^2}{4}}$$

where h is the height of the worn cap of the ball, R the radius of the ball and d the diameter of the worn cap.

Using this formula, the volume V can be calculated and reused into equation 1:

$$V = \frac{1}{3}\pi h^2(3R - h)$$

Therefore replugging into Equation 1:

$$\text{Wear rate}_{\text{partner}}: \frac{V}{s.F}$$

The other method of calculating wear rate through the amount of mass loss, using a highly sensitive balance and the density of the materials. However, this method is limited to the measurement of the balance and the accuracy of the density of the materials.

3.3.2.7 Conscan profilometer

Conscan profilometer (CSM Instruments SA, Switzerland) was used to conduct a scan over the surface of the metal samples for surface roughness and for the wear track profile.

For surface mechanical property measurement, the topography is very important, as it will give an indication of the behaviour of the material. Therefore, surface characterisation of the topography is essential before mechanical analysis.

The CSM Instruments Conscan, uses a raster scanning confocal light porfilometer to analyse the surface topography. In confocal profilometry, the basic principle of analysis of the surface is using chromatic aberration. Using white light and directing it towards the surface of the sample through a filtering optical component, the chromatic aberration can be used to separate the light using a dispersive lens into various wavelengths, which represent a z-coordinate in the optical axis. This transforms the visible light spectrum into a

z-coordinate as a ratio of the distance to the lens. As each wavelength of light reflects of the surface of the sample and returns to the lens, the variation of height of the sample at varying focal point produces a variation in the light wave. Therefore, the return wave can be used to correspond to a given height represented by z-height. Using a specific lens and specific scan area, raster scanning can form a large image of the micron lateral resolution and nanometer vertical resolution.

Using this technique the surface roughness of a polished sample, the wear track properties for Tribometer analysis and plastic deformation analysis of the material can be measured.

3.3.2.8 Nanosight

The particle size analyser used was the LM10-HS (Nanosight, Wiltshire, UK). This particle analyser allows analysis of particles in liquid. The particles can be counted and sized and also can perform this analysis upon nanoparticles too. It is a newly developed technique and can analyse the particles directly and under real-time visualisation. [Carr et al. 2007; Carr et al. 2007a]

The Nanosight instrument utilises a laser light source to illuminate the particles. The near-perfect black background, allows the particles to appear as individual entities with point scatter and move under Brownian motion. Brownian motion is the random movement of particles in a suspended fluid. The motion is captured and analysed using a CCD camera. The software involved tracks each individual particle simultaneously, but visualised separately. As the particles are analysed separately, the particle size and size distribution is not limited as intensity weighted, z-average distribution, which usually occurs in conventional particle analysers (dynamic light scattering (DLS) or photon correlation spectroscopy) in this nano-range of sizes. The Nanosight tracking analysis (NTA) can measure: particle size, particle size distribution as a direct number and as a frequency distribution, particle size

scattering intensity, which can allow heterogeneous particles mixture to be correlated and particle concentration. [Nanosight 2011]

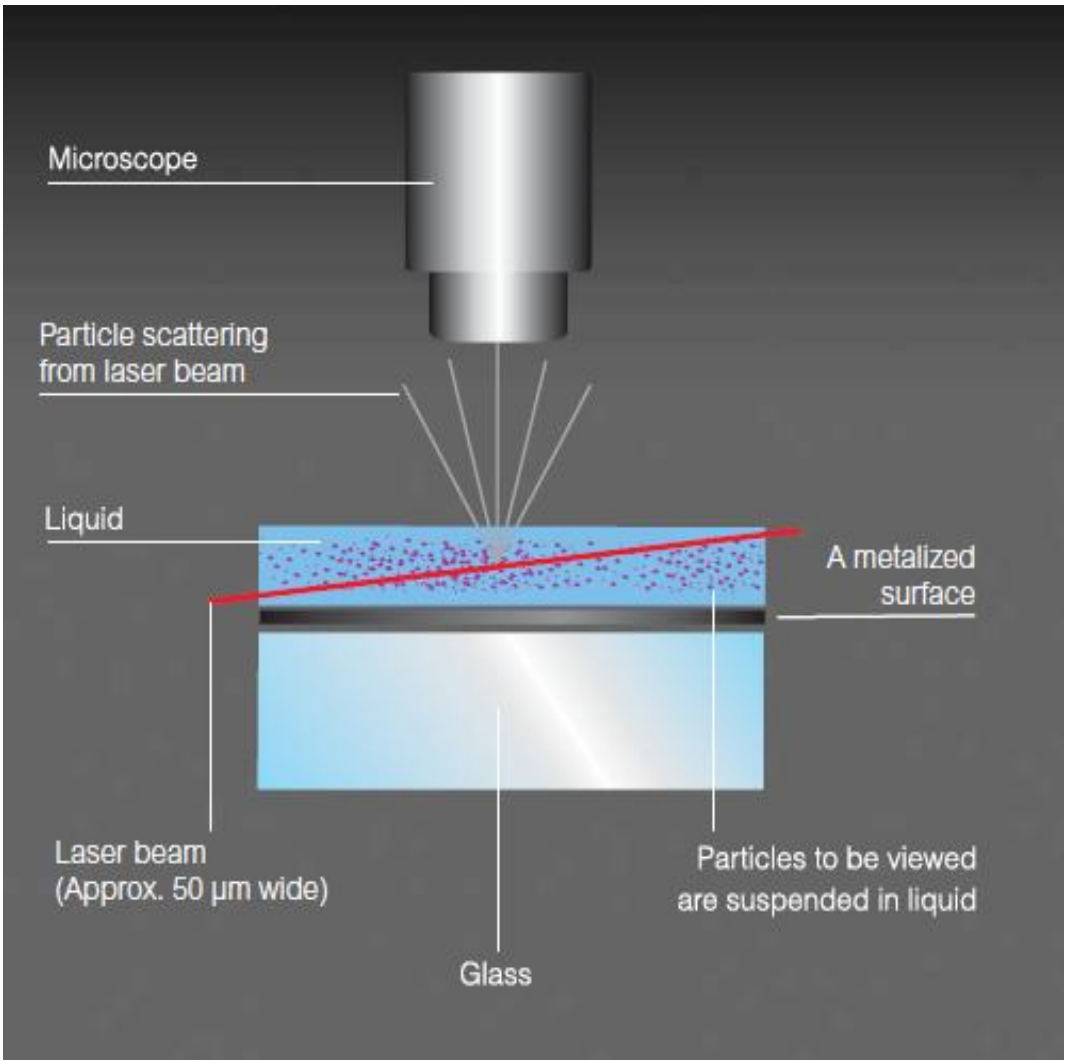

Figure 3.3: Representation of the technique of the Nanosight machine [Nanosight 2011]

3.3.2.8.1 Methodolgy of nanosight

The technique uses a finely focussed (635nm) laser beam which passes through a prism-edged optical flat (Figure 3.3). The refractive index of the glass is designed so that the beam refracts through the interface between the flat glass and the liquid layer upon it. The refraction causes the beam to be compressed into a lower profile and can illuminate the liquid layer to highlight

the nanoparticles present, using a x20 magnification objective lens fitted to a conventional microscopy with a long working distance. A CCD camera is mounted upon the microscopy to capture a video of the field of view of 100µm x 80µm, operating at 30 frames per second.

The particles moving under Brownian motion are simultaneously identified and tracked using the NTA software. Each particle is tracked frame by frame through the whole video segment, which are usually 900 frames or 30 seconds. The software makes calculations, depending upon the data received from the video: the average distance each particle moves in x and y directions. From these values the particle diffusion coefficient (Dt) is calculated. With the sample temperature (T) and the solvent viscosity (η) of the fluid known and with the other already obtained data the particle hydrodynamic diameter (d) can be acquired. The Brownian motion of the particles is taken in only two dimensions (x and y) from the video; however they are actually in three dimensional, therefore for this consideration a variation of the Stokes-Einstein equation is used to compensate for the dimensions.

$$\frac{\overline{(x,y)}^2}{4} = Dt = \frac{TK_B}{3\pi\eta d}$$

Where K_B is Boltzmann's constant.

The particle size limits of the NTA analysis depends upon the particle types. The lower limit is dependent upon the particle size and the particle's refractive index. Particles with a high refractive index, such as colloidal gold, are easier to track and so the accuracy of lower limit particle size can be down to 10nm. For the lower refractive index materials, such as biological molecules, the lower limit of particle size determination is between 25-30nm. The upper limits are dependent upon the Brownian motion of the particles, as the larger the particle size (1-2µm) the more difficult they are to track. For sufficient data to be acquired from an appropriate time period (~60 seconds) to give

statistically relevant and accurate particle size distributions, the sample requires to have between 10^7 and 10^9 particles/ml. Often, due to concentration range dilution is required.

3.3.2.8.2 Comparison to Dynamic Light Scattering

The most common method to analyse particles within a fluid is through Dynamic Light Scattering (DLS). The DLS uses a very similar method to NTA to analyse the particles through the Brownian motion and the Stokes-Einstein equation. In NTA, the motion of particles is captured through the video, in DLS the particle are analysed through a digital correlator, which analyses the time dependent scattering intensity fluctuations. The Brownian motion of the particles in the sample gives out fluctuations caused by interference effects of the particles with one another and its surroundings. Analysis of the resultant exponential autocorrelation function the average particle size and polydispersity index can be measured. However, for polydisperse particles, the multi-exponential autocorrelation functions cannot measure the particle size and polydispersity index accurately.

The main differences between the two techniques:

- The NTA measure particles in the range of 10-1000nm, the DLS measures particle from 1-2000nm
- NTA can measure all types of particle sizes, DLS is weighted more towards larger particle size
- DLS measures all the particles at once, NTA measures each and every one of the particles, but not as many as DLS.
- NTA can measure multimodal, polydisperse and heterogeneous/mixed samples with a high accuracy compared to DLS
- NTA requires no information upon the angle of detection, the wavelength used or the solvent refractive index, where DLS requires this to form the data

- NTA can provide information upon the particle concentration, DLS can not
- NTA shows the sample directly being generated to validate the particle size distribution, the DLS gives all the information once the data is collected
- The number of particles, the intensity of those particles and the size of the particles information is provide, DLS only gives the size and the polydispersity index
- NTA can analyse fluorescent nanoparticles as well as non-fluorescent, DLS can not

3.3.2.9 Inductively coupled plasma – mass spectroscopy

Inductively coupled plasma mass spectroscopy (ICP-MS), is an analytical technique that is used for identifying elemental characterisations. It is a highly sensitive device able to make measurements of concentration down to 10^{12}(parts per trillion) of metals and non-metals.

The inductively coupled plasma (ICP) is a system whereby plasma is used to make the gas electrically conductive. The plasma contains ions and electrons, which as electrically neutral, as the ions positive charge is balanced by the electrons. In the ICP spectrometry machine, there is a torch which consists of three concentric quartz tubes. The torch is placed in an induction coil, which has an applied radio-frequency electric current. The plasma gas, which is usually argon flows in the outer tubes and an electric spark produces free electrons into the gas. The electrons interact with an induction magnetic coil and are accelerated in one direction and then the opposite as the field changes. The argon atoms and electrons collide with one another and electrons off the argon atoms are lost in the process. These new electrons form part of the old electrons and repeat the process until the rate of released electrons balances the rate of recombination of electrons with argon ions. This process produces a high temperature plasma of around 10,000K. The torch enables the plasma

to flow in the outermost tubes and away from the wall enabling the ICP to remain stable. In the central tubing, a gas is introduced to flow through the plasma. This gas contains the sample and is administered as a liquid mist, produced using a nebuliser. As the nebulised sample enters the ICP, dissolved material is vaporised into liquid vapour, which subsequently breaks into atoms of the elements present. Due to the high temperatures, the atoms lose electrons and form singular charged ions, which can be measured.

3.3.2.9.1 Mass Spectroscopy

The ICP can be coupled with mass spectrometry (MS). The ions produced from the plasma are passed into the mass spectrometer where they flow through a series of cones, called a quadrupole. The ions are sieved out depending upon their mass-to-charge ratio and a detector analyses the concentration of ion signals. The concentration of the signals is referenced against a certified standard for single or multi- element materials.

The ICP-MS can analyse the range of elements with an atomic mass of between 7 and 250, which goes from lithium to uranium. Some atomic masses are excluded, such as 40 (argon), 80 (argon dimer) and 56 (argon oxide). The ICP-MS can measure sensitive of elements from 10 to 100 milligrams per litre to nanograms per litre.

Another chemical analysis device is atomic absorption spectroscopy, this uses an atomiser to atomise the sample. The atoms of the sample are then irradiate by optical radiation and passed through a monochromator. This splits the radiation of the source and the radiation of the element, which can be measured using a detector. With atomic absorption spectroscopy, only one element can be measured as a time, whereas the ICP-MS measure the whole spectrum range from lithium to uranium in one instance reducing time and allowing more samples to be analysed.

ICP-MS is used extensively in the medical and forensic fields, mainly for toxicology. Samples from patients can be collected from the blood, urine, plasma and serum and analysed for heavy metal poisoning, metabolic concerns and hepatologicl issues. It is also being used in the environmental field to analyse soil, water and material samples. In industrial environments, the exposure of metals is high and employers are having concerns for high metal content, therefore regular metal toxicity analysis is being undertaken using the ICP-MS systems. The samples tested in the system are usually high in concentration of materials such as clots in blood or solid samples in water. This has to be dissolved to avoid clogging in the system and diluents are used.

3.4 Method

3.4.1 Preparation of sample for alloy compositional analysis

Metallographic pieces (3 sampels) were cut from the supplied as-cast alloy and set in epoxy resin. They were ground and polished using 180P to 4000P graded silicon carbide paper, to create an excellent finish to view under the SEM.

3.4.2 Preparation for melting point analysis

Using Harris and Sikkengawork study [Harris & Sikkenga 1999], whereby the melting point of the F75 alloy is identified as 1377-1402°C, the temperature range was used as a reference to conduct the melting point analysis.

Metallographic specimens (3 samples for each temperature) were cut from the sample piece and heated to 1300°C, 1350°C, 1375°C, 1400°C and 1450°C in the furnace. Each sample was heated at a rate 5°Cmin^{-1} and allowed to dwell for a period of 1800 seconds and cooled to the ambient temperature within the furnace.

3.4.3 Preparation for heat treatment

Two cooling methods were used to cool the samples once heat treated. The two methods were annealing (cool within the furnace) and normalising (cool in air). Metallographic pieces (3 samples for each temperature) were cut from the supplied as-cast ally and were heated in the furnace. The range tested was 800-1200°C at intervals of 100°C. Each sample was heated at a rate 5°Cmin^{-1} and allowed to dwell for a period of 1800 seconds. One set was cooled in the furnace and the other in air.

3.4.4 Preparation for F75 and F1537 alloys

The F75 and F1537 alloys were supplied in a 20mm x 3mm discs and were polished using 180P to 4000P graded silicon carbide paper, to create an excellent finish.

3.4.5 Preparation of powder for spark plasma sintering

Table 3.4: Composition of elements for SPS alloy formation

Element	Co	Cr	Mo
Composition	66	28	6

50g of the Co–Cr–Mo powder was measured in the 66:28:6 wt% ratio, respectively (Table 3.4), and added to a nylon ball-milling pot containing zirconia slenders. A process control agent (120 ml ethanol) was added to the milling pot and the mixture was milled for 72h. The ethanol reduces oxidation and breaks up any agglomerates that may have been formed. The milled mixture was removed into a stainless steel pan and heated to 80°C for 24 h to evaporate the ethanol, leaving a dry powder. A 250 μm sieve was used to remove any agglomerates. Cobalt, chromium, molybdenum and ball milled powders were examined for confirmation of size using field emission SEM (FE-SEM; FEI Inspect F).

3.4.6 Conditions for spark plasma sintering

SPS was performed using a HPD25/1 (FCT Systeme, Germany) furnace under vacuum (5 Pa). Batches containing 3.5g of mixed powder were loaded into the 20 mm diameter cylindrical graphite die. The heating rate was set at 50°Cmin-^{1} and the cooling rate at 130°Cmin^{-1}. Table 3.5 shows the sintering conditions that were adopted for each sample.

Table 3.5: Details of SPS sample processing conditions

Sintering Temperature /°C	Dwell Time /min	Pressure /MPa
1050	10	75
1050	10	100
1075	10	100
1100	10	75
1150	3	75
1175	3	75

3.4.7 Characterisation for alloy compositional analysis

The field emission SEM (FE-SEM JEOL JSM-6300) was used to observe the microstructure of the alloy. The FE-SEM was operated at 10kV at a distance of 10mm. EDX analysis was used to determine the elemental composition of the medical grade Co-Cr-Mo alloy.

3.4.8 Characterisation of heat treated samples

3.4.8.1 Optical microscopy

Sample pieces once heat treat were set in epoxy resin and polished using silicon carbide paper. An optical microscopy (Nikon Eclipse ME 600, Nikon, Japan) was used to observe the microstructure of the specimens.

3.4.8.2 Measuring carbide phase

The carbide phase was measured using the optical images and UTHSCSA Imagetool 3.0 software. The carbide phase was threshold out and measured as a percentage of the entire image to determine the amount of content present.

3.4.8.3 Microhardness

Microhardness of the samples was measured using a Leco M-400-G hardness tester and the Vickers indentation method [ASTM Standard E92 2003].

3.4.8.4 XRD analysis

Phase analysis was conducted upon the annealed samples using X'PERT PRO Philips diffractometer operated with CuKα radiation at 45 kV and 40 mA in the scanning range of 5–70° with a step size of 0.03° and a scan time of 400s per data point.

3.4.9 Characterisation of F75 and F1537

3.4.9.1 Microstructure and Phase analysis

The microstructure was analysed using a SEM (Hitachi S-3400N). The phase analysis is conducted with an X'PERT PRO Philips diffractometer operating with CuKα radiation at 45 kV and 40 mA in the scanning range of 30–90° with a step size of 0.03° and a scan time of 400 s per data point.

3.4.9.2 Microhardness and Nanohardness

Microhardness was conducted upon a Leco M-400-G under Vickers indentation method [ASTM Standard E92 2003]. Five measurements were taken on the alloys. Nanohardness was measured using a CSM Instruments Nano Hardness Tester with a diamond Berkovich indenter with a linear loading/unloading rate of 100mN/min and maximum load of 50mN. The Nanohardness was calculated through the load/displacement curves and the Oliver and Pharr method [Oliver & Pharr 1992]. Five measurements were taken on the alloys.

3.4.10 Characterisation of SPS compacts

3.4.10.1 XRD analysis

The three elemental powders and ball-milled powder were analysed for their phase content using an X'PERT PRO Philips diffractometer. For the powder the XRD operated with CuKα radiation at 45 kV and 40 mA in the scanning range of 30–90° with a step size of 0.03° and a scan time of 400s per data point. For the compacts the XRD operated CuKα radiation at 45 kV and 40 mA in the scanning range of 5–70° with a step size of 0.03° and a scan time of 400 s per data point.

3.4.10.2 Scanning Electron Microscopy

The microstructure was observed using the field emission SEM (FE-SEM; FEI Inspect F) operated at 10 kV with a working distance 10 mm. Element mapping of elements was carried out using an integrated X-ray energy-dispersive attachment with an EDAX UTW detector.

3.4.10.3 Density

The densities of the sintered samples were studied using SEM images of the surface after thresholding the porosity using UTHSCSA Imagetool 3.0 software.

3.4.10.4 Measuring the grain structure

To measure the grains the sample had to be etched. The samples were dipped in an etching solution of 25 ml ethanol, 5 ml 1.0 M HCl and 1 g of $CuCl_2$ for 10 s and rinsed out with acetone to remove any excess etchant [Tang et al. 2008]. The samples were observed in the SEM and using UTHSCSA Imagetool 3.0 software the grains were measured.

3.4.10.5 Measuring the chromium oxide content

The chromium oxide content was measured using the optical images and UTHSCSA Imagetool 3.0 software. The oxide phase was threshold out and

measured as a percentage of the entire image to determine the amount of content present.

3.4.10.6 Microhardness and Nanohardness

Microhardness of the samples was measured using a Leco M-400-G hardness tester and the Vickers indentation method [ASTM Standard E92 2003]. Nanohardness was measured using a CSM Instruments Nano Hardness Tester with a diamond Berkovich indenter with a linear loading/unloading rate of 100mN/min and maximum load of 50mN. The Nanohardness was calculated through the load/displacement curves and the Oliver and Pharr method [Oliver & Pharr 1992]. Five measurements were taken on the alloys.

3.4.11 Tribological performance

The F75, F1537 and SPS alloy (sintered at 1075°C, with a dwell time of 10min and a pressure of 100 MPa) were formed into a 20mm x 3mm disc and tested for their tribological performance.

3.4.11.1 Alumina counterpiece

A 6mm diameter ball of alumina was supplied by Atlas Ball and Bearing, UK, for use in the wear test as the counterpart of the discs.

3.4.11.2 Wear test

Wear test was conducted upon CSM Instruments Tribometer. The discs were polished using silicon carbide paper from 120 to 4000P grading paper. The initial surface roughness was analysed using a ConScan surface profilometer. The average roughness (R_a) was measured at 0.015μm, 0.01μm and 0.01μm for the F75, F1537 and SPS alloys, which is lower than the 0.05μm maximum recommended by the Standard F732 [ASTM Standard F732 2006].

Three samples of each alloy were tested against the 6mm diameter alumina ball under the G133 and F732 standards [ASTM Standard G133 2002; ASTM Standard F732 2006]. The wear mode was a rotational motion with a 1.5mm

radius, linear speed of 0.04m/s and a normal load of 5N. Temperature set was 37°C with a humidity of 40%. The sliding distance was ~2.4km (250,000 laps). Both alloys and balls were cleaned with isopropanol before wear testing commenced. The lubricating fluid was 25% Bovine Serum with distilled water and 0.01% sodium azide. Serum was collected after testing and frozen for wear particle analysis. The total wear volume was measured through the wear profile. The wear profile was constructed using ConScan surface profilometer. Images of the wear track were taken using SEM (Hitachi S-3400N).

3.4.12 Wear particle analysis

The wear particles were analysed for the size and size distribution using Nanosight LM10-HS. 1ml of unfrozen serum collected fluid was diluted x100,000 using Pure Water (Rathburn Chemicals Ltd, Walkerburn) and measured. Serum analysis for metal element concentration was conducted using a high-resolution ICP-MS (Element2; Thermo Finnigan, Bremen, Germany). Acid oxidative digestion was used to digest the material within the serum for analysis, including the metallic nanoparticles, the proteins and other insoluble material. 0.5ml of extracted serum fluid was digested with 5ml of nitric acid (Super Purity Solvents grade, Romil) at 100°C for 240 minutes, using a dry heating block (DigiPrep, SCP Science, Quebec, Canada). After digestion, the remaining fluid is further diluted to 20ml ready for analysis. The concentrations of the metal elements are expressed in μg/l.

3.4.12.1 Wear particle shape

1ml of fluid from the frozen serum of the wear generation debris was placed upon a glass slide and sputter coated for 3mins with gold using a sputtering machine (Edwards sputter coater S 1 50B) to enable conduction of the sample for view using the SEM (JEOL JSM-6301F). The particles were characterised using digital image analysis software (SemAfore 5.21, JOEL (Skandinaviska) AB, Sweden) for their aspect ratio. Aspect ratio (AR) is a common measure of shape, which is the ratio of the major diameter (d_{max}) to the minor diameter

(d_{min}). The major diameter is the longest straight line that can be drawn between any two points on the outline. The minor diameter is the longest line perpendicular to the major diameter; AR is defined as:

$$AR = \frac{d_{max}}{d_{min}}$$

3.4.13 Metal element leaching

Test conducted under the ISO 10933-12 standard [ISO 10933]. The F75, F1537 and SPS alloy were placed in a beaker of 50ml of distilled water and placed in the incubator. At time intervals of 24h, 72h and 148h (±1h), 5ml of fluid was taken out for elemental content analysis.

3.4.13.1 Metal element content study

The 5ml fluid removed from the beaker was analysed for its elemental content of Co, Cr and Mo. The metal element concentration was conducted using a high-resolution ICP-MS (Element2; Thermo Finnigan, Bremen, Germany). The fluid is diluted to 20ml for analysis and the concentration of metal elements is determined and expressed in μg/l.

3.4.13.2 Microstructure characterisation after leaching study

The three alloys were examined for their microstructure after leaching experiments using SEM (Hitachi S-3400N) and elemental analysis of the surface was carried out using the integrated X-ray energy-dispersive attachment with an EDAX UTW detector.

Chapter 4

Processing, Microstructure and Phase Analysis

4.1 Introduction

This section gives an insight into the actual orthopaedic alloy used in the bearing surfaces of the hip replacement. Heat treatment upon the orthopaedic alloy is investigated to determine the effects it has on the microstructure and phase analysis. Two commercial medical grade alloys are also characterised to determine their microstructure and phases present. A novel processing technique is investigated to determine its feasibility to form cobalt based alloys and to identify and explained how the microstructure has formed.

4.2 Investigating the current orthopaedic alloys

Alloys used in clinical applications may be slightly different to the standard alloys available in the market. Therefore, evaluating the alloy used in an actual orthopaedic device will enable an understanding of the alloy in terms of its microstructure and compositional analysis.

4.2.1 Microstructure and Medical Grade

The microstructure was analysed using SEM and EDX analysis was used to determine which medical grade was supplied.

The microstructure of the supplied as-cast Co-Cr-Mo alloy (Figure 4.1) consists of a solid matrix (dark background) and secondary phases (light phases). There are also tiny black dots scattered within the microstructure, these are carbides.

The solid matrix is a soft ductile Co-based matrix. As Co has different crystalline structure, HCP and FCC depending upon the casting conditions

either structure can form. Usually, the FCC structure is more favourable due to the carbides present. The Cr and Mo elements are HCP stabilisers, but they form carbides and secondary phases and so have little influence on the crystal structure of the Co matrix. Different properties are exhibited depending on the crystal structure; the HCP structure with its lower slip systems shows a more brittle orientated structure whereas the FCC is more ductile.

The secondary phases are inter-metallic phases. Carbides are complex hard phases rich in Cr and Mo. They act as blockers in the movement of dislocations to limit slip and plastic flow. Their size and shape depends upon the cooling rate and changes in the chemistry. They also affect the mechanical properties of the alloy with their presence in grains and at grain boundaries. The grain boundary is strengthened by limiting grain boundary migration through either the carbide particles preventing sliding action or in high carbide regions a grain boundary skeletal network forms to support the load and hindering sliding action.

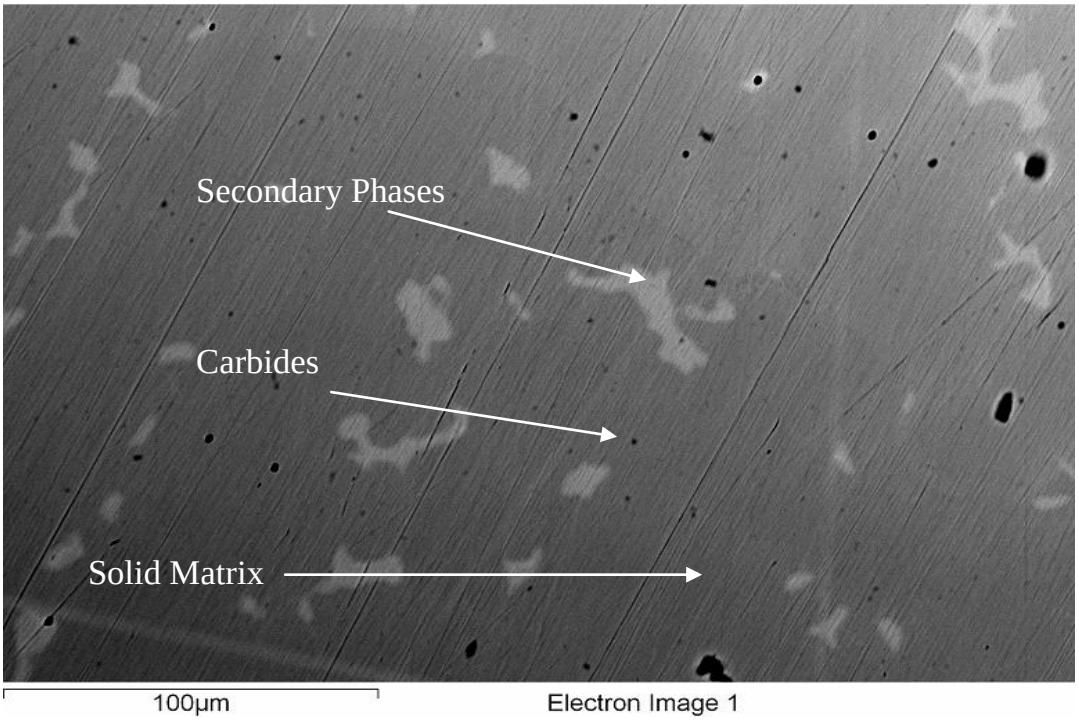

Figure 4.1: Microstructure of the as-cast supplied Co-Cr-Mo orthopaedic alloy, indicated in the diagram are the solid matrix, carbides and the secondary phases.

Subsequently, EDX analysis was carried out on various positions on the alloy via point and box analysis (Figure 4.2).

Table 4.1: Average chemical composition of the elements analysed via EDX analysis of the as-cast supplied alloy

Element	Average Percentage (%)
Co	65.0
Cr	29.4
Mo	5.6

Comparing Table 4.1 values with the composition of the cobalt-based surgical alloys (Table 4.2), it shows that the average percentages of the Co, Cr and Mo elements lie within the range of the surgical graded alloy F75 alloy. Hence, it can be assumed that the supplied as-cast alloy is the F75 Co-Cr-Mo alloy, with a chemical composition of Co28Cr6Mo. Also, the microstructure (Figure 4.1) exhibits the same characteristics found in the as cast F75 alloy [ASTM Standard F75 1998]. This will help when comparing properties for subsequent work.

Table 4.2: Composition of Cobalt base surgical implant alloys [Davis 2001]

ASTM Specification	Composition (wt%)						
	Co	Cr	Ni	Mo	Fe	C	Other
F75	Bal.	27-30	1	5-7	0.75	0.35	
F90	Bal.	19-21	9.0-11.0		3 (max)	0.05-0.15	14-16 W
F562	Bal.	19-21	33-37	9-10.5	1 (max)	0.025 (max)	1 Ti (max)

4.2.2 Melting point analysis

To investigate the effects of heat treatment upon the F75 alloy, firstly the melting point analysis was required to determine a suitable temperature range to study the heat treatment. The work by Harris and Sikkenga which stated the melting occurred between 1377-1402°C was used as the reference [Harris & Sikkenga 1999].

The melting point analysis was determined from the state at which melting had occurred from a macro point of view, which when observed after heating was in the 1350°C sample. Subsequently, looking at the SEM images shown in Figure 4.3 one can determined the melting point at a micro point of view between 1375-1400°C.

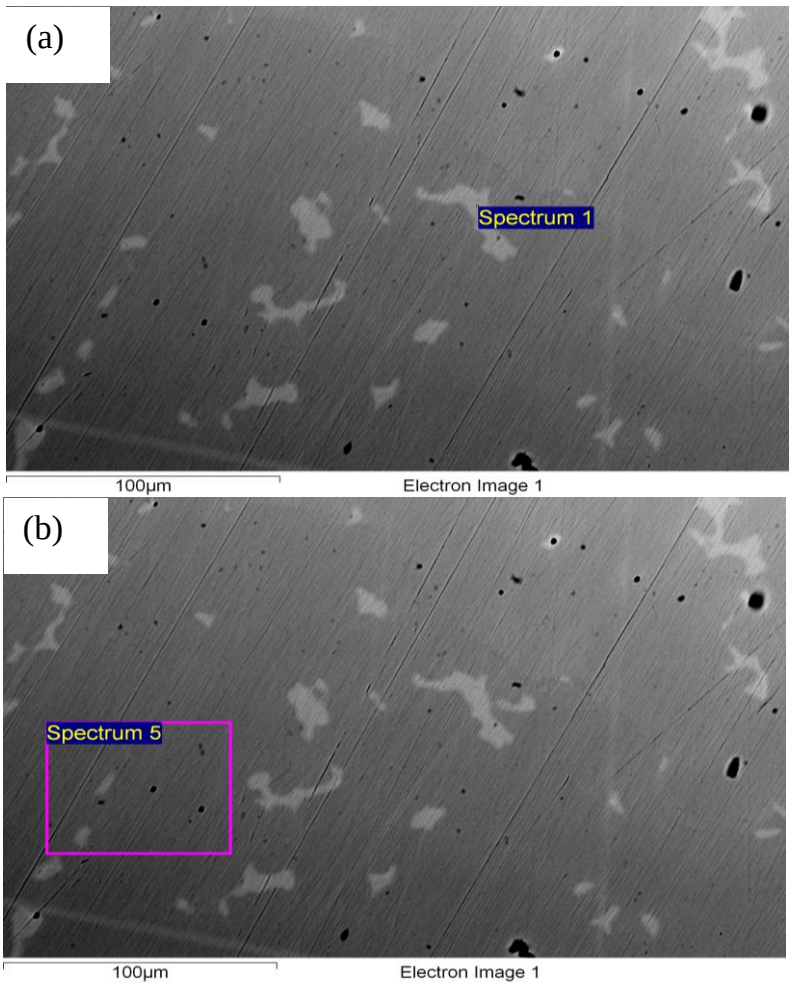

Figure 4.2: EDX analysis of the as-cast supplied alloy using point (a) and box (b) analysis.

From Figure 4.3a, the image shows the matrix to be intact and the secondary phases still present. Porosity voids begin to appear in the matrix represented by the dark dots, indicating that point melting is occurring in certain regions. Carbides have disappeared and the secondary phases have become stretched and many have disappeared. But an increase of 25°C (Figure 4.3b), the matrix and the secondary phases have become highly distorted and damaged and larger voids have begun to appear. The secondary phases have significantly reduced in size and many have been plucked out either during the polishing process or due to the heating. No carbides are present in the structure. With further investigation into this work one could narrow the melting point range even further.

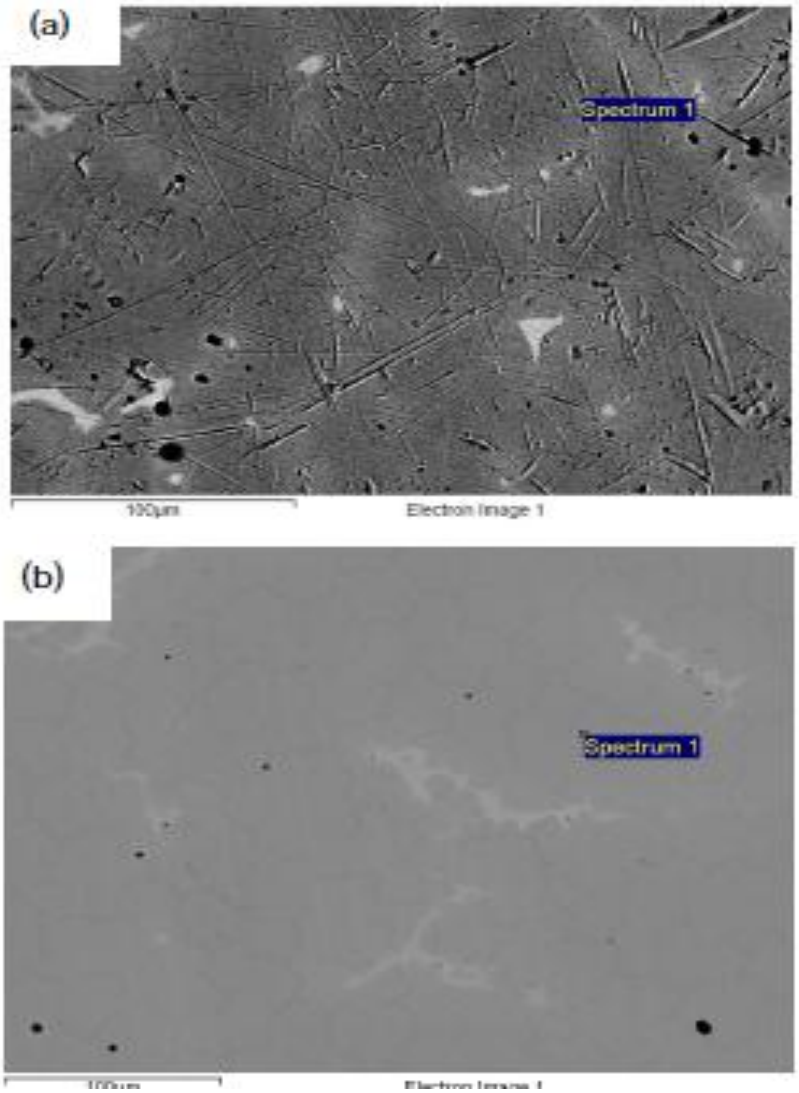

Figure 4.3: SEM images of (a) 1375°C and (b) 1400°C heat treated as-cast supplied annealed alloy

4.2.3 Heat treatment

Once the melting point was determined this gave a range of heat treatment values to investigate. The range 800-1200°C at intervals of 100°C was chosen as the microstructures of 1300°C and 1350°C had no significant changes. Two cooling methods were applied, one annealing and the other normalising.

Observing the optical images (Figure 4.4) of the annealed alloy, it can be seen that the number of carbides increases with temperature until 1100°C and suddenly decreases significantly at 1200°C. From ambient temperature to 1000°C (Figure 4.4a-d) the carbide content increases gradually and a rapid increase can be seen in Figure 4.4e. The maximum number of carbides in the image is seen at 1100°C. The secondary phases do not really change much in the images, but in Figure 4.4f at 1200°C the secondary phases are significantly reduced. The solid matrix does not show any distortion or the formation of voids as seen in Figure 4.3.

Observing the optical images (Figure 4.5) of the normalised heat treated alloy, shows no significant changes in the carbide content. The carbide content remains fairly stable with the increasing temperature. The number of secondary phases has increased in 1100°C (Figure 4.5e), but decrease again in 1200°C (Figure 4.5f).

Relating these observations of the heat treated alloys with the carbide content (Figure 4.6 and Figure 4.7), it can be seen they are the similar. The annealed alloy (Figure 4.6) carbide content gradually increases from 0.09% at ambient temperature to maximum of 0.58% at 1100°C. Suddenly, the carbide content decreases to its lowest of 0.05%. The carbide content (Figure 4.7) in the normalised heat treated alloy indicate the carbide content increases from ambient temperature of 0.26% but then remains fairly constant to maximum of 0.37%. The carbide content remain stable at an average 0.35%.

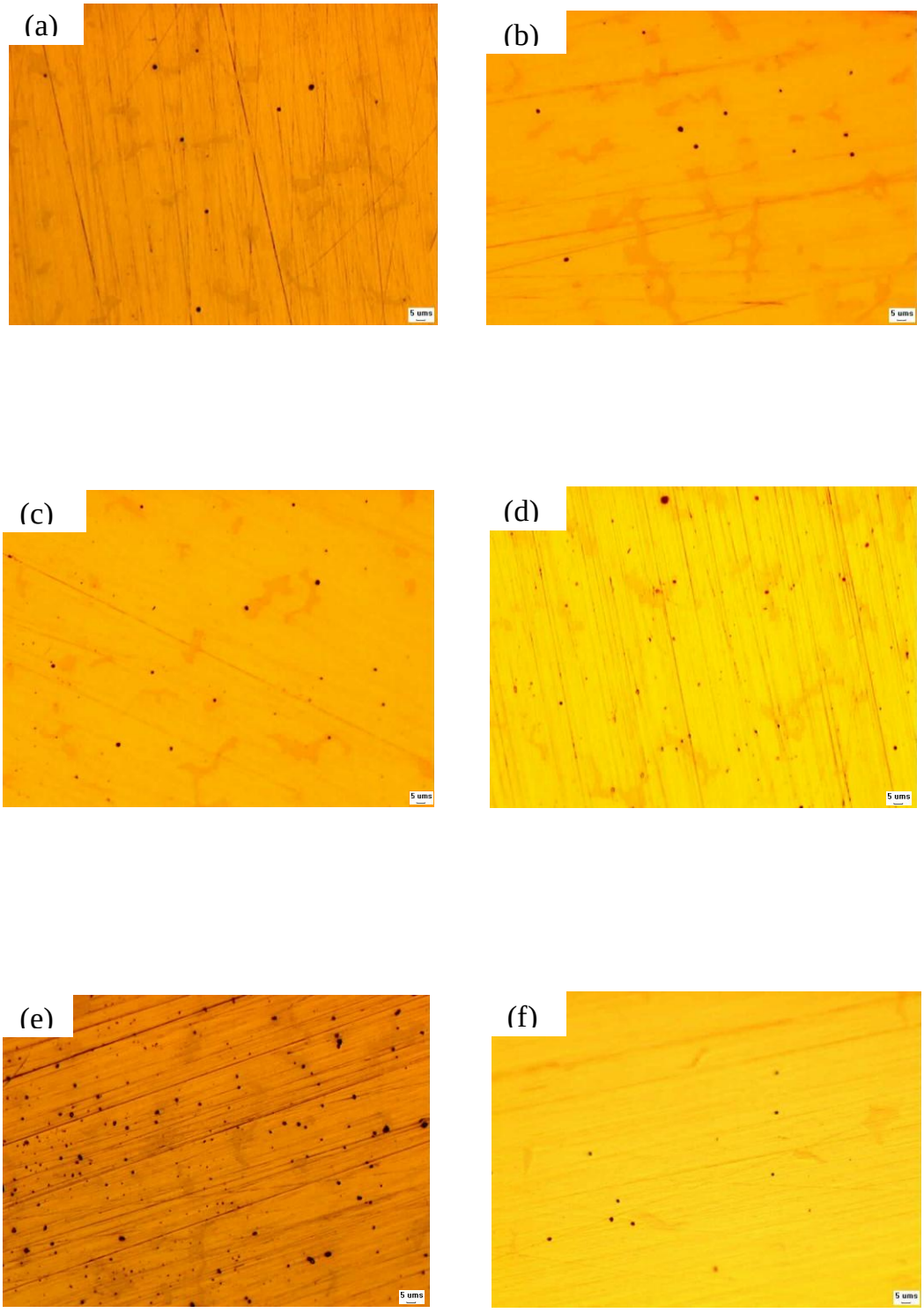

Figure 4.4: Optical Images of the (a) ambient temperature, (b) 800°C, (c) 900°C, (d) 1000°C, (e) 1100°C, (f) 1200°C heat treated via annealing of as-cast supplied F75 alloy

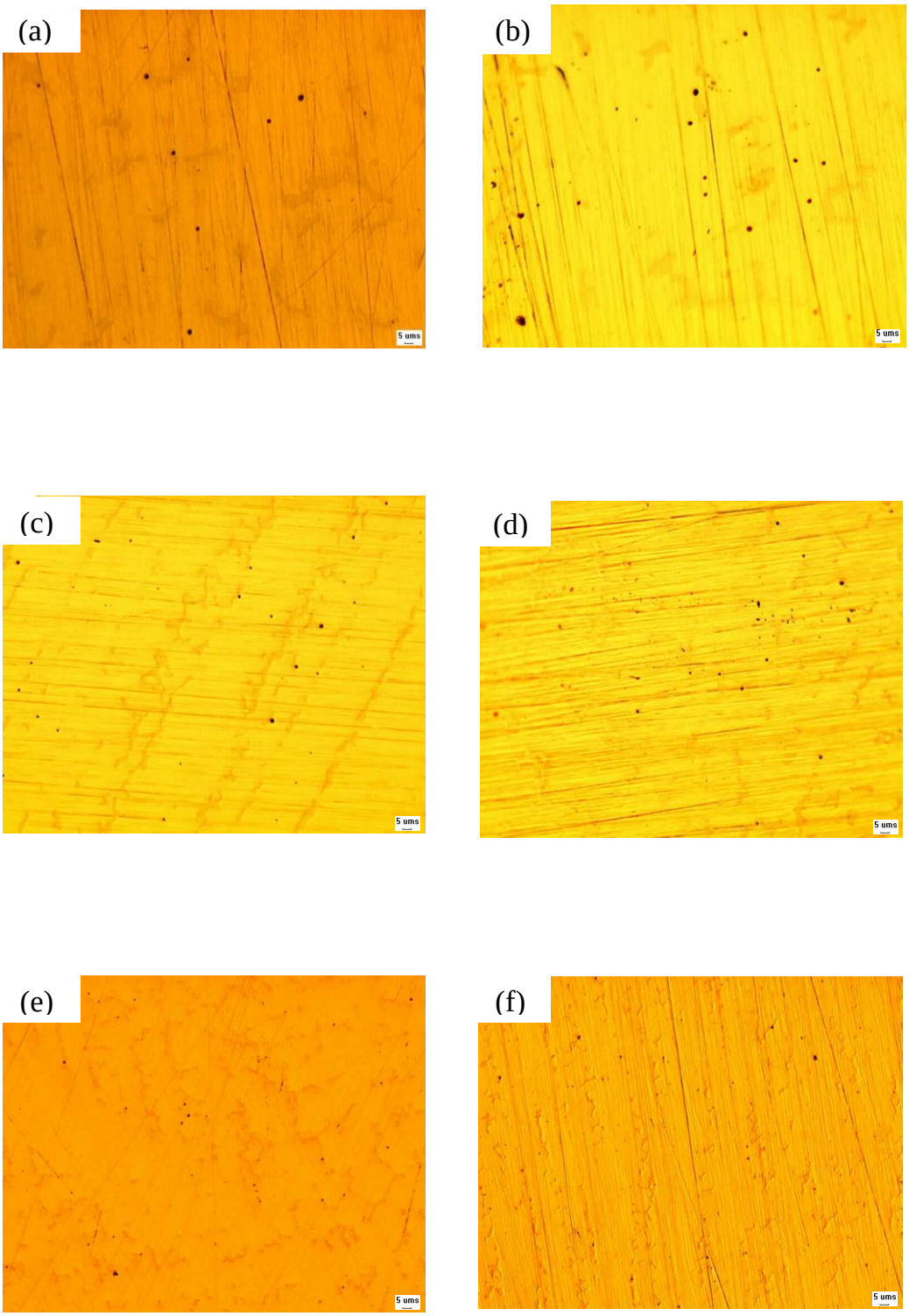

Figure 4.5: Optical Images of the (a) ambient temperature, (b) 800°C, (c) 900°C, (d) 1000°C, (e) 1100°C, (f) 1200°C heat treated via normalising of as-cast supplied F75 alloy

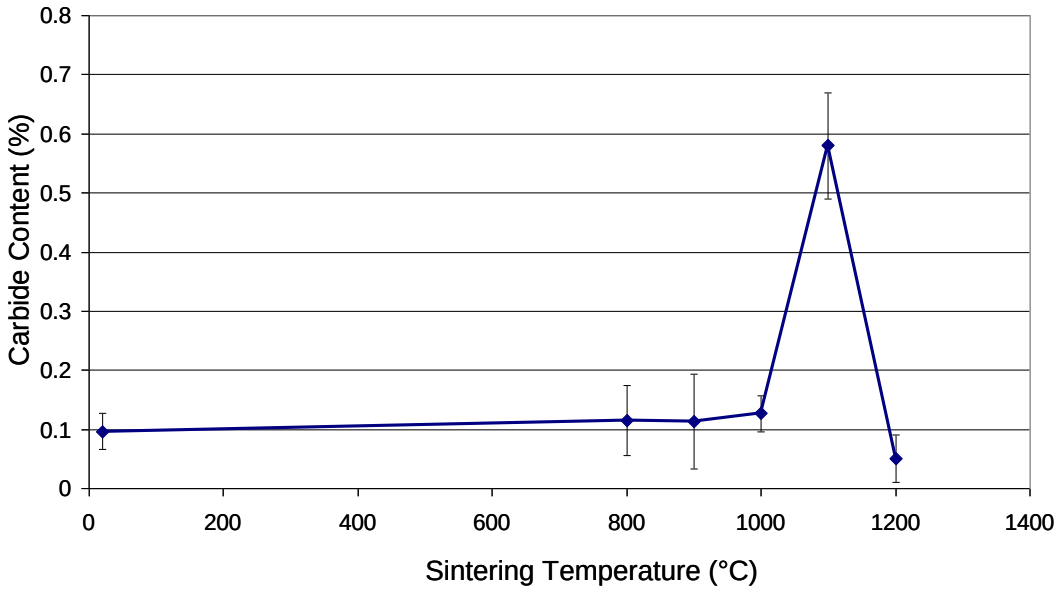

Figure 4.6: Temperature against carbide content of annealed heat treated as-cast supplied alloy, with error bars plotted to represent the standard deviation

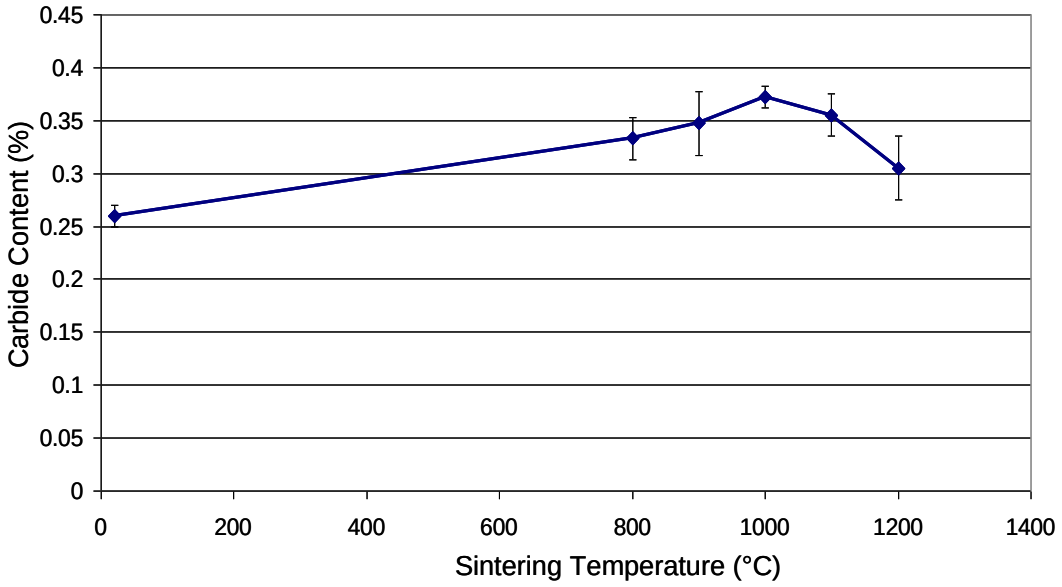

Figure 4.7: Temperature against carbide content of normalised heat treated as-cast supplied alloy, with error bars plotted to represent the standard deviation alloy

The annealed heat treated alloy shows the classic case of carbide dissolution [Clemow & Daniell 1979]. It is known that heat treatment temperatures above 1160°C, show a significant loss of carbide content as the carbides are dissolved into the matrix. The normalised heat treatment (Figure 4.7) results contrast the annealing study (Figure 4.6) and other studies where carbide content changes with temperature [Caudillo et al. 2001]. It can be assumed that the cooling method in air has caused no carbide increase or dissolution and no significant changes in the microstructure. The normalising treatment has shown to produce scale on the surface due to the higher oxygen content. This scale has known to consist of a combination of cobalt oxide and chromium oxide [El Dahshan et al. 1975]. It has been known that chromium oxide is a protector against corrosion resistance, but it may also provide additional protection against microstructural changes usually affected by heat. Therefore, the changes in the microstructure usually occur in the cooling period and not in the heat period.

4.2.4 XRD Analysis

The as cast (Figure 4.7a) x-ray diffraction peaks shows the presence of precipitates found in the Co matrix. The precipitate identified are σ phase, the $M_{23}C_6$ and M_6C-$M_{12}C$ carbides. The σ phase and the $M_{23}C_6$ phases are the most common phases found in the F75 alloy [Rosenthal et al. 2010]. The σ phase usually occurs in the alloy with high amounts of chromium and has an approximate composition of Co:Cr [Davis 2001]. The $M_{23}C_6$ is the most common carbide found in cobalt based alloys. It forms from the metastable σ phase transforming into the $M_{23}C_6$ carbide at temperatures below 1150°C [Rosenthal et al. 2010].

The M_6C-$M_{12}C$ is not that commonly found and rarely shows up in the XRD of the F75 alloy. But in other cobalt based alloys it shows up more regularly [Jiang et al. 1999]. This phase usually occurs in alloys with high molybdenum or tungsten content (>6%). The formation is determined by this high

percentage known as the "M_6C rule" [Sims et al. 1972], in this case as the molybdenum content of F75 alloy is lower than 6% (Table 4.2), the carbides are considered to occur due to the segregation of the molybdenum in certain regions to form the M_6C carbide [Yang et al. 2001]. The M_6C and the $M_{12}C$ carbides have very similar crystal structures and so overlap in their diffraction peaks. These results agree with the results in other studies [Weeton & Signorelli 1955; Youdelis & Kwon 1983]. The secondary phases indicated in Figure 4.1 can be attributed to σ phase and the black tiny dots attributed to the $M_{23}C_6$ and M_6C-$M_{12}C$ carbides.

Increasing the temperature to 800°C (Figure 4.8b) shows presence of the FCC Co (γ) phase, the $M_{23}C_6$ and the σ phase. The M_6C-$M_{12}C$ carbide peak has disappeared. This occurs as the M_6C-$M_{12}C$ have been known to transforms into the more favourable $M_{23}C_6$ carbides during the cooling of the alloy [Ramirez et al. 2002]. These results are similar to the study by Mineta et al. that showed, increasing the heat temperatures causes the disappearance of most of the other phases and only $M_{23}C_6$ and σ phase remain [Mineta et al. 2010]. The γ phase represents the matrix of the alloy.

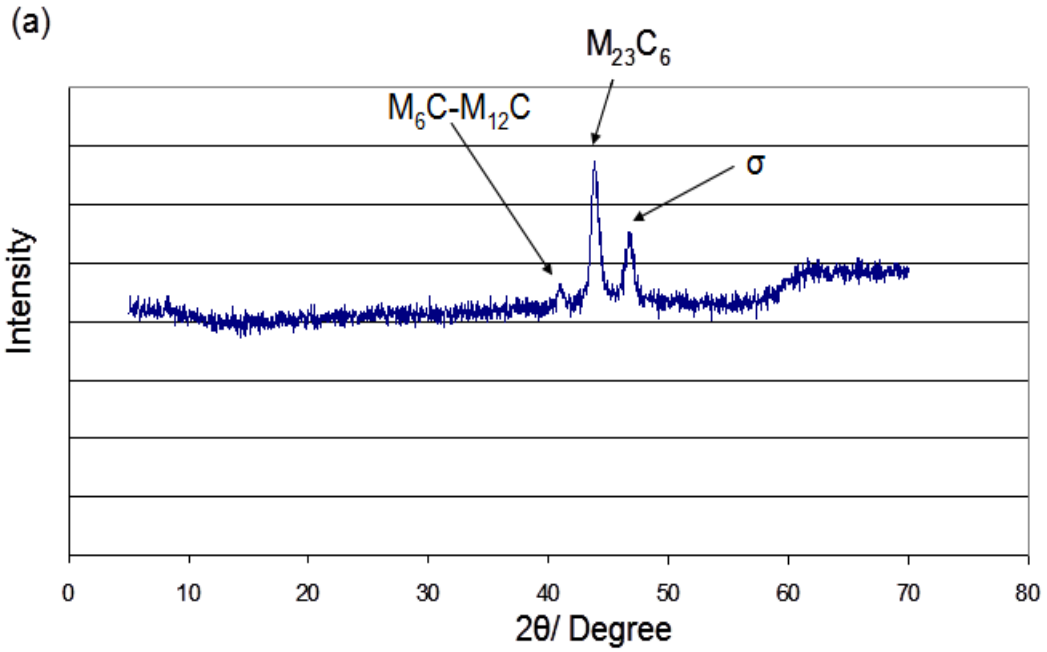

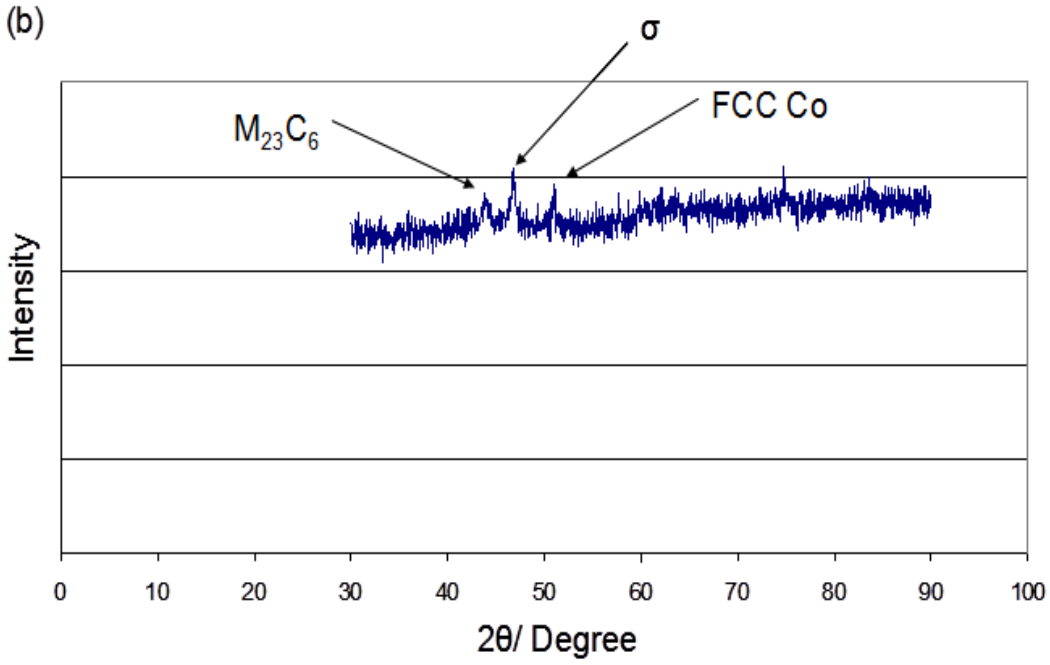
(b)
σ
FCC Co
$M_{23}C_6$
Intensity
0
10
20
30
40
50
60
70
80
90
100
2θ/ Degree

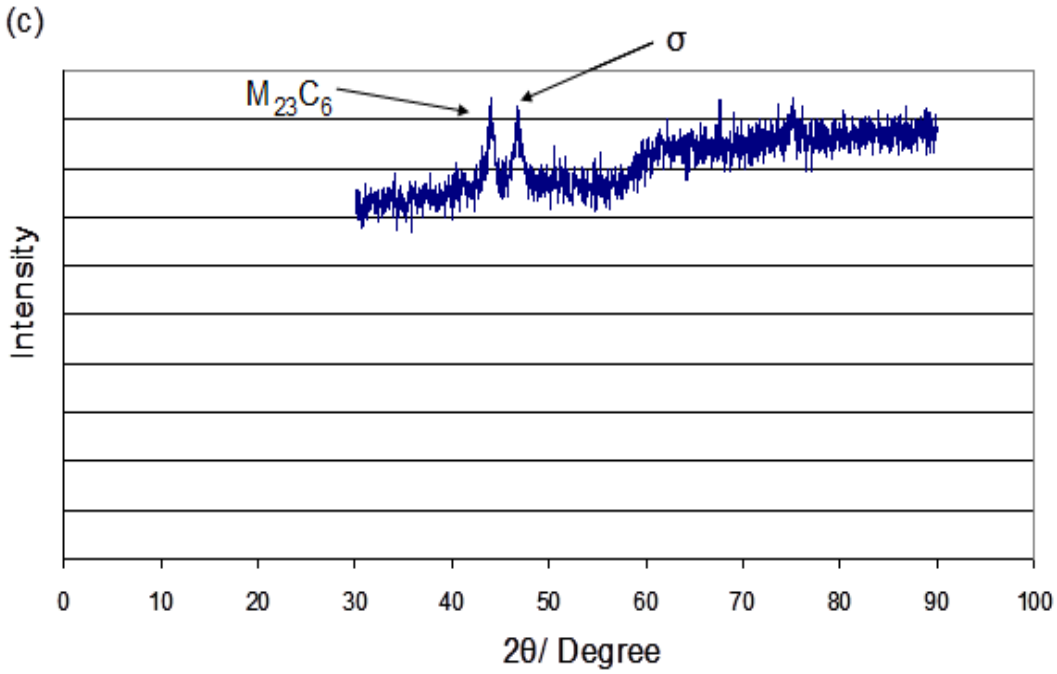
(c)
σ
$M_{23}C_6$
Intensity
0
10
20
30
40
50
60
70
80
90
100
2θ/ Degree

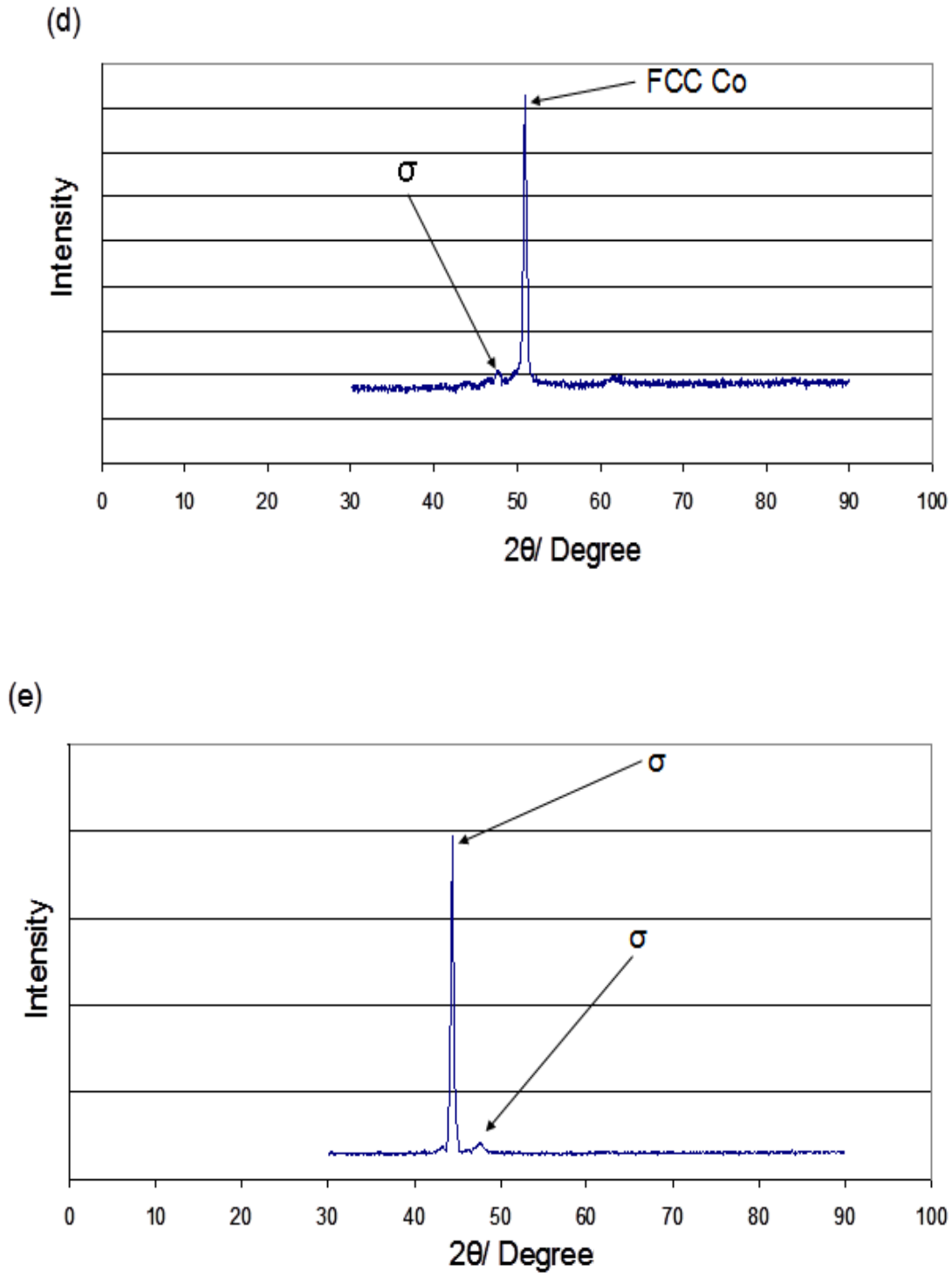

Figure 4.8: X-ray diffraction pattern of (a) ambient (b) 800°C (c) 1000°C (d) 1375°C (e) 1400°C Co-Cr-Mo as-cast supplied heat treated alloy

Further increasing of the temperature to 1000°C (Figure 4.8c), shows only the presence of $M_{23}C_6$ and the σ phases. In Figure 4.6, it has shown that the carbide content increases, therefore the amount of $M_{23}C_6$ has increased. This occurs from the transformation of the σ phase into the $M_{23}C_6$ carbides as the increased carbon reacts with small σ phases to form the favourable $M_{23}C_6$ precipitate [Rosenthal et al. 2010].

Analysis of the x-ray diffraction of the onset of melting (1375°C) (Figure 4.8d) indicates the presence of σ and the γ phases. The presence of carbides is no more, due to the dissolution of these phases into the matrix at 1160°C [Clemow & Daniell 1979]. Figure 4.6, shows the reduction in the carbide content attributed to this phenomenon. At higher heating rates it has been suggested that $M_{23}C_6$ carbides can transform into σ phase [Clemow & Daniell 1979]. However, the heating rate used in this experiment was much lower. The σ phase remains as is more stable at the higher temperature above 1150°C and cannot be transformed with the lack of carbon present [Ramirez et al. 2002]. As no carbide phases are present the γ phase is not being overshadowed and can be distinguished, also the onset of melting may have unstabilised the matrix causing the peaks to become present.

At 1400°C (Figure 4.8e), the only phase present is the σ phase as the carbides have undergone dissolution and the γ phase may have stabilised. As mentioned the more higher the temperature towards complete melting the σ phase remains fairly stable. The precipitates present within the Co matrix are ultimately dependent upon the carbide content below the dissolution temperature.

4.3 A new method to manufacture F75 orthopaedic alloys

This section describes a new method used to manufacture the F75 orthopaedic alloy using nanopowders and SPS. The current research work upon cobalt based alloys for orthopaedics has not produced any significant effects upon the properties of the alloy to enhance its reputation as a bearing surface material. Here, I have investigated the powder processing technique to produce the alloy using electrical current technology of heating the powders.

The images of the individual powders (Co, Cr, Mo) and ball milled powders are shown in Figure 4.9. The Co and Mo powders are shown to be in the nanoscale, the Cr powder is in a much larger scale. This may due to the agglomerates that have formed. The ball milled powder (Figure 4.9d) shows a thorough mixing of the powders, but there are still some agglomerates present. The peaks of the elemental phases are shown in Figure 4.10. In the case of Co, oxide peaks are also identified; this is probably because of surface coatings on the powder in order to reduce its oxidation and enable safe handling. Ball milled powder showed no significant contamination as the peak identified only came from the individual element powders (Figure 4.10).

SPS has resulted in the formation of new phases in the bulk material and these are identified in Figure 4.12. The phases identified in the SPS alloy differ from the phases in the as-cast alloy (Figure 4.10a). The SPS alloy shows the presence of FCC Co, Cr, Mo, HCP Co and Cr_2O_3. The microstructure of the SPS compacts is different from that of typical cast or wrought alloys. The conventional methods form a Co matrix with carbides distributed randomly [ASTM Standard F75 1998], but the SPS microstructure (Figure 4.11) consists of a Co matrix with Cr- and Mo-rich regions. Also, from Figures 4.12 and 4.12, it is clear that the Cr in association with O forms Cr_2O_3 in the microstructure. The necessary O could have come from two sources: from Co powder or from the atmosphere during mixing. The Co matrix has both crystal structures of Co, the FCC and HCP. The FCC is present from the Co powder.

HCP Co structure has been formed because of the martensitic transformation [Montero-Ocampo et al. 2002]. Also, Cr and Mo are known to be HCP stabilisers. No carbides are present in the microstructure, which corresponds well with the XRD peaks identified in Figure 4.10.

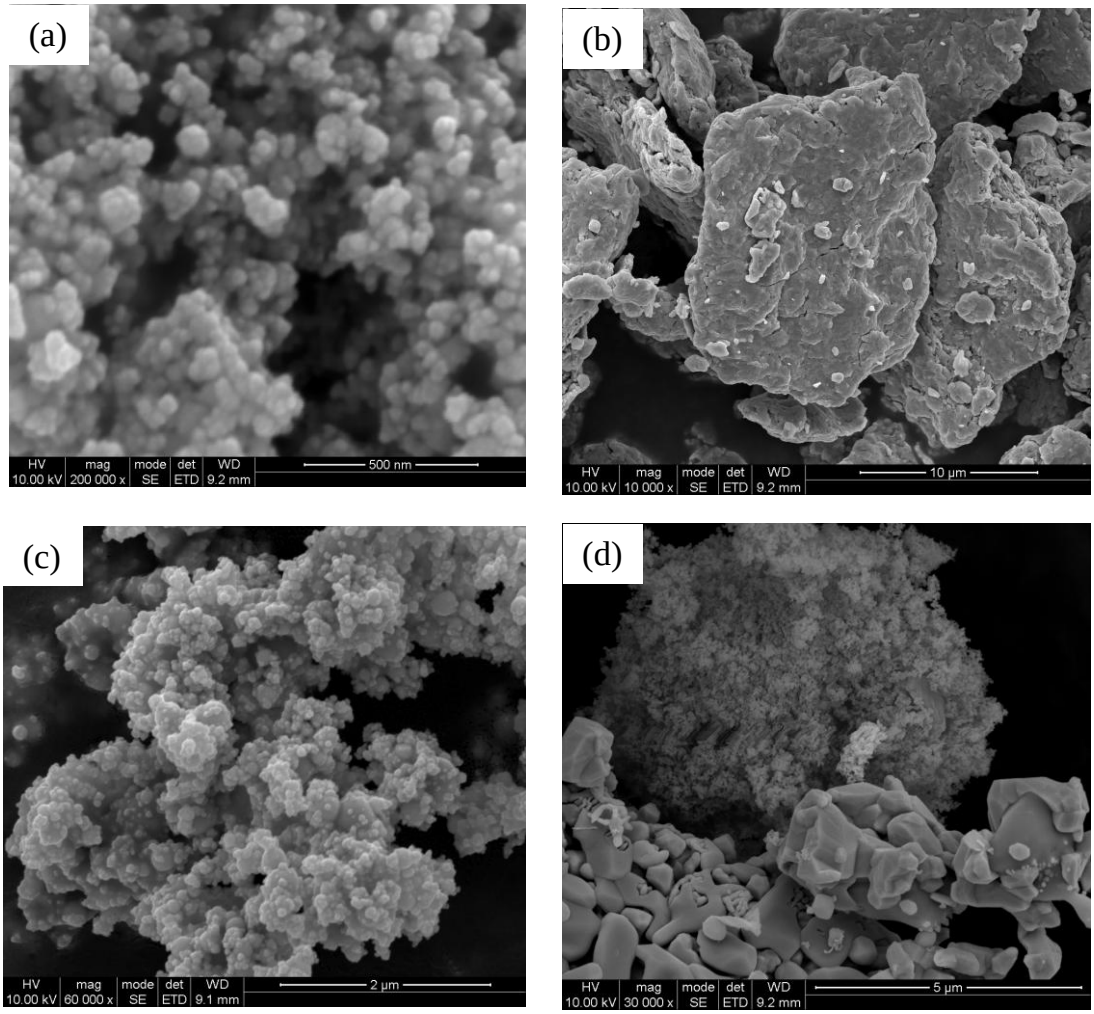

Figure 4.9: SEM images of powder: (a) cobalt, (b), chromium, (c) molybdenum and (d) after ball milling of the three elemental powders together

Table 4.3: Details of ball milled SPS sample processing conditions and density

Sintering Temperature /°C	Dwell Time /min	Pressure /MPa	Density (%)
1050	10	75	99.3
1050	10	100	99.2
1075	10	100	99.5
1100	10	75	98.3
1150	3	75	98.1
1175	3	75	98.1

All ball-milled sintered compacts (Table 4.3) were near-full density (>98.1%). The compacts had very limited porosity, which is one of the advantages of this processing technique. Above 1075°C, melting occurred, whereby small droplets appeared at the rim of the die after sintering, which reduced the relative density to 98%. During SPS, the powder particles are heated by electric discharge action through the electrical current and because of the high pressures and rapid cooling, the molten mix is forced outward, forming droplets [Tang et al. 2008]. The forced out material would leave gaps within the microstructure of the alloy where voids will form. These voids will increase the porosity and this can reduce the strengths of the alloy in terms of its mechanical properties, which will be analysed in Chapter 5. Also, for hip replacement devices the bearing surfaces where these alloys are mainly used need to be fully dense otherwise they may not be adequate for their function.

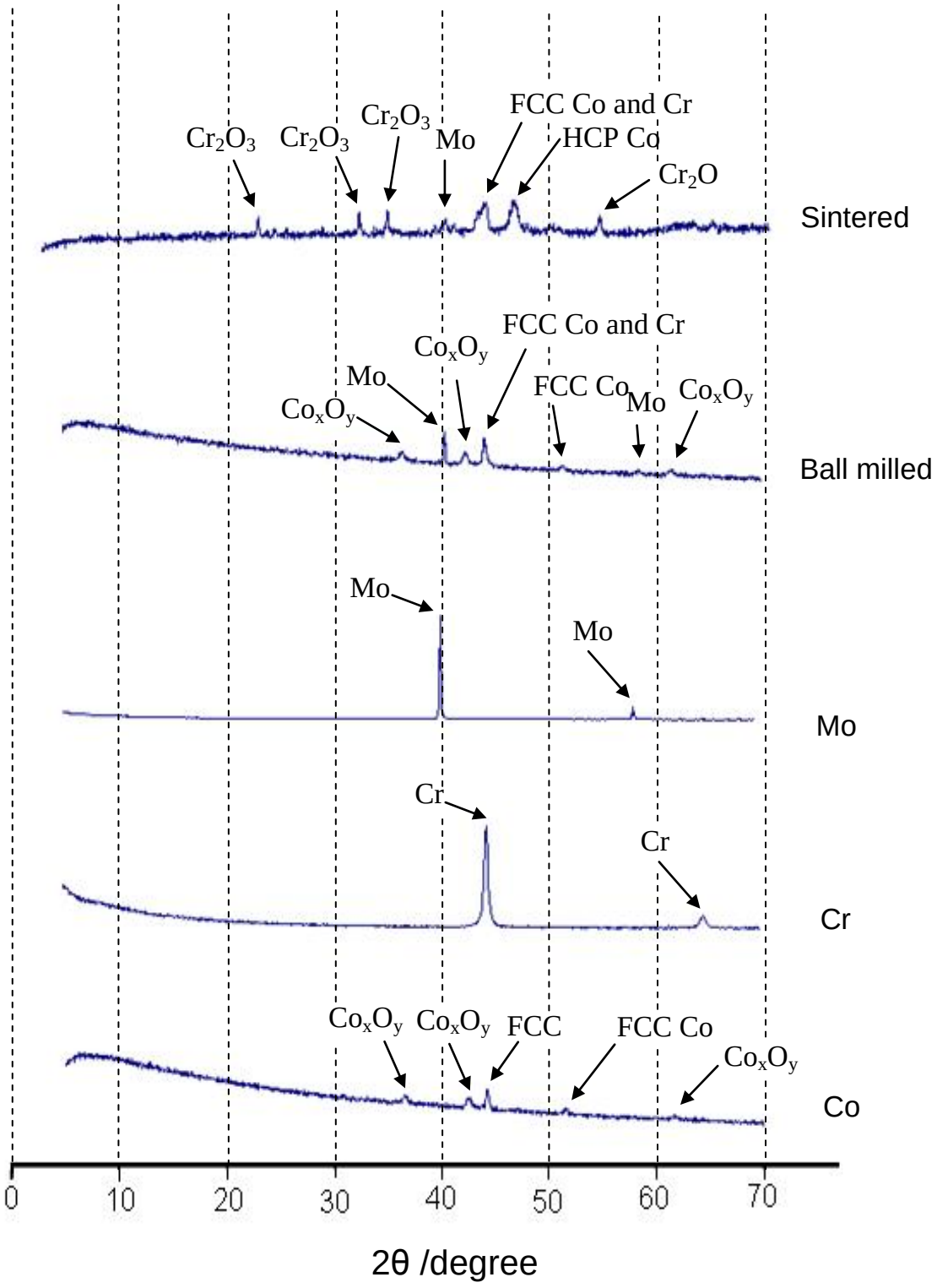

Figure 4.10: XRD results of the as received, ball milled and sintered powders. Indicated are the various phases present of the powders and compact.

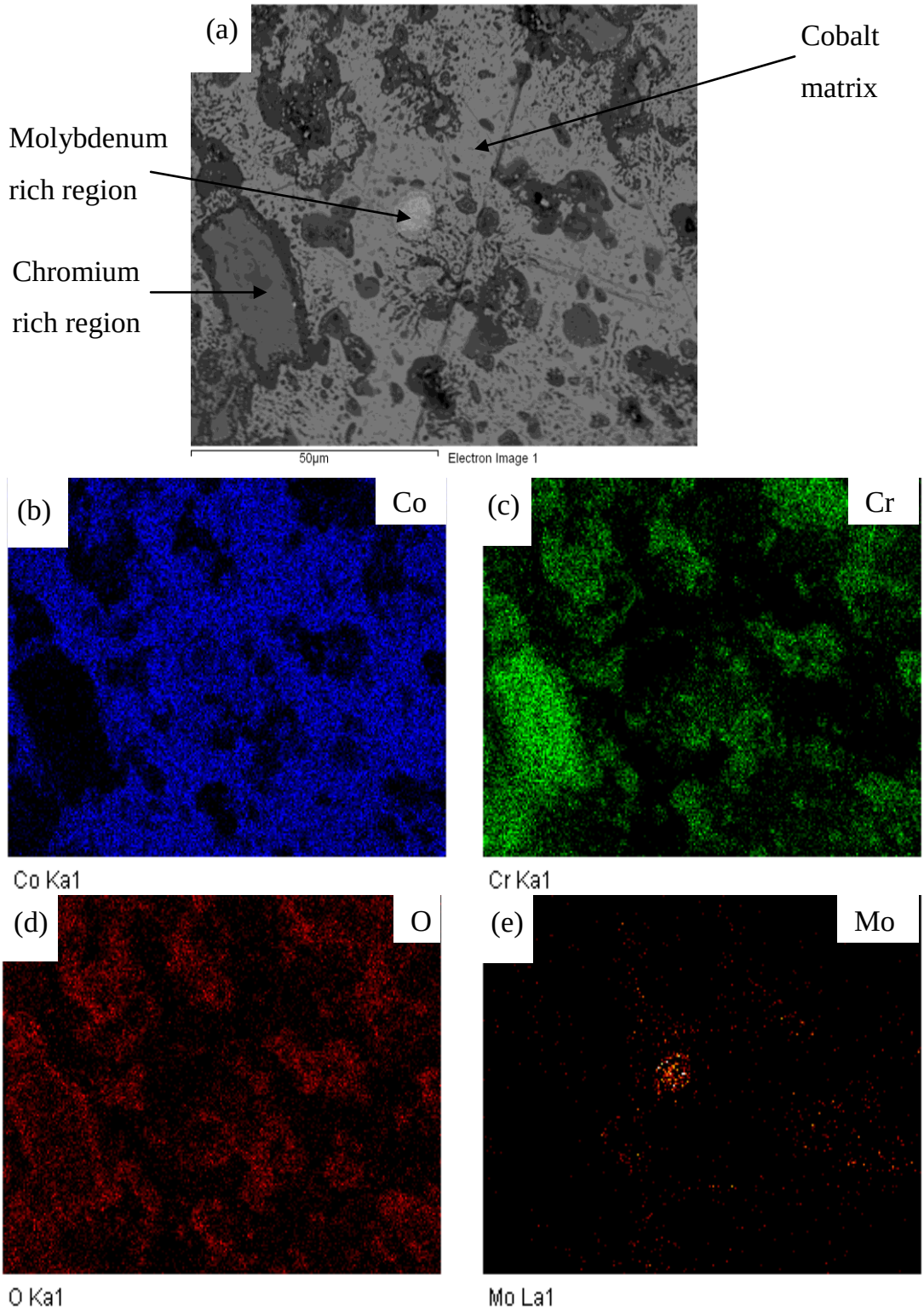

Figure 4.11: (a) Typical microstructure with labelled phases prepared by ball milling of SPS compact and heated to 1075°C with (b) Co, (c) Cr, (d) O and (e) Mo distribution highlighted

4.4 Mechanism for the formation of Chromium Oxide in the microstructure

It is well known that the surface of components can be treated to produce chromium oxide as a protective coating. The chromium reacts with oxygen and forms the oxide which is one of the hardest oxides, and has excellent tribological properties as well. It is a ceramic that has high corrosion and wear resistance with a low coefficient of friction. Currently, to have chromium oxide present within the microstructure, the chromium oxide needs to be added as a dispersion to enhance the strength of the alloy [Riu et al. 2000]. The SPS route requires no added material to form the chromium oxide within the structure of the F75 alloy.

4.4.1 Phases

The three elemental powders were analysed for their phases (Figure 4.12). The Cr and Mo powders show only peaks for their expected body centred cubic element phase. The Co powder shows the peaks for FCC Co and CoO (cobalt II oxide) peaks. The FCC Co peaks are present and not the more thermodynamically stable HCP Co due to the FCC phase being the more stable phase in nanoparticles, whereas the HCP phase is more stable in larger particles [Petit et al. 1999]. The CoO peak is present due to the partial passivation of the powders to enable their safer handling. Otherwise, this volatile powder in the presence of air can be dangerous due to its high reactivity with oxygen. The sintered samples show the presence of all the peaks from the powders and also two other peaks: HCP Co and Cr_2O_3.

The HCP Co formation occurs due to a martensitic transformation [Lopez & Saldivar-Garcia 2008]. This phase transformation is difficult to accomplish. The martensitic transformation of Co occurs due to cooling from a critical temperature. In pure Co, the critical cooling transformation temperature is below 417ºC [Montero-Ocampo et al. 2002]. With the addition of Cr and Mo

the temperature increases [Sims 1969]. A study by Weeton and Signorelli has suggested that this critical cooling temperature ranges from 965 to 1230ºC [Weeton & Signorelli 1955]. This range coincides with the operating temperature used in this investigation. Certain elements such as Cr and Mo are HCP stabilisers, whereas carbides are FCC stabilizers. As no carbides were detected in our samples, the production of the HCP phase is favoured by increasing stability [Sullivan et al. 1970].

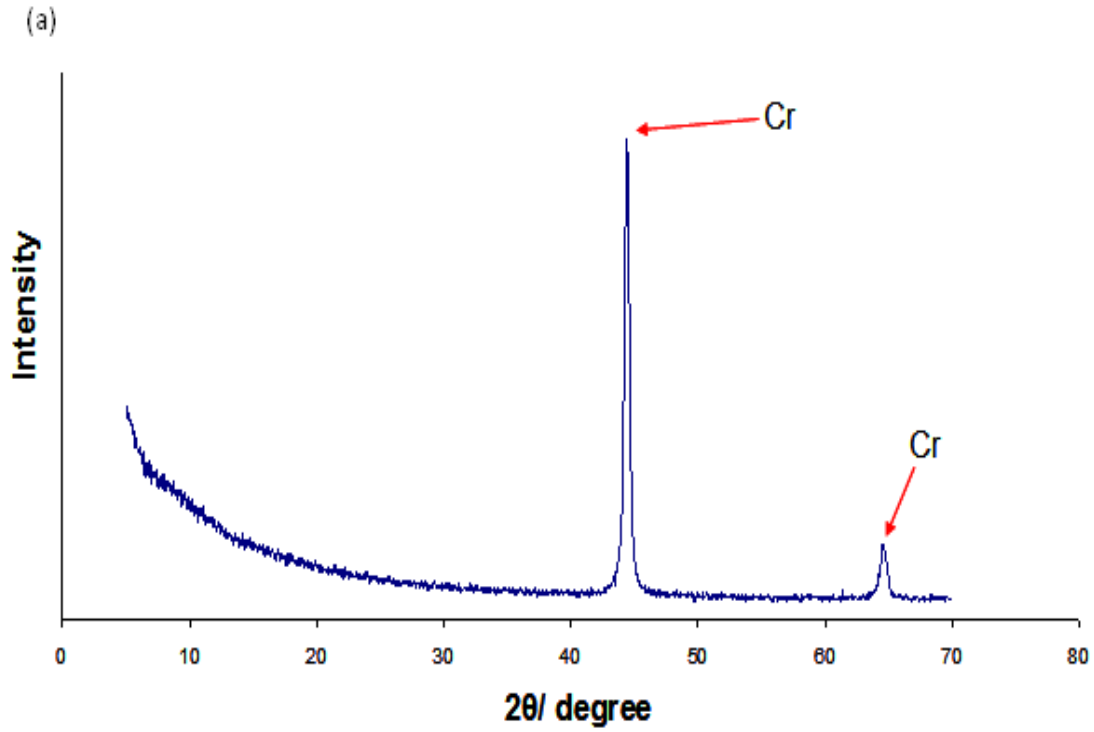

(b)

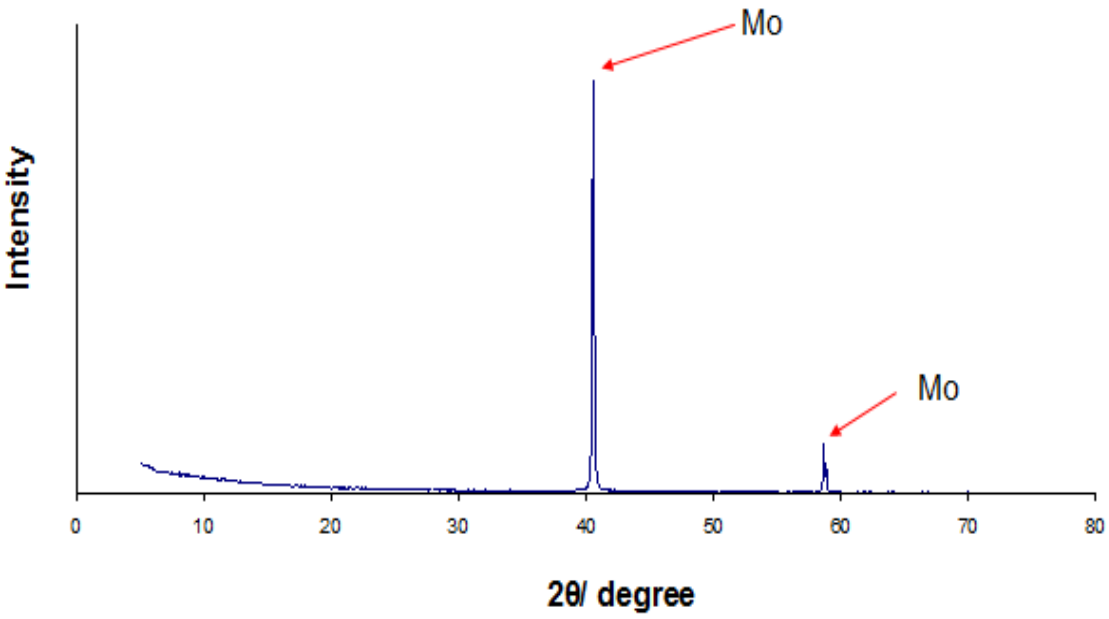
Mo
Mo
Intensity
0
10
20
30
40
50
60
70
80
2θ/ degree

(c)

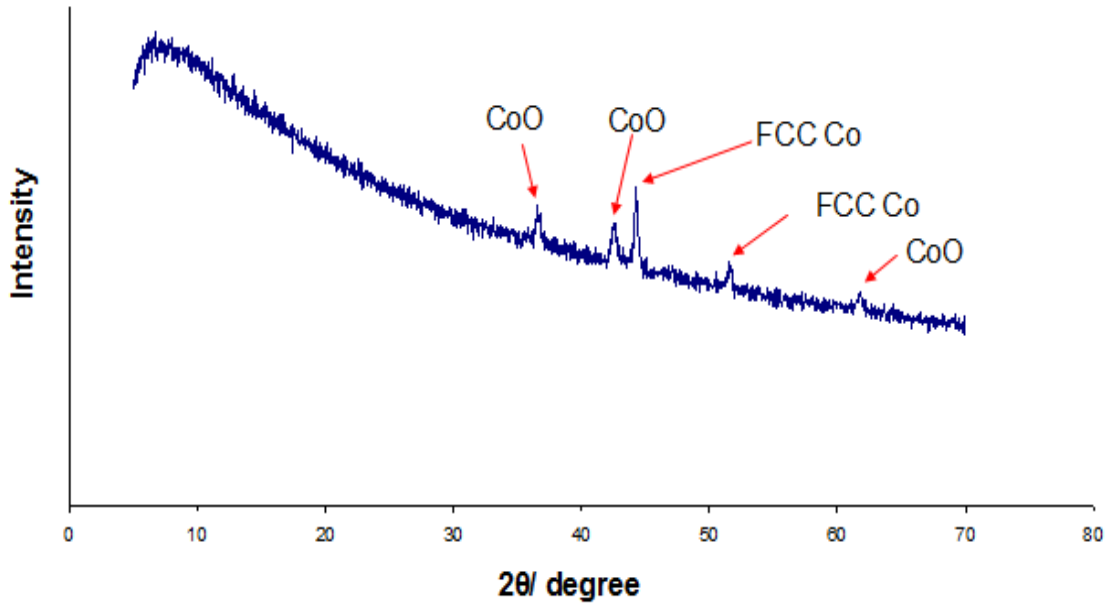
CoO
CoO
FCC Co
FCC Co
CoO
Intensity
0
10
20
30
40
50
60
70
80
2θ/ degree

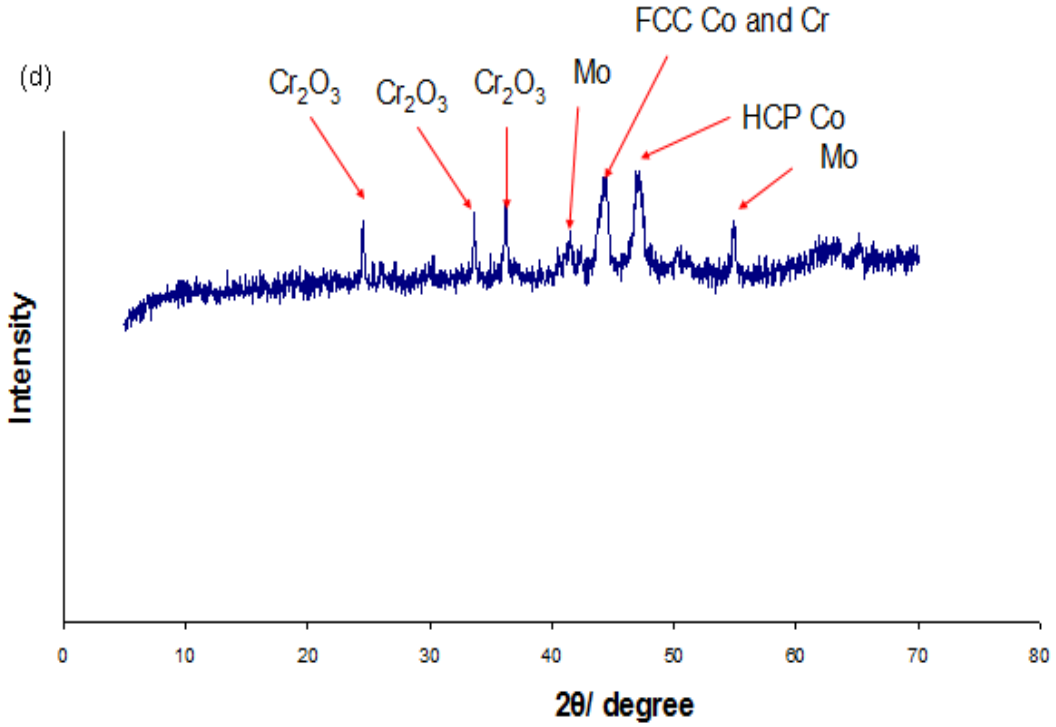

Figure 4.12: XRD patterns of powders and sintered compact, (a) chromium powder, (b) molybdenum powder, (c) cobalt powder, (d) sintered compact

The formation of the Cr_2O_3 is explained in the next few sections.

4.4.2 Sintering

The mechanism behind the sintering of powders in the SPS process is primarily due to the ON-OFF pulsed DC current. Due to the conductivity of metallic powders and the graphite die, the electrical current can flow through the system and heat the powders via the Joule effect. In terms of chromium oxide formation, this method of powder sintering via SPS in the presence of the cobalt oxide provides a means of producing it. Firstly, in the SPS process, the powders are activated through electric current heating. Any coatings or impurities present upon the particles are removed or if the surface coatings has

a low boiling point in the range of the sintering process, this coating is decomposed. The only surface coating present is that of cobalt oxide on the cobalt powder. This has a higher melting point (1935°C) than sintering temperature and so does not decompose [Young 2001]. Figure 4.13 summaries the mechanisms involved in the evolution of the SPS alloy microstructure. With the activation of the powders, this coating becomes active. The other powders, Cr and Mo are activated simultaneously. Due its high affinity of O, Cr reacts with the cobalt oxide and displaces the oxygen and forms chromium oxide. Any extra minute quantities of O in the graphite die can also help the formation of chromium oxide. Thus, the cobalt oxide reduces to Co and forms the matrix of the alloy together with the bulk Co present in the core of the Co powder

4.4.3 Mapping

The three metal elements and O are mapped in Figure 4.14. The Co shown corresponds to the matrix, the Cr and Mo mapping consists of the particulate phases. These particulate phases are produced due to the process not reaching total equilibrium as defined by the phase diagram of Co-Cr-Mo system for the F75 composition [Gupta 2005]. The equilibrium present in the SPS processed alloy is a solid solution of all three metals. The O elemental mapping mirrors certain areas of the Cr mapping, indicating that a combination of Cr and O is present, which indicates the chromium oxide phase.

There are individual phases of the chromium oxide and around the edge of the chromium rich phase the chromium oxide is visible. The edge-on chromium oxide develops as the oxygen cannot get into the centre of the Cr rich region, so the oxide phase forms at the edge, similar to the formation of oxide film or coating on the surface of alloys. The bulk of the oxide phase forms as the smaller Cr rich regions combine with O.

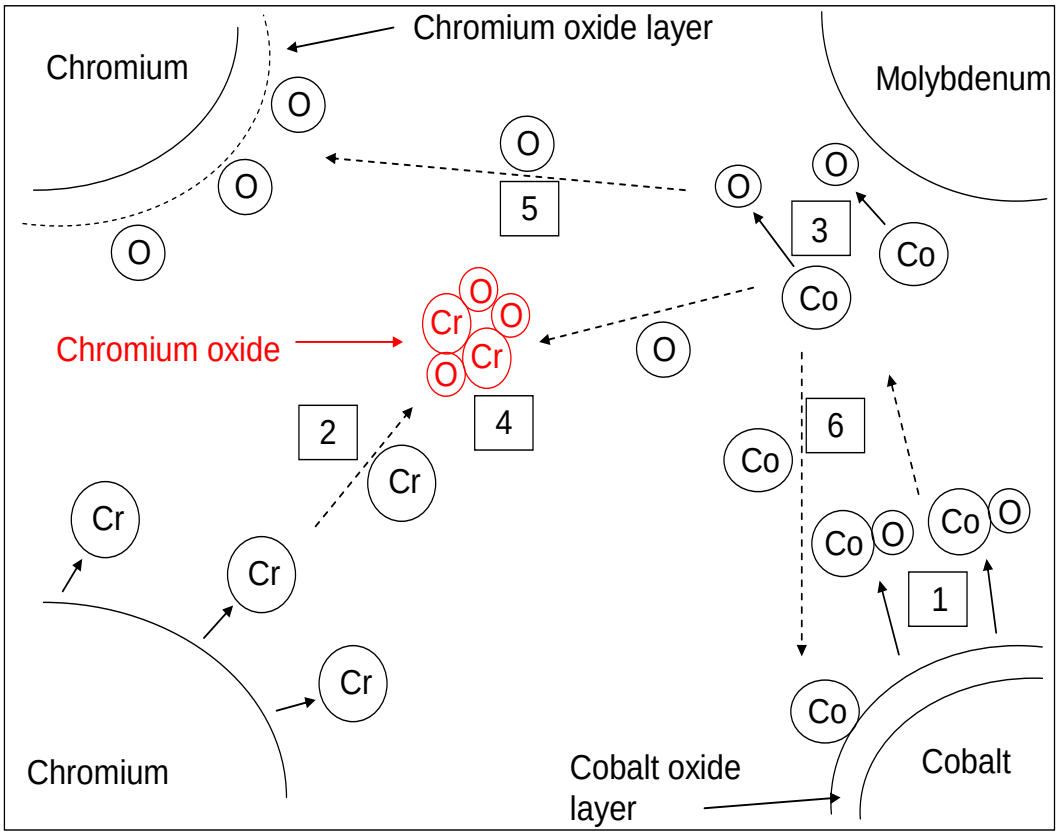

Figure 4.13: Diagram illustrating chromium oxide formation within the SPS alloy, with a numbered flow map describing the path of reaction to form the oxide

The numbers are explained below:

1. Activation of powders causes cobalt oxide layer to be active
2. Chromium particles are activated too
3. The cobalt oxide breaks up, due to the chromium ions' high affinity for oxygen
4. The chromium and oxygen combine to form chromium oxide
5. Some of the oxygen combines with other chromium particles to form a layer around the chromium rich phases
6. The cobalt from the cobalt oxide is reduced and together with bulk cobalt in the core of the cobalt particles forms the matrix

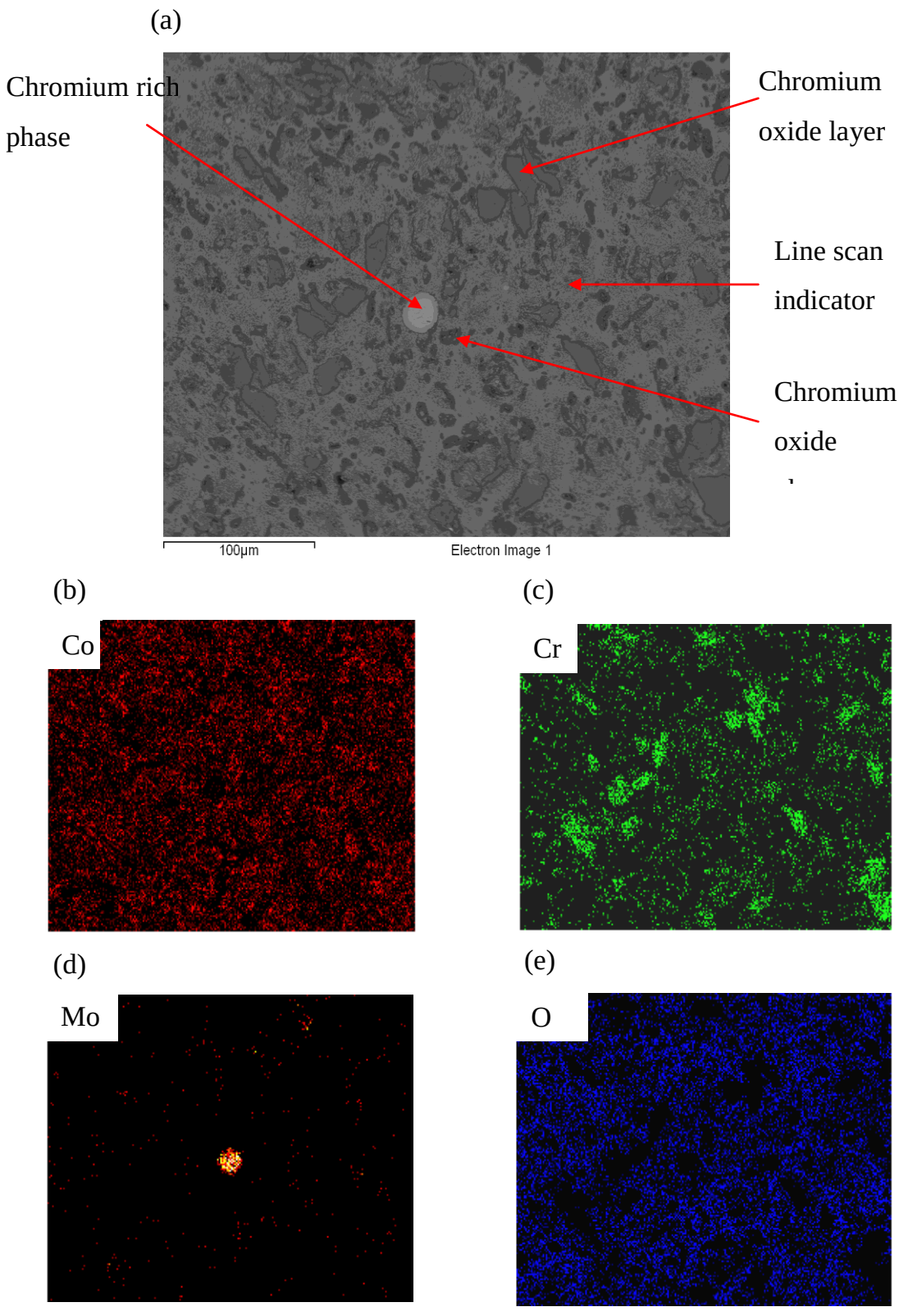

Figure 4.14: Elemental mapping of phases, (a) microstructure of the SPS fabricated compact with labelled phases, (b) oxygen, (c) chromium, (d) molybdenum and (e) cobalt mapping

The milled powder, produces a random distribution of the elemental powder, certain areas will have higher content of an element compared to others.

The line scan image (Figure 4.15) shows the presence of Cr, chromium oxide, Co and Mo. As the line scan begins from left to right, the phases can be identified. In the early stages of the scan, the Cr intensity is high, and the rest of the element intensities' are low, indicating a Cr rich phase is present. Continuing with the scan, the O intensity begins to increase with the Cr intensity still high, showing a combination of Cr and O present, which is the chromium oxide boundary or border edge. The decrease in the O shows a reduction in the Cr too at the same stage and the Co and Mo both rises. The Mo intensity is the lowest of all the elements, showing no phase has formed, but it is present in solid solution in the matrix. The Co intensity increases rapidly to indicate the matrix between the chromium oxide boundary and the next phase of chromium oxide. Subsequently, the Cr and O intensity increases again to represent the small chromium oxide phase, as the scan width is not very narrow, the surrounding Co matrix is still picked up and the Co intensity only dips slightly. Once the chromium oxide phase is scanned, the intensity of both elements decreases rapidly and only the Co and Mo remain, until another chromium oxide is identified.

The SPS system can be considered a closed system once the die is placed in the holder for sintering. The die is surrounded by vacuum (5Pa), causing no external matter to enter the die and form other phases. Also, no carbides were formed, as shown in Figure 4.12, indicating no carbon diffusion took place from the graphite die to the compact. This enables the O present in the system to be freely available and so reacts with the chromium to form oxides.

The chromium oxide formed from the natural oxygen is easy to understand, due to the oxygen present and the way chromium readily forms the oxide when oxidised at elevated temperatures. The method of formation in the SPS

alloy is due to a displacement reaction [Singh & Birks 1979]. The reaction that takes place in the graphite die is described below.

4.4.4 Reaction

Before sintering the three elements Co, Cr and Mo are present with the additional cobalt oxide from the Co powder. After sintering, the three elements still remain as Co, Cr, Mo and the O from the cobalt oxide is displaced by Cr to form the chromium oxide. Since Mo forms no compound phases and so has no real influence in the redox reaction, it can therefore be removed giving an overall net reaction:

$$3CoO + 3Cr + Co \rightarrow 4Co + Cr + Cr_2O_3$$

The resulting formation of chromium oxide and no other compounds from the reaction coincide with the Ellingham diagram for the various oxides that could be produced using these elements [Reed 1971]. The Ellingham diagram indicates the most likely oxide phase to form between the elements is chromium oxide.

In terms of O affinity of the three elements, the order is as follows: Cr>Co>Mo [Zimmermann & Ciacchi 2010; Tyurin 2003]. Therefore, chromium has the highest affinity for O, indicating that any freely available O present will bind with Cr first to form an oxide phase and also any oxides present can be reduced to their metal form.

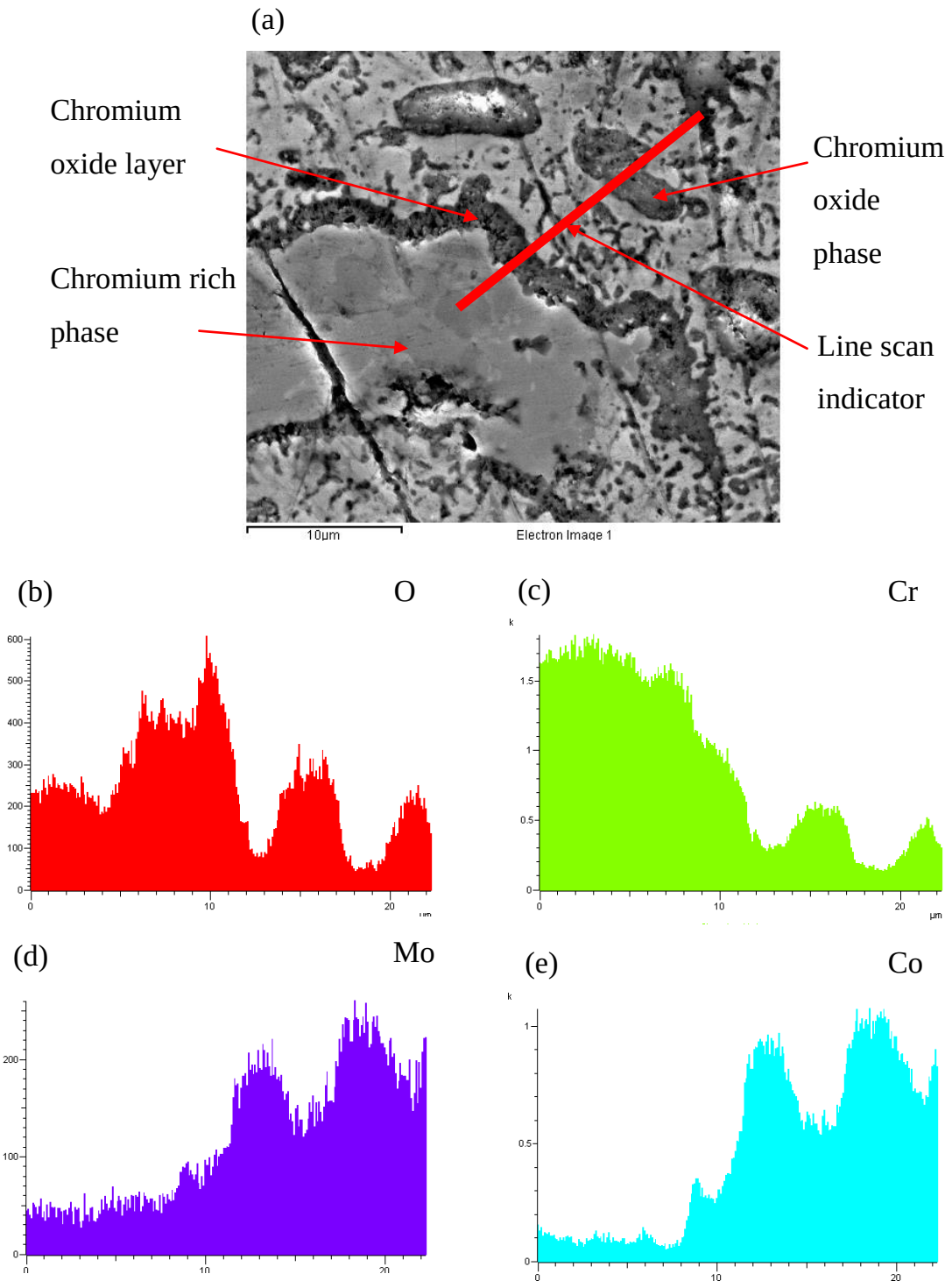

Figure 4.15: Line scan of phases and associated intensities of elements, (a) microstructure image with line scan and labelled phases, intensity of (b) oxygen, (c) chromium, (d) molybdenum and (e) cobalt

4.4.5 Effects of Oxides

The strengthening mechanism in the conventional cast/wrought F75 alloy is produced by the carbides. These are usually a combination of chromium and molybdenum carbide. These are the hardest phases in the microstructure. However, chromium oxide is much harder than the carbides (Table 4.4). The Vickers hardness of chromium oxide is approximately twice as hard as the carbides. The carbides are known to cause accelerated wear, as they become dislodged between the bearing surfaces causing third body wear [Que & Topoleski 2000].

Table 4.4: Properties of the materials and compounds that have been found in cobalt based alloys [Davis 1996; Brandes & Brook 1992]. For comparison, the average hardness of the SPS alloy is 730HV [Patel et al. 2010]. However, the conventional cast/wrought alloy has hardness of 300-480HV [Devine & Wulff 1975]

Materials	Density (kg/m^3)	Vickers Hardness (HV)
Cobalt	8900	1043
Chromium	7190	1060
Molybdenum	10280	1530
Chromium (III) Oxide (Cr_2O_3)	5220	2898
Chromium carbide	6680	1200-1600
Molybdenum carbide	8900	1500

Chromium oxide coatings on these alloys have been investigated to increase the wear resistance and due to its high hardness have shown lower wear rates compared to other coating materials currently used [Cellard et al. 2009]. This produces less wear debris, reduces the amount of osteolysis occurring and

improves the life span of the implant. It also has a lower density than the carbides and would make the alloy lighter than the current alloys.

Oxides are generally good for corrosion resistance; chromium oxide has been shown to be excellent for hot corrosion, due to its ability to withstand high temperatures and chemical stability [Sidhu et al. 2006; Whittle et al. 1980]. This makes the compound more stable than the carbides to attack from other chemicals and heat. The carbides in the microstructure improve strength but are known to change due to heat treatment; above the carbide dissolution temperature strength is lost due to carbides dissipating into the matrix. With the addition of chromium oxide in the matrix, the metallic alloy approaches the hardness of ceramic implants. Ceramic implants are known primarily for their significantly lower wear rates, due to their extreme hardness and produce less wear debris [Clarke 1992; Essner et al. 2005].

The toxicity of metallic implants is still a problem, as the metal ions have deleterious effects upon body tissues, especially surrounding the implant. The metal ions interact with the biomolecules and cause immune reactions leading to necrosis or damaged tissues [Hanawa 2004]. The metallic ions released from these cobalt-based alloys are usually more cobalt and chromium [Yan et al. 2008]. As chromium oxide is present in the microstructure, some of the chromium is now associated with the oxygen and due to the oxides insolubility in water the compound will not break up and expose chromium ions [Deren et al. 1963]. It has also been tested at elevated levels over a prolonged period in rats with no toxicity or carcinogenicity being identified [Ivankovic & Preussmann 1975].

In the current cobalt-based alloys, the metal ions are only released once the oxidic surface layer is disturbed and stop being released once the layer is regenerated [Hanawa 2004]. This layer is composed of oxides of cobalt and chromium [Smith et al. 1991]. The additional chromium oxide present

provides additional surface resistance and could reduce the release of metallic ions.

The materials used in the bearing surfaces of hip replacement devices are very specific for their function. This function is enabled through the motion of the acetabular cup and femoral head. The subsequent motion is related to the wear of the device and this is the main property of the device. This property's performance is measure through tribology. The wearing of the devices results in wear particles and debris and by reducing this; the device's lifespan can be increased. The measurement of wear is essential to determine the performance of the material for bearing surfaces in hip replacement devices.

4.5 Microstructure and Phase Analysis of F75 and F1537

The F75 and F1537 were evaluated for their microstructure and phase analysis. The F75 and F1537 alloy are the most common commercially used alloys in hip replacement devices. The F75 alloy is manufactured in the traditional casting method. The alloy elements are mixed together and heated above their melting point (1350-1450°C) and the molten liquid poured into ceramic dies and allowed to cool [Ratner 2009]. The F1537 alloy is manufactured using the wrought method. It can be done either hot or warm and can be annealed or unannealed. The annealed condition is hot rolled and annealed, the hot worked condition is hot rolled and unannealed and the warm worked is thermomechanically processed [ASTM F1537 Standard 2000]. Their microstructures (Figure 4.17) show similarities due to the similar elemental content (Table 3.2). The microstructures consist of a solid cobalt matrix with interdentric phases and carbides. The carbides are a combintion of either of Co, Cr or Mo and carbon and are denoted as M_nC_n where M is either Co, Cr or Mo and C is carbon. The microstructure and the phases of the F75 can be different depending on the casting condition. There have been known to exist three different types of microstructures depending upon the casting conditions. One microstructure forms as a Co-rich matrix with interdendritic

and grain boundary carbides. The other two consists of the same phases as the first one with either Co and Mo rich sigma (σ) intermetallics or Co based gamma(γ) phases [Archard 1953]. The F1537 comes in two types either low LC or high carbon HC, depending upon the C content. LC is typically <0.05% and HC is typically >0.2% [ASTM F1537 Standard 2000]. The increased C content is meant to increase the strengths alloy by reducing dislocation movement, therefore the HC alloy has increased wear resistance [Frenk & Kurz 1994; Streicher et al. 1996]. The F1537 alloy used in this study is of the LC as indicated in Table 3.2, with the C content <0.05%. XRD analysis of the F75 and F1537 alloys (Figure 4.18) show the same phases, they consist of the FCC Co, $M_{23}C_6$ and σ phases.

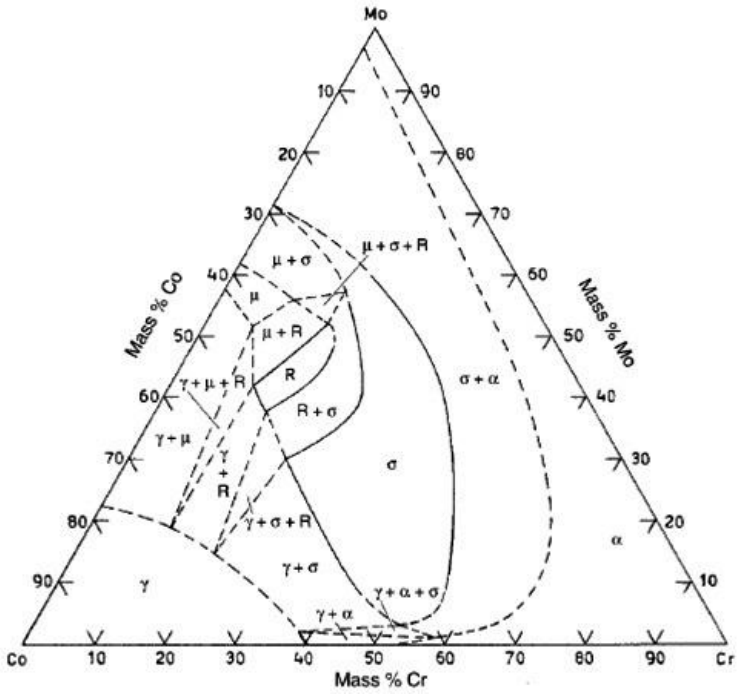

Figure 4.16**:** Co-Cr-Mo phase diagram [Gupta 2005]

Some of the phases formed in the F75, F1537 and SPS alloy coincide with the phase diagram of the Co-Cr-Mo (Figure 4.16) [Ragan 1974; Gupta 2005]. The phase diagrams for this cobalt system (Co28Cr6Mo) show that at low temperatures (~650°C) the most likely phases to form are the HCP Co and σ phases. As the temperature increases (~950°C) further the phases likely to form are σ, HCP Co and FCC Co phases. Further increase of temperature

(1200°C), the γ Co phase is most likely and further increase to 1300°C the same γ phase is the most likely to form [Rideout et al. 1961; Darby & Beck 1955]. In terms of the F75 and F1537, these are the phases that are mostly found in the microstructure, however, the addition of C makes carbides and gives more favourability to the formation of FCC Co phases (γ), rather than the more thermodynamic HCP Co phase formed at the low temperature ends [Petit et al. 1999; Sullivan 1970].

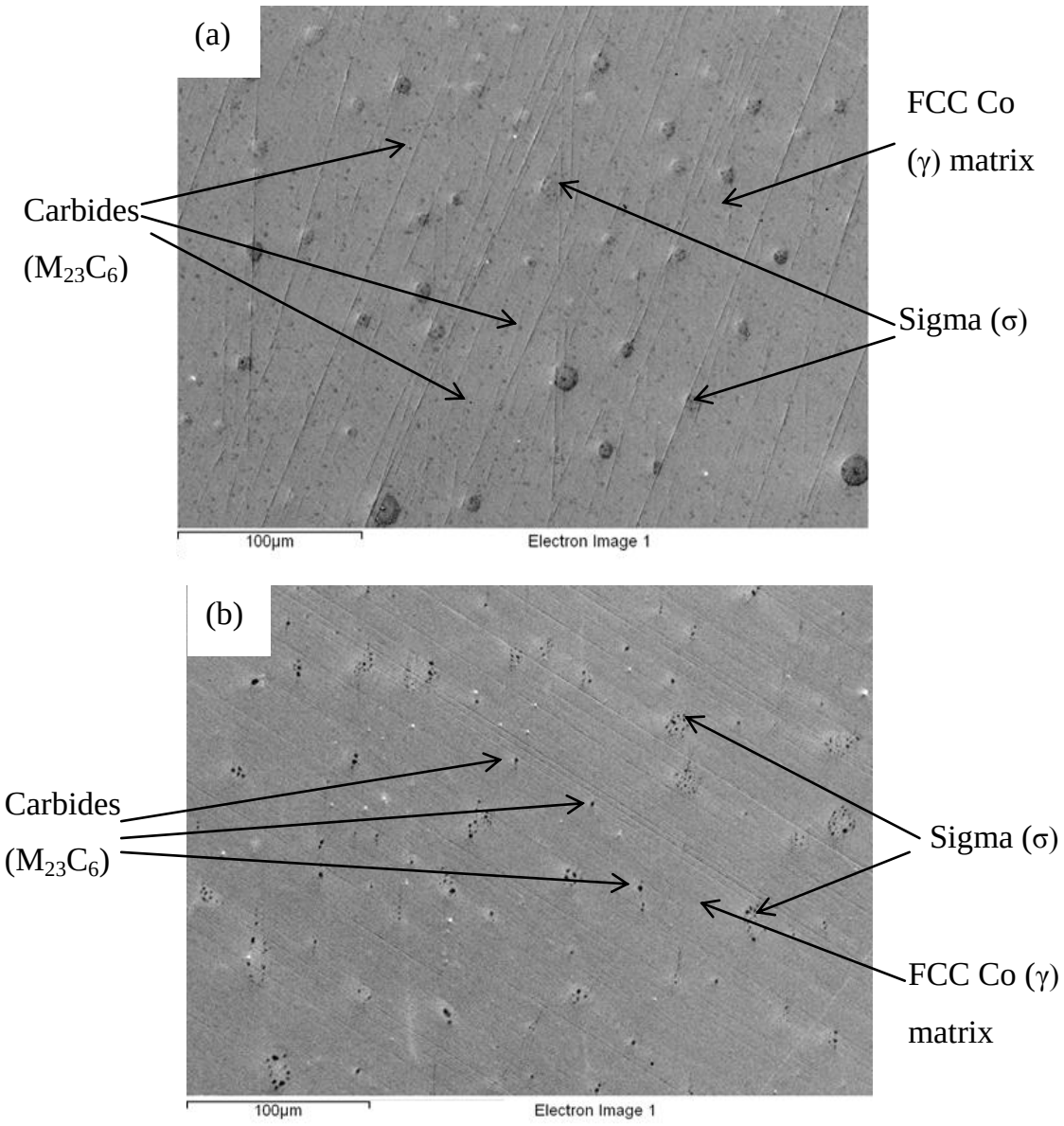

Figure 4.17: SEM images of the microstructure of the (a) F75 and (b) F1537 alloys before wear testing with phases labelled

In terms of SPS, as no carbides are present the most likely phases to form are the γ, HCP Co and σ phases or a combination of these. However, only some of these phases form, such as HCP Co and γ. As there is no carbon present HCP Co is also present as well as the γ cobalt. The rich Cr and Mo phases form as the solubility of the Cr and Mo seems to be low in the SPS alloy, whereas in the Co-Cr and Co-Mo phase diagram under the SPS sintered conditions the Cr and Mo are highly soluble and form γ phase [Massalski 1990]. With C present these phases are made less soluble as the C binds to form the carbides [Peissl et al. 2006]. The formation of Cr_2O_3 as described in Section 4.4 and is unique to the SPS system. The Co powder used to form the alloy is passivated with O to enable safer handling as it is very volatile when exposed to air. The unique sintering technique of the SPS provides the means for the formation of the Cr_2O_3 phase, as the oxygen from the Co powder is displaced by the Cr due to its higher affinity for oxygen and the formation of Cr_2O_3 within the microstructure proceeds, and this a very favourable according to the Ellingham diagrams [Zimmermann & Ciacchi 2010; Tyurin 2003; Reed 1971].

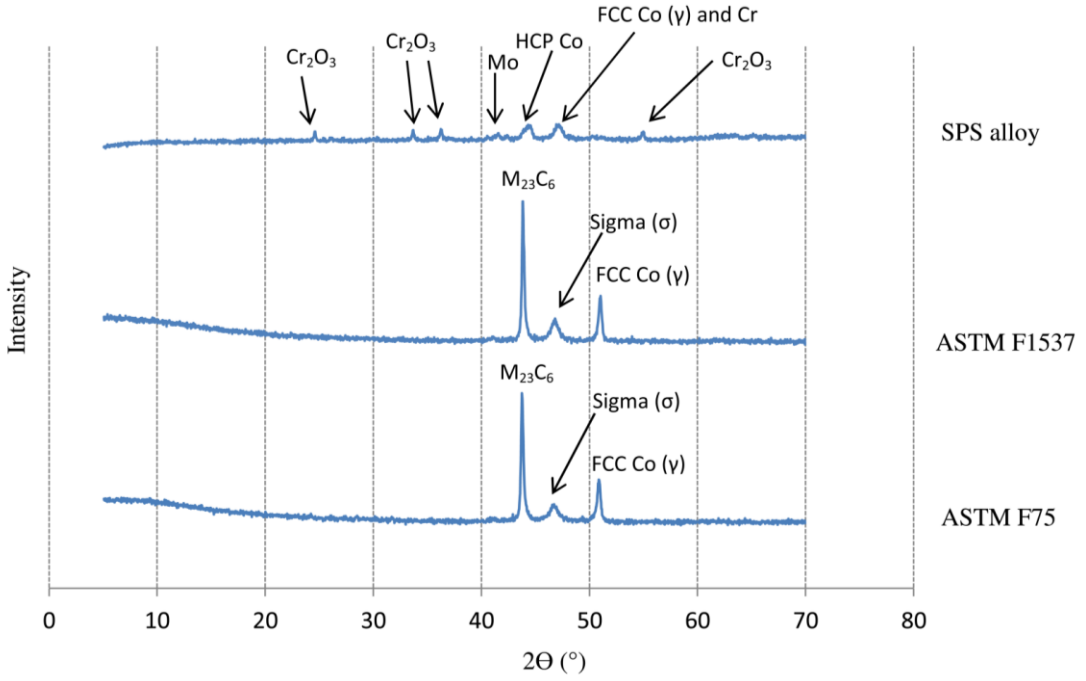

Figure 4.18: XRD phase analysis of F75, F1537 and SPS alloys with phases labelled

Chapter 5
Properties

5.1 Introduction

This section describes the properties of the alloys processed and supplied. The heat treatment conducted in Section 4.2.3, is evaluated for its hardness. The SPS compact formed in the Section 4.3 is evaluated for its grain size, hardness and tribological performance against two commercial used orthopaedic alloys, with their initial hardness being measured too. The wear particles generated from the tribological testing are evaluated for their size, size distribution, elemental content and shape. Metal element leaching studies are conducted upon the SPS processed alloy and the two conventional manufactured alloys to evaluate the elements that are being leached and the performance of the alloys for their application.

5.2 Heating treatment Properties

The annealed and normalised heat treatment alloys were tested for their microhardness. The annealed alloys (Figure 5.1) showed an increase in hardness from 296HV to its maximum of 565HV at 1100°C. Above 1100°C, the hardness decreases dramatically. The normalised alloys (Figure 5.2) showed a slight increase in the hardness to 363HV and remained fairly constant, with a maximum hardness of 383HV. The hardness values coincide with the ones in similar studies [Cawley et al. 2003].

The hardness of the alloy in the cobalt based alloys is meant to be influenced by the carbide content. Comparing Figure 5.1 and 5.2 with Figure 4.6 and 4.7, the carbide content of both annealed and normalised heat treated alloys have similar trends indicating that this phase has an influence on the hardness. This theory, of carbide content influencing the hardness has been known [Dobbs &

Robertson 1982]. This is due to the fact the carbides provide the main strengthening mechanism by reducing dislocation movement and strengthening the alloy [Dobbs & Robertson 1983]. Therefore, the decrease in the hardness in the annealed alloy at 1100°C, must be due to the carbide dissolution that occurs in the alloy in that temperature range.

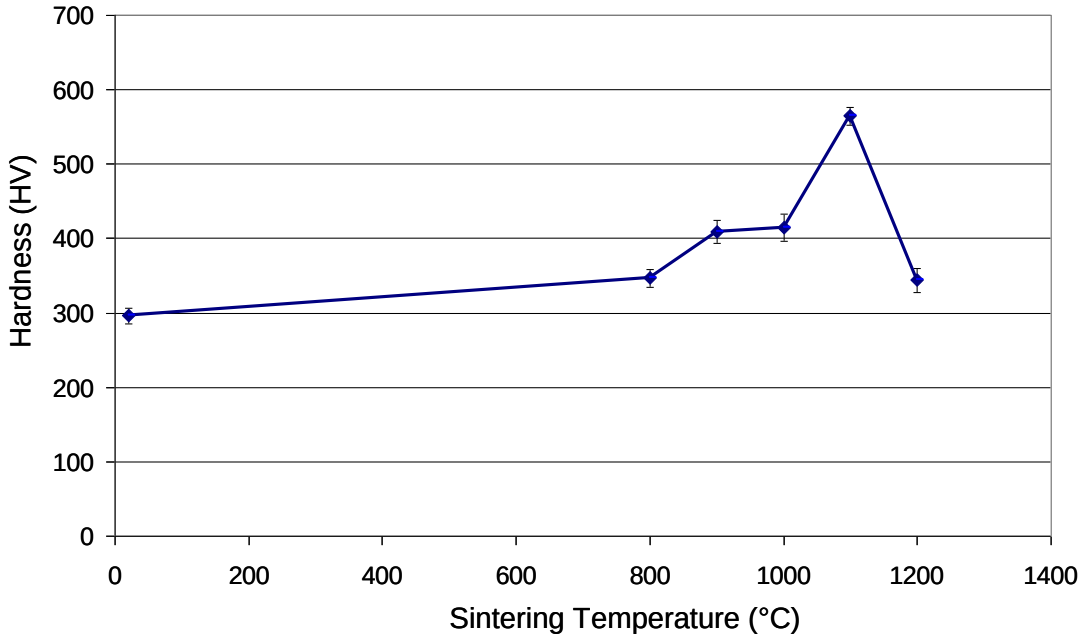

Figure 5.1: Temperature against hardness of annealed as-cast supplied heat treated alloy

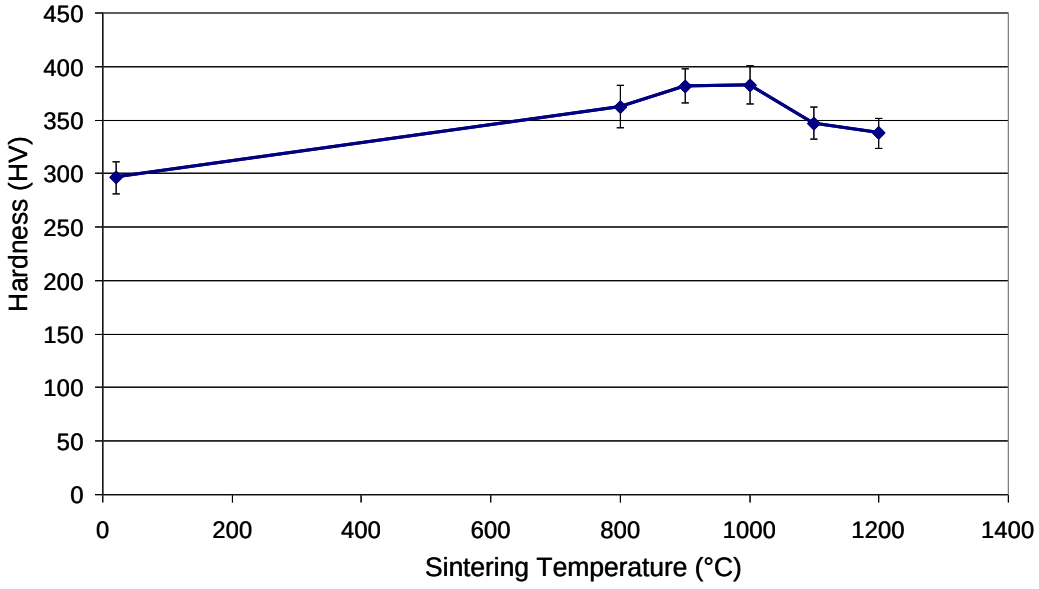

Figure 5.2: Temperature against hardness of normalised as-cast supplied heat treated alloy

5.3 SPS alloy Properties

5.3.1 Grain size and Hardness

The grain size and hardness of the SPS alloy are indicated in Table 5.1.

Table 5.1: Details of ball milled SPS sample processing conditions, grain size and hardness.

Sintering Temperature /°C	Dwell Time /min	Pressure /MPa	Average Grain Size /μm	Average Hardness /Vickers
1050	10	75	1.3	742
1050	10	100	1.2	754
1075	10	100	1.4	797
1100	10	75	1.0	707

Compared with the conventional processing methods, which produce samples with a grain size of approximately 7 μm [Salinas-Rodriguez & Rodriguez-Galicia 1996], the SPS compacts originating from nanopowders have a much finer grain structure, as indicated in Table 5.1, and this is beneficial for achieving high strength and high toughness products. The grain structure produced via SPS produces grain of a maximum of 1.5 μm, which is significantly less than conventional. The use of rapid heating and cooling in SPS limits the increase in grain size. Increasing the temperature above 1075°C where melting and resolidification is accompanied by an even slightly lower grain size of 1.0 μm. The variation of hardness and grain size as a function of sintering temperature shows similar profiles (Figures 5.3 and 5.4). Compared with the conventional routes of forming similar materials, which result in a hardness of 300–480 Vickers [Devine & Wulff 1975], the SPS compacts are much harder, as indicated in Table 5.1. The increase in the sintering temperature increases the average hardness of the compact initially (Figure 5.4). However, above 1075°C the hardness decreases, probably because of the

melting observed and melting reduces the density of the alloy and increased porosity is known to reduce strength. The maximum average hardness achieved was 797 Vickers, and this must be owing to a combination of factors such as fine grains and the distribution of the oxides in the microstructure.

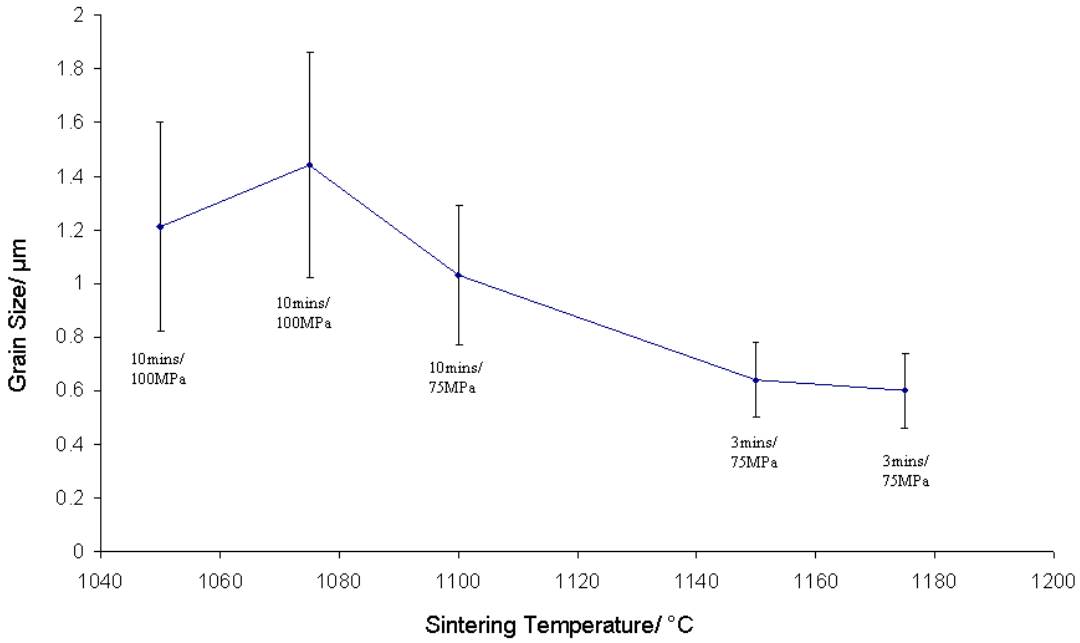

Figure 5.3: Variation of grain size as a function of sintering temperature of the SPS compacts

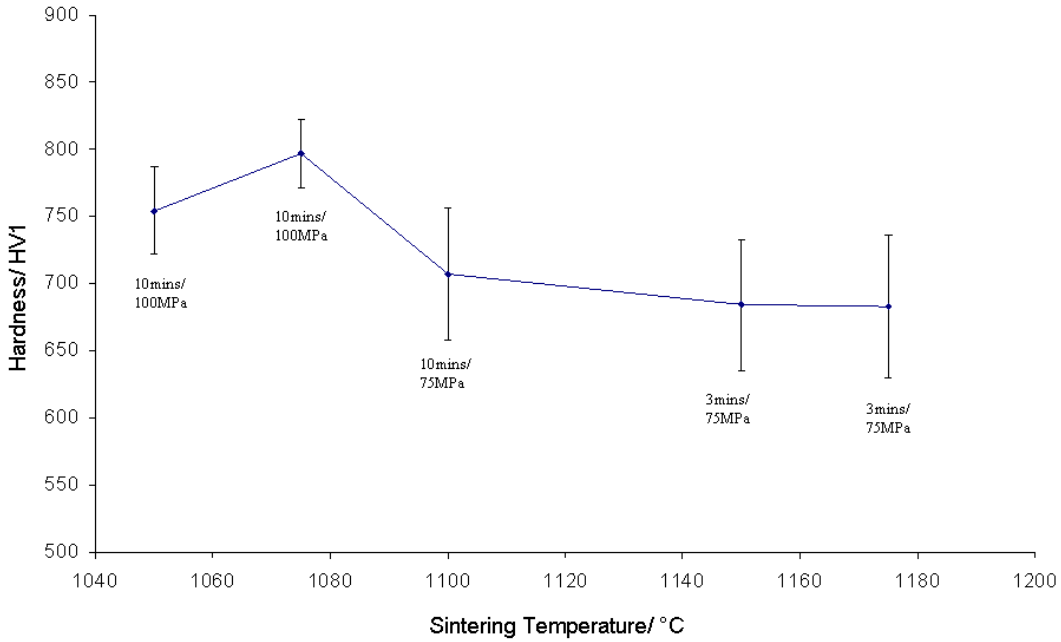

Figure 5.4: Variation of hardness as a function of sintering temperature of the SPS compacts

5.3.2 Chromium Oxide

The chromium oxide content is measured in the microstructure of the SPS sintered compacts and shown in Figure 5.5. As the sintering temperature is increased the oxide content increases to 17% from 15%, however it begins to fall dramatically to 12% and then to 8%.

Comparing, Figure 5.5 and Figure 5.4 it can be evaluated for the influence of the oxide content on the hardness. Like the carbide content of the heat treated alloys it can be observed that the chromium oxide content with increasing temperature has a similar trend to the SPS compact hardness with varying processing temperatures. The oxide phase being the hardest in the SPS alloy shows it has the greatest influence. This can be critical in being able to make an alloy of significant hardness, however due to the brittle nature of the phase as it is a ceramic, having too much present can make the alloy more brittle and prone to sudden fracture, which may not be ideal in a predominantly wear functional application.

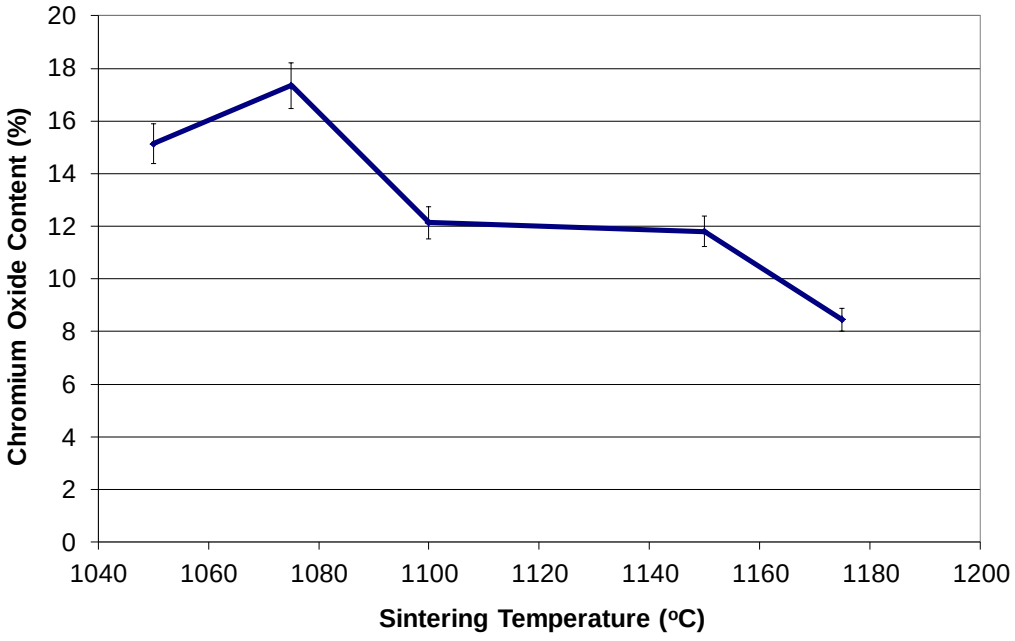

Figure 5.5: Variation of Chromium oxide content as a function of sintering temperature in the SPS compacts

5.4 Tribological Performance

The most common mode of failure in the hip replacement devices is Wear. During wear of materials, wear particles are produced that can become dislodged in the bearing surfaces and increase the risk of failure. There are two types of wear, abrasive and sliding. Sliding wear is simpler to determine through experiments, whereas abrasive requires addition material to be added to act as the abrasive. Wear testing of hip replacement devices is usually carried out in a hip simulator nowadays as this can simulate the movement in the body much more accurately. But to test newly developed materials simpler techniques are used usually pin on disk or variations of this such as ball on flat.

This section explains the tribological performance of the F75, F1537 and SPS alloy against an alumina ball under the G133 and F732 conditions.

5.4.1 Microhardness and Nanohardness

The micro- and nano- hardness is an important property when evaluating the tribological properties of the material. It gives an indication of the resistance of the alloy in terms of wear as the two properties are directly related [de Mol van Otterloo & De Hosson 1997]. The microhardness of the material is an indication of the hardness of the surface of the material as the indenter penetrates through the first few micrometres of the surface. The nanohardness is usually used to measure the hardness of thin films and the interaction between the coated films upon a substrate [Sun et al. 2008]. In this case, it can indicate the hardness of the individual phases and any passive oxide film upon the surface [Pang et al. 2001; Dourandish et al. 2008].

The micro- and nano-hardness are shown in Figure 5.6 which indicates that the SPS alloy has the highest micro and nano hardness. This explains that the microstructure is very hard upon the surfaces and through the top of surface. The nanohardness due to the small area of resistance measured can measure

the hardness of individual phases. As indicated by the standard deviation, the F75 and F1537 have small standard deviations indicating that the microstructure is uniform in terms of the its hardness. The standard deviation of the SPS alloy is much larger due to the variations of the hardness. The phases within the microstructure have different hardness; within the F75 and F1537 the hardness is correlated to the carbide content as these phases are the hardest phases found in the microstructure [Dourandish et al. 2008]. For the SPS alloy the much high hardness is attributed to the formation of the Cr_2O_3 phases.

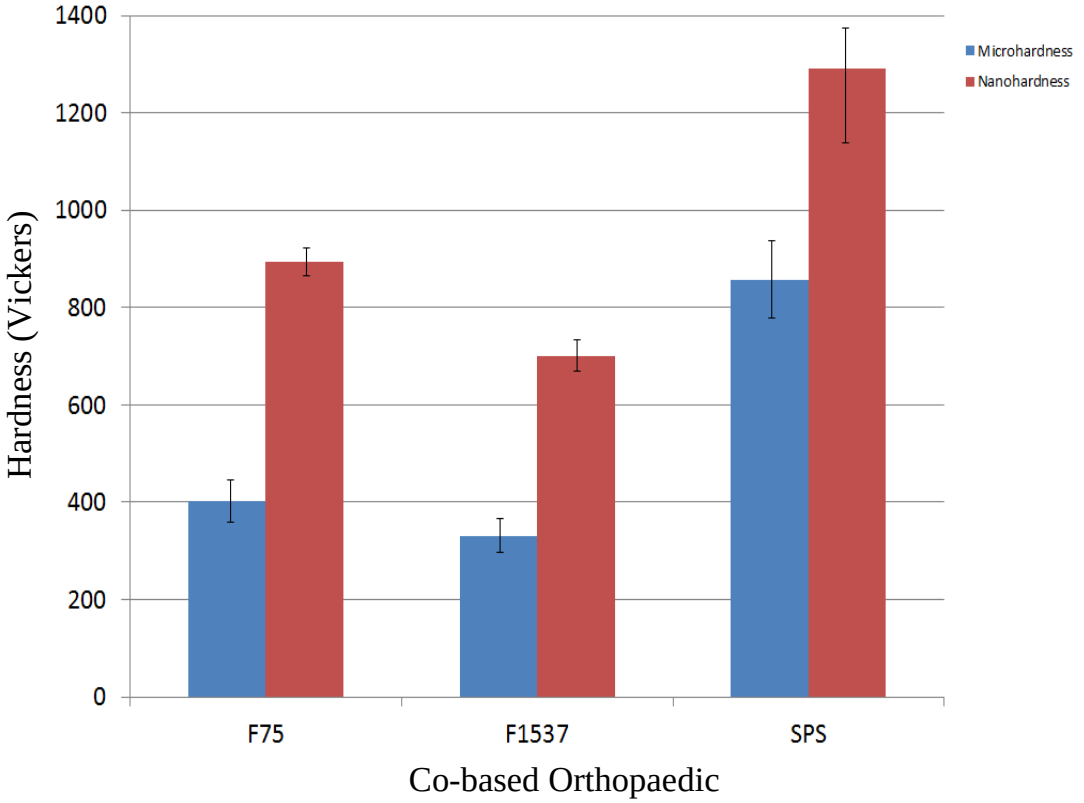

Figure 5.6: Microhardness and Nanohardness of F75, F1537 and SPS alloys before wear testing

This phase is a ceramic material that exhibits high corrosion resistance and high wear resistance, ideal qualities for a hip replacement device [Cellard et al. 2009; Sidhu 2006; Whittle & Stringer 1980]. Compared tiny carbides this is a larger phase and therefore can influence the hardness. The Cr_2O_3 hardness

(2898 Vickers) compared to the hardness of the carbides (1200-1600 Vickers) formed in the F75 and F1537 is much higher, therefore the oxide in the microstructure gives the alloy a higher hardness [Davis 1996; Brandes & Brook 1992]. The Cr and Mo rich phases also help in increasing the hardness as they can act as solid solution hardeners hindering dislocation movement. The HCP Co phases has been known to have fewer slip systems compared to the FCC Co, with lower number of slip systems the dislocation movement is limited and this can increase the hardness [Buckley 1976; Ratner et al. 2004]. The nanohardness measurements of the three alloys is higher than the microhardness measurements due to the formation of passive oxide layers. In all three alloys, due to the presence of Cr the formation of passive layer consists majorly of Cr_2O_3, and some minute oxides of Co and Mo [Kocijan et al. 2004]. This oxide as mentioned has extreme hardness and therefore the nanoindentation measurement would have this film taken into consideration as it forms around the surface of the alloys. Due to the relationship between hardness and wear, the SPS alloy should have the lowest wear rates and least amount of material loss.

5.4.2 Wear and Friction Coefficient

The total material volume loss due to wear is shown in Figure 5.7. This shows that the two conventional manufactured alloys have a much higher volume loss of material compared to the SPS alloy. This can be related back to the hardness in Figure 5.6. The higher hardness alloy exhibits lower loss of material, as the microstructure is more resistance to the wear. This material loss can be translated into a wear rate coefficient and shown in Table 5.2. This rate expresses the amount of wear material loss, over a specific distance, under a specific load. The wear rates show that SPS has the lowest wear rate.

Table 5.2 also shows the friction coefficient. The low friction coefficient of the SPS alloy indicates that the contact between the surfaces has a low resistance to friction. The lower friction resistance will provide smoother

contact between the surfaces and therefore reduce the wear. The friction coefficient graphs are shown in Figure 5.8. The SPS alloy also has the lowest coefficient of friction.

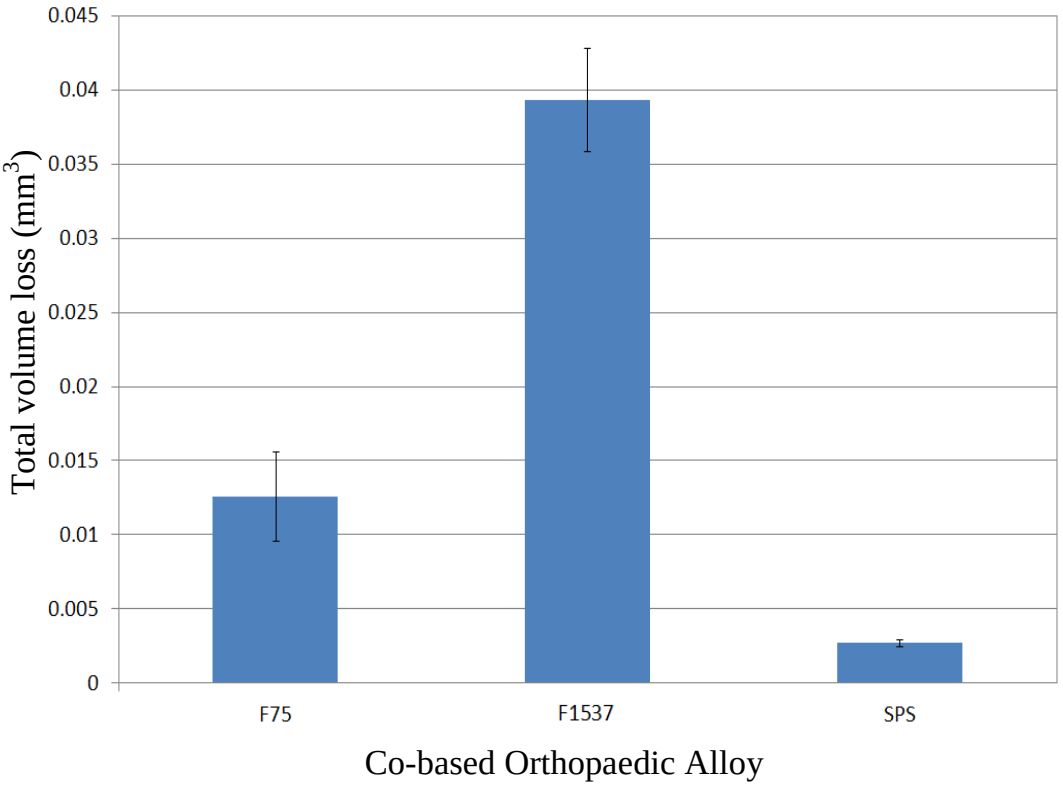

Figure 5.7: Wear material loss of the F75, F1537 and SPS alloys after wear testing

Table 5.2: Wear rates and friction coefficient of the alloys after wear testing

Alloy	Wear Rate ($x10^6$ mm^3/Nm)	Mean Friction Coefficient (μ)
F75	1.0 (0.26)	0.18 (0.009)
F1537	2.6 (0.30)	0.21 (0.003)
SPS	0.2 (0.002)	0.17 (0.002)

The friction coefficient has a large influence on the wear rates as can be seen in Table 5.2, they complement each other. Having a higher friction coefficient gives higher wear rates as the two surfaces in motion have increased friction and therefore a larger resistance to movement. For smooth motion between surfaces a low friction coefficient is beneficial as it can prevent friction forming and provides a low energy surface [Streicher et al. 1996]. It also prevents the friction to cause phase changes due to point heating as the cobalt based alloys are known to undergo phase changes after wear from a FCC phase to a HCP phase due to strain induced deformation [Varan et al 2006; Salinas-Rodriguez & Rodriguez-Galicia 1996]. The increased friction can cause the surfaces to become fused due to the heat produced during wearing and the sudden movement could remove large amounts material. The friction coefficient graphs in Figure 5.8 show how the friction coefficient changed during the wear test. In Figure 5.8, all graphs have a small amount of run-in phase after which the steady state phase is formed. The F75 and F1537 (Figure 5.8a, b) have more "noisy" lines, as the friction coefficient fluctuates during the test, indicating that the test runs less smoothly. The SPS alloy (Figure 5.8c), has a smoother line in the steady state phase, indicating that during the test the friction coefficient remained fairly stable and the motion between the surfaces was smooth.

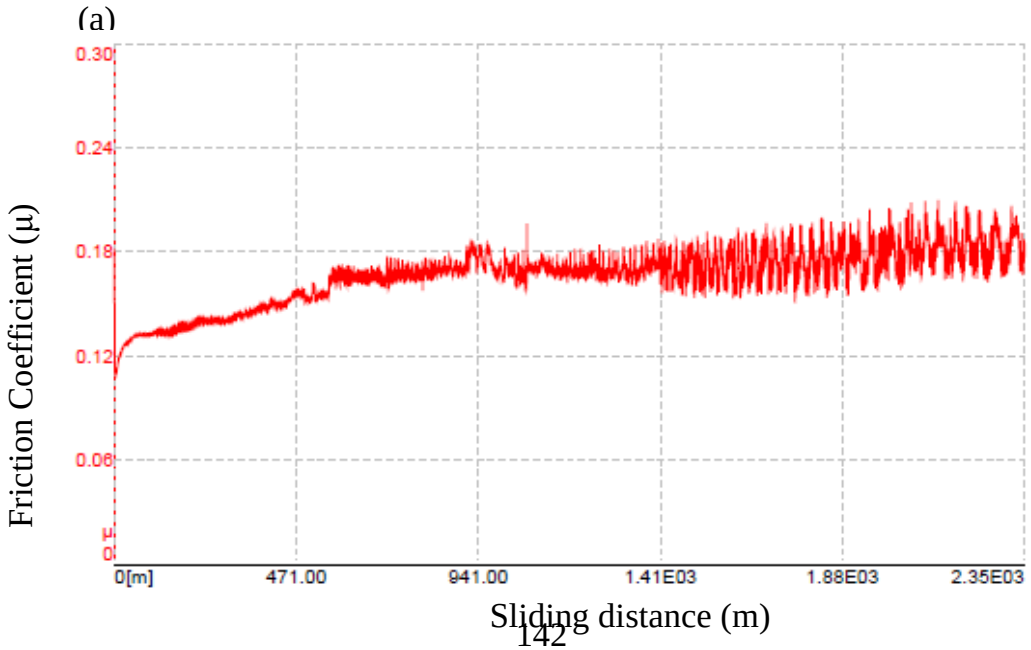

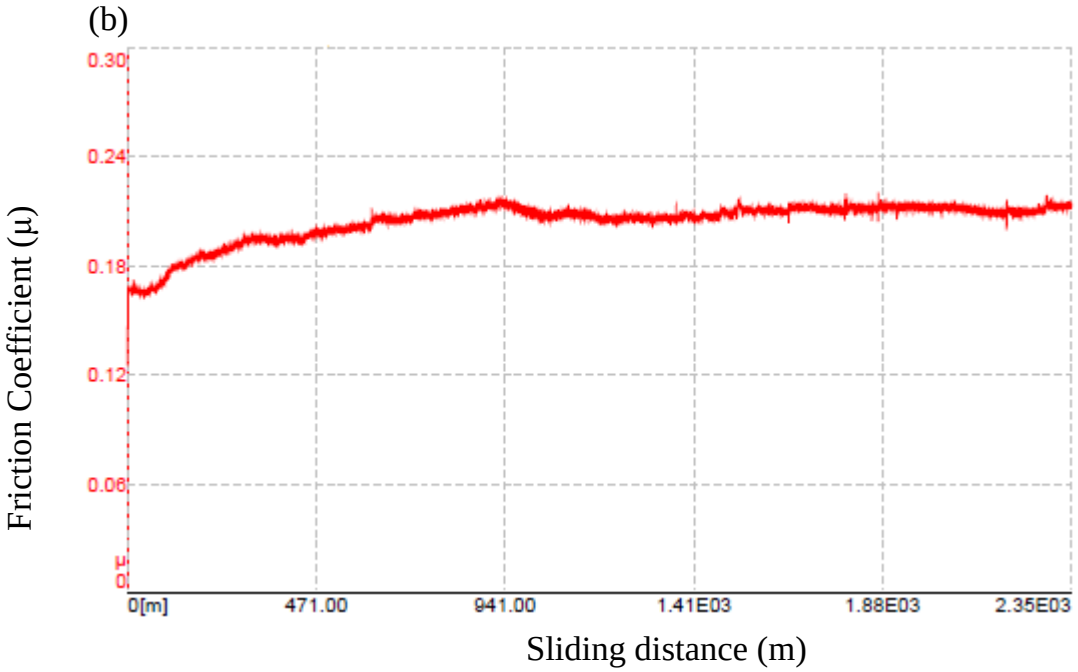

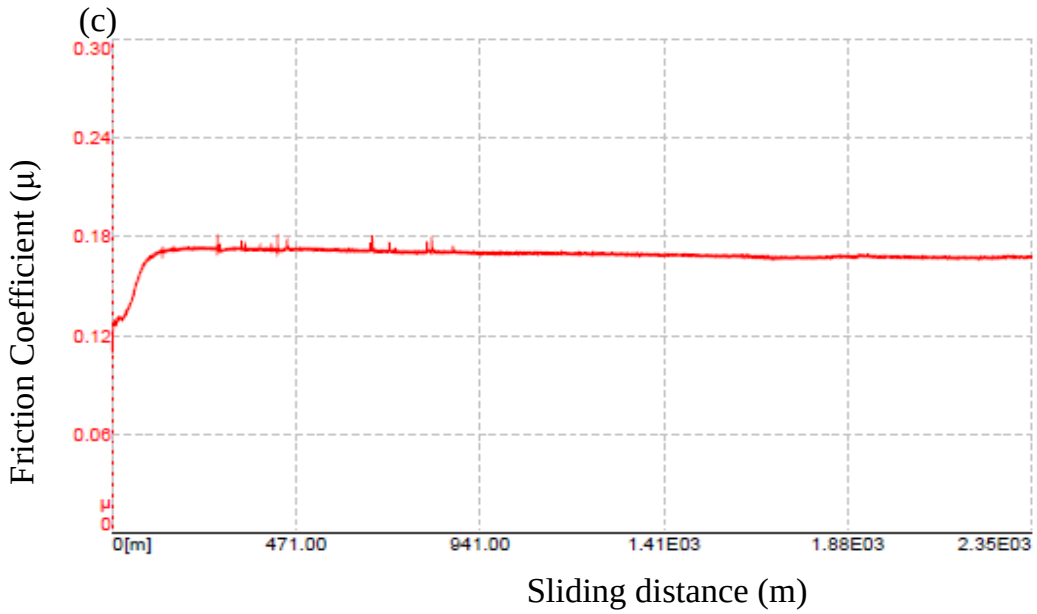

Figure 5.8: Friction coefficient (μ): (a) F75, (b) F1537, (c) SPS alloys during wear testing

In hip replacement devices, one of the major failures is due to the aseptic loosening of the implant and this is related to the wear debris and high coefficient of friction [Sundfeldt et al. 2006; McGee et al. 2000]. The wear debris when still circulating near the region can become entrapped between the bearing surfaces and during motion this accelerates wear. This phenomenon is known as abrasive wear. The other form of wear that usually occurs is sliding wear, where no abrasive particles are involved. The images of the wear track (Figure 5.9) show the type of wear that has occurred. F75 and F1537 (Figure 5.9a,b) show small areas of abrasive wear, where small grooves can be seen identifying the marks of the particles that may have been entrapped between the surfaces, which is common in wearing of these materials, where the actebular cup or femoral head show large striations upon the surfaces indicating large amount of abrasive wear [St. John et al. 2004; Doorn et al. 1998].

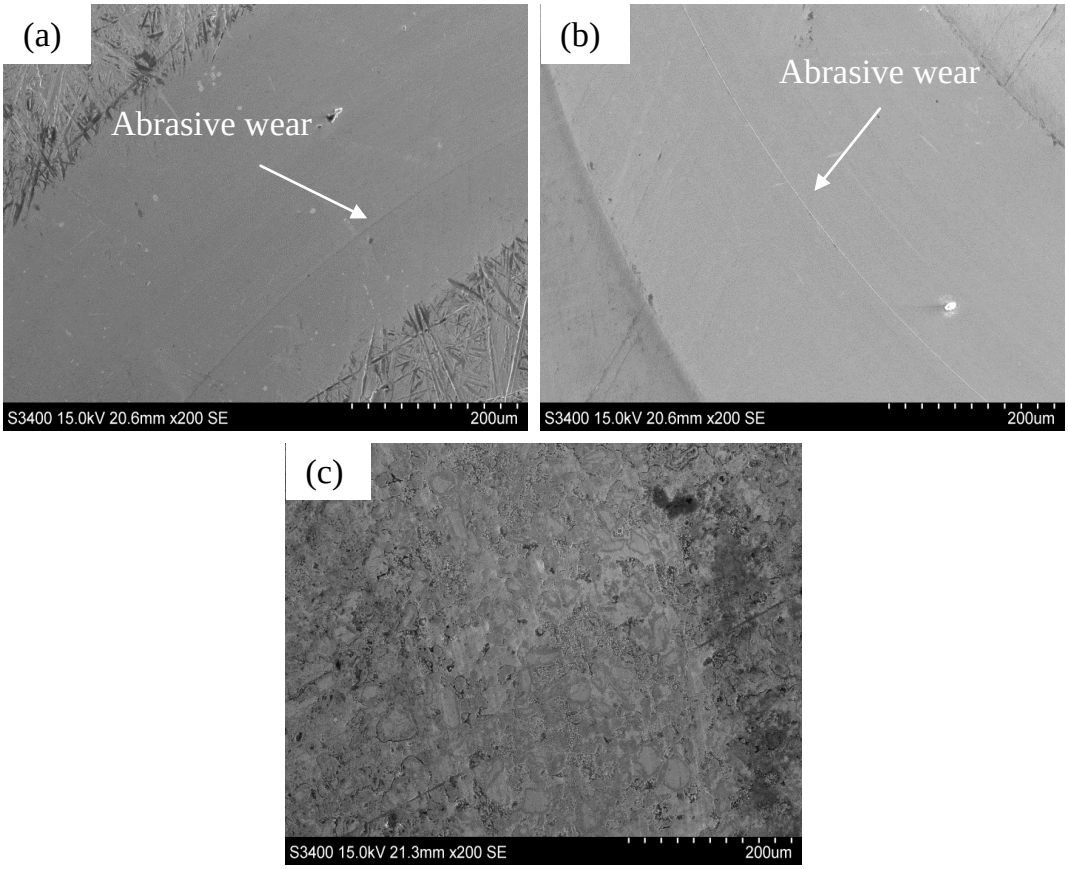

Figure 5.9: SEM images of the wear tracks: (a) F75, (b) F1537, (c) SPS alloys after wear testing

The SPS alloy (Figure 5.9c), has no distinctive marks of abrasive wear indicating that only sliding wear may have occurred upon the alloy. With the SPS alloy having lower wear rate and coefficient of friction compared to the other conventional manufactured alloys, the amount of wear debris produced is less and therefore the risk of aseptic loosening is reduced.

The wear profile of the three alloys is shown in Figure 5.10. The cross sectional view can be used to determine how the wear has occurred. While the wear track image shows only the top surfaces with the grooves and other defects, the wear profile can indicate the amount of material loss, due to the area under the surface and the profile of the wear erosion. The F75 and F1537 wear profiles' are very similar, and show a U bend shape, probably due to the hard alumina ball wearing upon the surface. The softer material enables the harder ball to penetrate deeper into the surface, and the shape of the curve can be attributed to the alumina ball. The F1537 alloy has a lower and wider depth indicating that it is softer material compared to the F75, which can be confirmed by the hardness results (Figure 5.6). The wear profile of the SPS alloy has a shallower depth and is not so rounded off at the end, indicating that the material is being worn away more steadily, instead of being gauged completely out, representing a harder alloy.

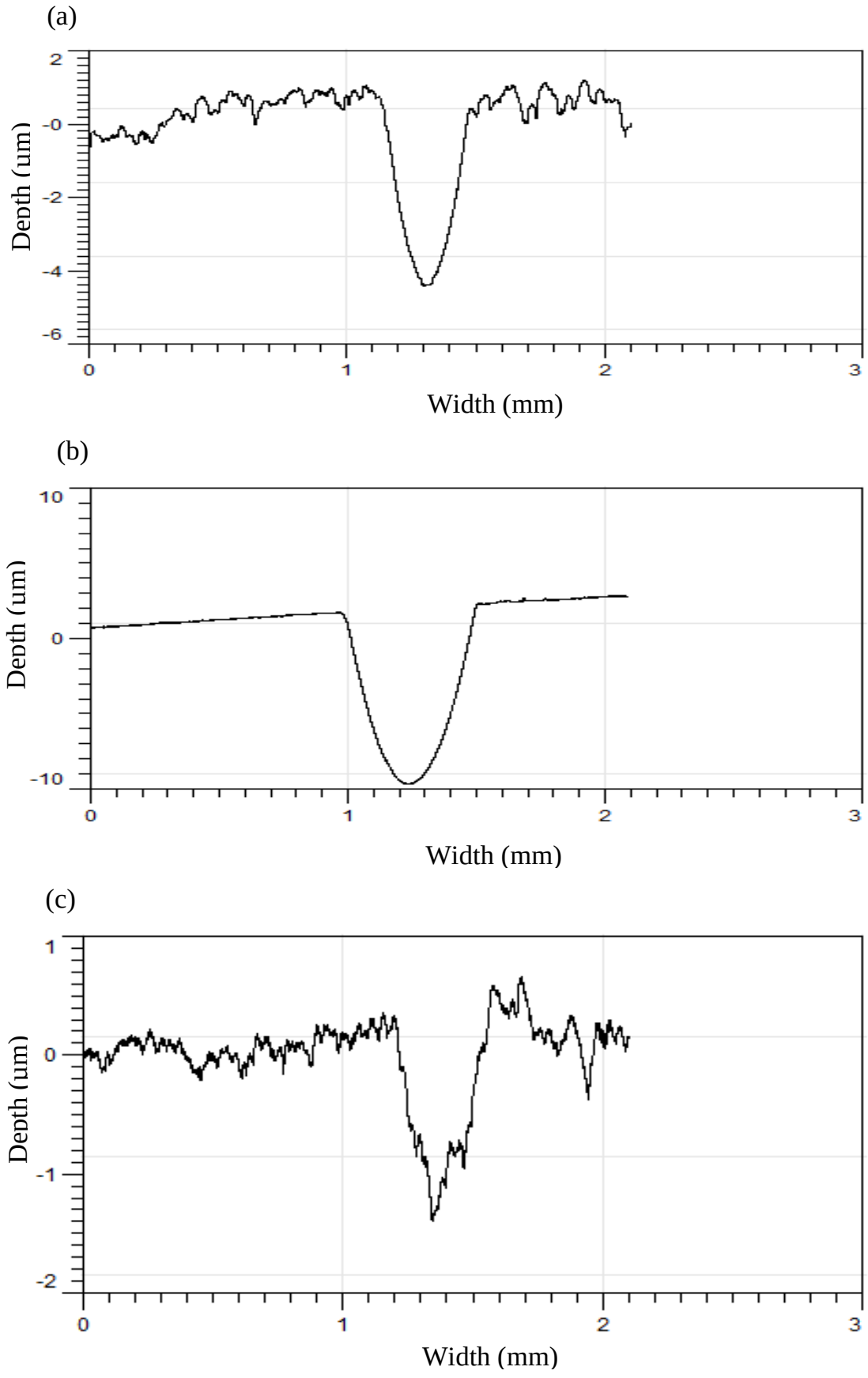

Figure 5.10: Wear track profile: (a) F75, (b) F1537, (c) SPS alloys

5.5 Wear particle analysis

5.5.1 Size and Size Distribution

The wear debris particle size of the alloys is shown in Table 5.3. The SPS alloy shows the smallest particle size with the smallest standard deviation. The SPS alloy shows the narrowest size distribution indicating the particles are of more monodispersed size compared to the size distribution of the other alloys. These results are similar to the wear debris size and size distribution generated in metallic hip replacement devices [Doorn et al. 1998].

Table 5.3: Wear debris particle size details

Alloy	Particle size (nm)	
	Mean	Standard Deviation
F75	74	44
F1537	71	34
SPS	69	33

The mode of the particle size distribution is in Figure 5.11. In the bovine serum there are materials such as proteins, salts and other molecules and these have certain sizes (Table 2). The Nanosight LM10-HS measures the particle size of all the material present in the solution and therefore, the sizes of these materials are also measured. Some researchers isolate the particles using reagents that could cause changes to the size of the particles [Schmiedberg et al. 1994; Catelas et al. 2001]. The wear debris particles size is smaller than the other material present and therefore the mode of the wear debris gives a clearer indication of the wear debris particle size without the other materials measured. In Figure 5.11a, the mode of particles size for F75 shows some peaks at the lower end around 32nm and the main one at 60nm, indicating that the particles could be of different sizes. The F1537 mode map (Figure 5.11b), has two characteristic peaks at 22nm and 54nm, also indicating different sizes of particles. The SPS mode map (Figure 5.11c), has one characteristic peak of

50nm, showing that the particles are more of one size than a wider "distribution" of sizes.

The smaller the wear debris particles size, the higher the increase in the surface area for reactivity with biological material, this can be a positive and a negative feature [Yue et al. 2010]. Larger wear debris size is harder to remove by the macrophages and therefore requires giant cells to remove the material [Pazzaglia et al. 1985; Murray & Rushton 1990; Jacobs et al. 1994]. With smaller size particles, the macrophages would find it easier to engulf the foreign material ready for excretion. Also, larger material would need to be consumed and then transported, increasing the time for excretion and the processes involved [Doshi & Mitragotri 2010].

5.5.2 Shape

Wear particles generated are of different shapes, from prism-like to needle-like particles. The shape of the particles can influence their biological activity as their surface area can vary and biological molecules may or may not interact with the debris.

The debris particles are in two types of shape, either prism or needle shaped. The prism (Figure 5.12a-c) are much more spherical and uniform shaped compared to the needle-like shaped particles (Figure 5.12d-f).This can indicate that during wear testing, the particles generated are either being chipped away or being scrapped out. The chipping would represent the prism shaped particles whereas the scrapped would indicate the elongated needle-like shape.

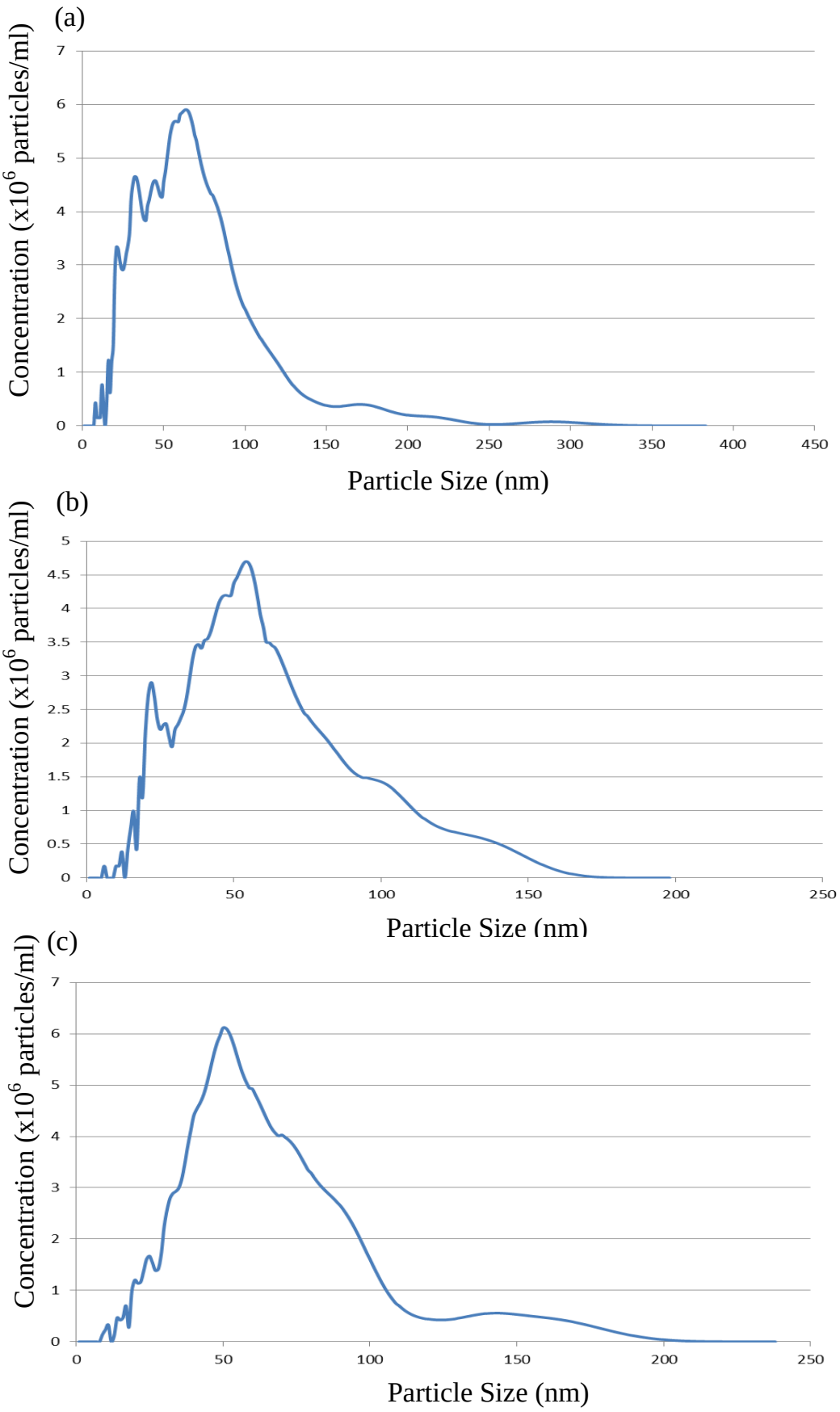

Figure 5.11: Mode of wear particle debris size distribution: (a) F75, (b) F1537, (c) SPS alloys

The prism-like particles have a smaller surface area compared to the elongated needle shaped. Surface area is an important factor as this determines the opportunity of biomolecule interacting with and causing reactions. The higher the surface area of the particles, the increased risk of reactions and this therefore induces adverse effects with surrounding tissues [Shanbhag et al. 1994; Campbell et al. 1999].

5.5.3 Elemental Content

The wear debris elemental content is shown in Figure 5.13. The F75 shows the lowest level of Co detected with F1537 indicating the most Co present. The SPS shows a higher level of Co than the F75, but the levels of Cr and Mo are much lower than the other two alloys. The low Cr and Mo content in SPS alloy can be attributed to the present of Cr rich and Mo rich phases and the Cr_2O_3 phase, these phases have a high chemical stability within the matrix [Hashimoto et al. 1979; Ma et al. 2004]. The Cr and Mo found in F75 and F1537 is found in the matrix or attributed to the carbides. The carbide formation reduces the degradation resistance of the alloy and causes the release of metallic ions into the body [Pardo et al. 2007]. The relatively high Co content in the SPS alloy is due to less Cr and Mo release. Most of the content of wear debris is made up of Co and this is being detected from the particles. The lower overall detection levels from the SPS alloy can be attributed to the low wear rates, as less wear debris would be formed and therefore less elemental count can be detected. The level of Co and Cr found in the blood and urine of patients implanted with hip replacement devices has been a very serious issue for surgeons [Milogev et al. 2005].

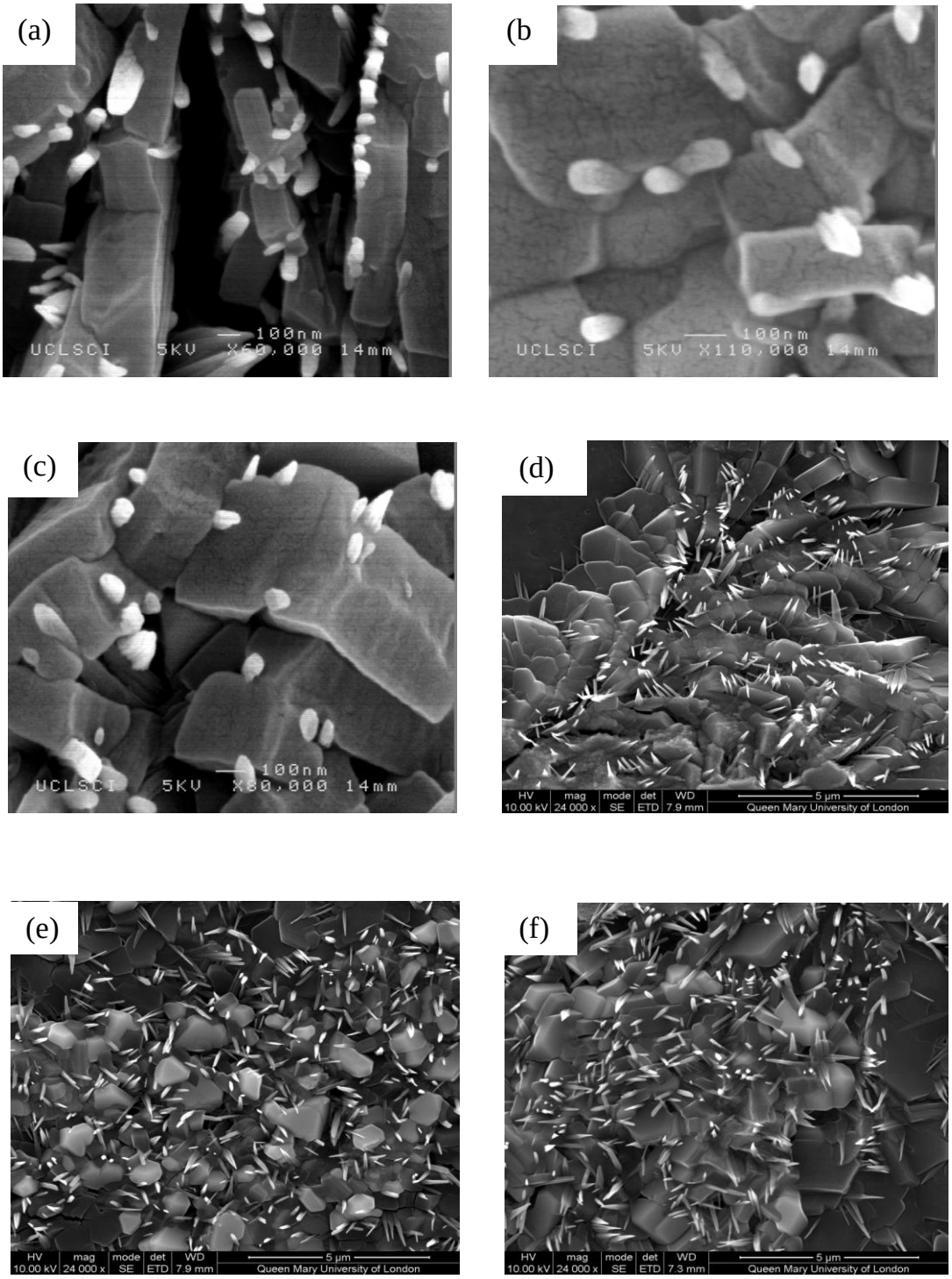

Figure 5.12: Wear debris particle of prism shaped: (a) F75, (b) F1537, (c) SPS and needle-like particles: (d) F75, (e) F1537, (f) SPS

Reactions with their ions and compounds formed within the body have caused major problems to surrounding tissues and other organs, such as the kidneys and the liver [Case et al. 1994; Michel et al. 1991; Cobb & Schmalzreid 2006]. Having the ability of the metallic microstructure to produce low wear rates and also be able to release less metallic ions can reduce this overall problem and ensure that the implant material for hip replacement devices is safer than the current material, causes less immune responses and reducing the risk of failure and revision rates.

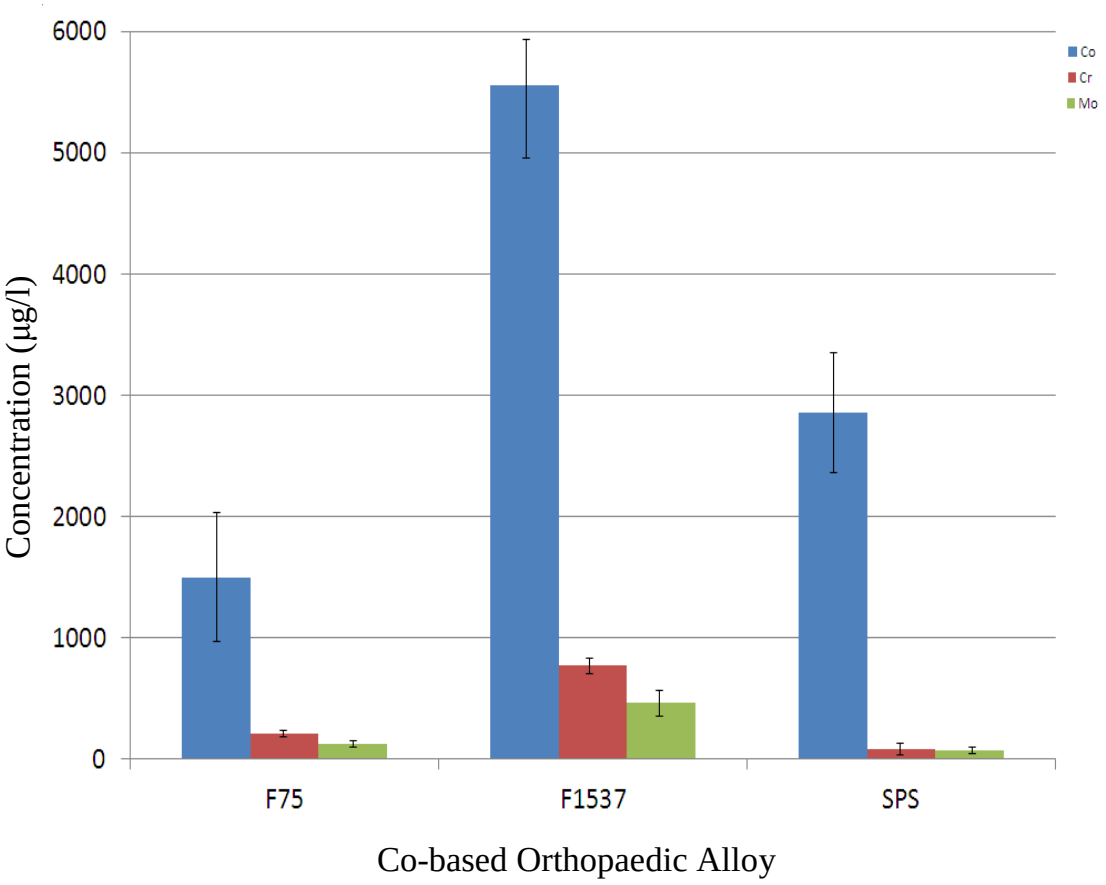

Figure 5.13: Metal element content of serum after wear testing of F75, F1537 and SPS alloys

5.6 Metal element leaching

Even though it has been suggested no proof has been shown that indicates metallic ions cause damage to the surrounding areas, resulting in sarcomas or necrosis [Merritt & Brown 1996]. The release of ions may not be ideal in terms of excess amounts of ionic content circulating the human system. All metallic materials release metallic ions over time, the limiting of these ions would significantly improve the biocompatibility and reduce the risk of failure of the implant and enable patients to be satisfied with the new device in the long term. The metallic ions are released due to the passivity layers on the surface of the material that protect against degradation, becoming broken due to the wearing process and the metallic ions are released due to the attack from ions within the blood [Hanawa 2004].

Metal ions are atoms or groups of atoms with a positive charge. They either form by a reaction or released from the bulk material during exposure to certain environments. Ions are usually not deemed to be harmful but depend upon the composition. Most ions would try to return back to a stable state, as the ions have a high energy and would combine with other material to stabilise themselves.

The metal materials used in the bearing surfaces are usually cobalt based alloys, which have chromium and molybdenum as other elements in the microstructure. Bearing surfaces of the devices are usually in the form of metal-on-plastic, metal-on-metal, ceramic-on-plastic and ceramic-on-ceramic. The use of plastic has shown that the plastic particles cause osteolysis due to the composition of the plastic (UHMWPE). The use of metal has shown to release metallic ions during function. The use of ceramic has been deemed to be the best due to the extremely low wear rates and no plastic or metals, however ceramics are susceptible to sudden fracture and the fabrication of the two ceramics in constant motion needs to be very accurate in terms of the

shape and roughness and this can be expensive or if wrong cause major problems.

The metal ion leaching study results are depicted in Table 5.4. The F75 and F1537 alloys show a steady increase in the Co, Cr, Mo element content. The SPS alloy in the initial stage shows a very high level of Co count and Mo count. The Mo count reduces dramatically over the next 148h showing that the Mo may have stabilised in the fluid or the high factor could be due to the oxidative degradation used to make the solution. The cobalt in the first 24 hours is very high. And subsequently falls dramatically over the next 148 hours. The Cr in the SPS alloy remains much lower than the other two alloys and remains fairly stable. This could be interrupted as bad news for the SPS alloy due to the concerns over metal ion leaching, as some of this high content can be related to having higher amounts of metallic ions floating around the blood system ready to interact with biomolecules.

The microstructure of the three alloys may indicate why the high elemental counts for the cobalt are observed in the SPS alloy. Figure 5.14 shows the microstructure of the alloys after leaching. Compares these to Figure 4.13, the microstructures are different. The F75 alloy (Figure 5.14a) has a stretching in the sigma phases and carbides are still present. The F1537 alloy (Figure 5.14b), has not much change, carbides are hardly visible, but this may be due to the low carbon content or due to the presence of chromium oxide that may have formed during the leaching experiment. The chromium oxide being an oxide is non-conductive making it more difficult to visualise the microstructure underneath. The SPS alloy (Figure 5.14c) is inherently different compared to Figure 4.14; the surface of the alloy has material present (Figure 5.15). The microstructure seems to have a film formed on the surface. These cobalt based alloy have been known to form a protective surface upon the alloy for corrosion resistance. When analysed using EDX (Table 5.5) the surface of the alloy have a distinctive oxide formed upon the surface. This

oxide consists predominantly of Co and O, indicating a form of cobalt oxide has formed during the leaching studies.

Table 5.4: Metal elemental content of leaching studies

Alloy	Elements		
	Co (µg/l)	Cr (µg/l)	Mo (µg/l)
24h			
F75	96	0	7.5
F1537	153	0	8
SPS	1912	0	171
72h			
F75	110	0.5	6.1
F1537	193	0.61	15
SPS	1877.32	0.34	143
148h			
F75	132	1.14	11.26
F1537	143	0.99	19
SPS	1402.72	0.34	4.25

As mentioned films form due to corrosion resistance and therefore it can be assumed the cobalt oxide film has formed due to the alloy in the presence of distilled water. The cobalt count in the first 24h was really high as the cobalt oxide films begins to develop and increases the count of the Co found in the fluid. As the oxide surface is formed the amount of cobalt leaching can be interrupted to be gradually reduced, showing the reduction in the count of Co as the study proceeds. With further increase in time, the oxide surface can fully cover the surface of the oxide reducing the Co count and trying to achieve stability.

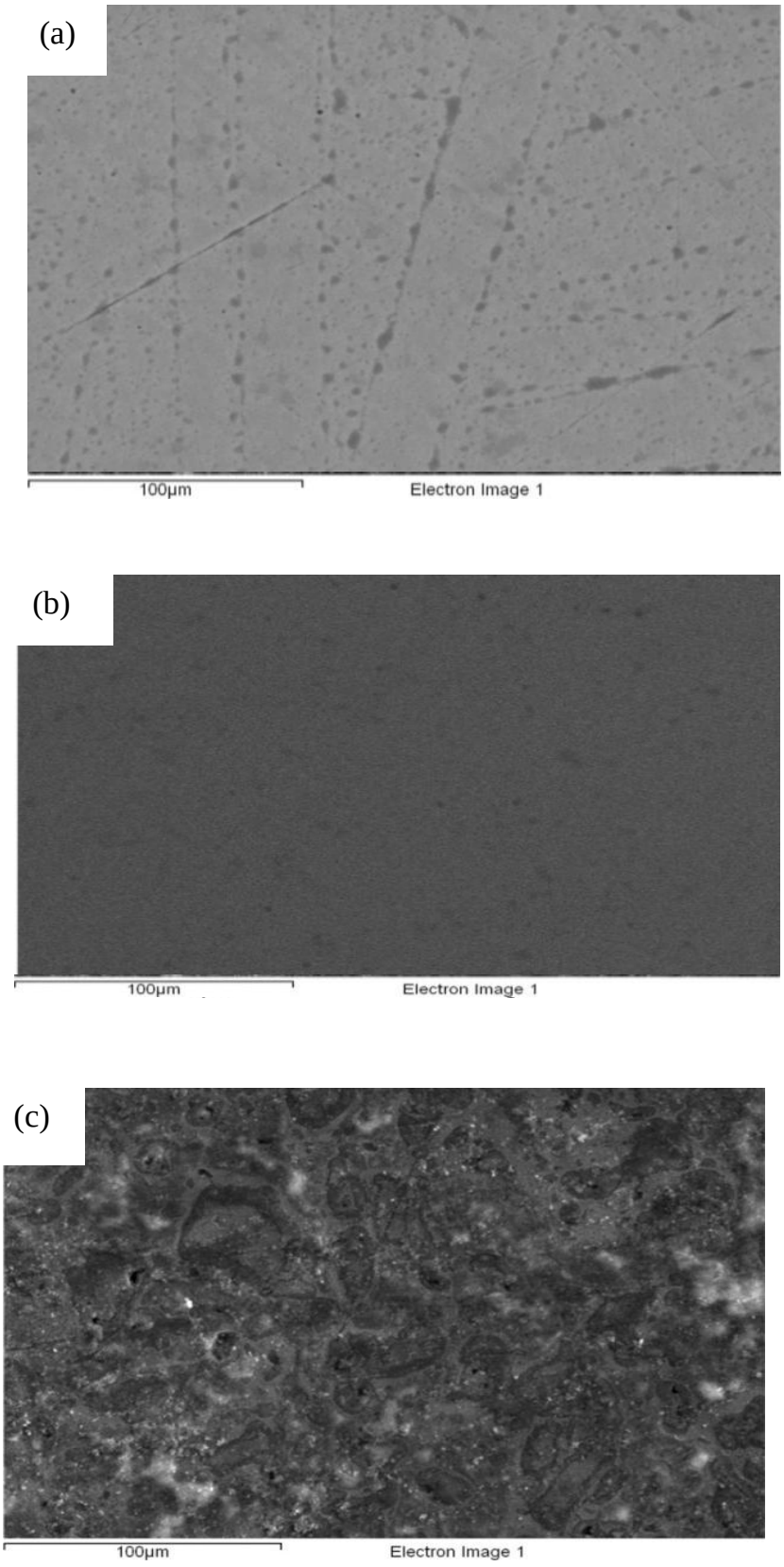

Figure 5.14: Microstructure of (a) F75, (b) F1537 and (c) SPS alloy after leaching studies, with the F75 and F5137 alloys showing no signs of change in the microstructure and SPS alloy having material present on the surface

As mentioned in Section 2.11, the way oxidic films develop in different environments can be seen through this example. The alloy placed in the new environment (distilled water) adapts to the new surroundings. Over time a film begins to develop to protect the alloy from attack from species within the fluid and forms an oxidic covering. Once formed, susceptible of attack to the alloy is reduced.

Using this scenario in the body, the alloy once implanted could form a covering of this cobalt oxide and as oxides are known to be non-toxic, due to their high chemical stability compared to other compounds, the covering would be beneficial. The cobalt oxide would cover the alloy, enabling the biomolecules, such as the macrophages, fibroblasts and giant cells to not interfere with the surface, ensuring no reactions or biological responses can occur.

Table 5.5: Elemental content of EDX analysis upon the microstructure of the SPS alloy after leaching

Element	Average Content (%)
O	30
Cr	1
Co	65
Mo	3

The alloy functioning as it is, produces its wear debris particles and these would also slowly form a surface coating of cobalt oxide, ensuring that they become less toxic to the cells that are engulfing and transporting them for excretion. Also, having surface coating has been beneficial to cobalt based alloys. Different coatings have been tried upon the surface to ensure an increase in surface hardness and to protect against ion leaching as the surface prevents the ion being released.

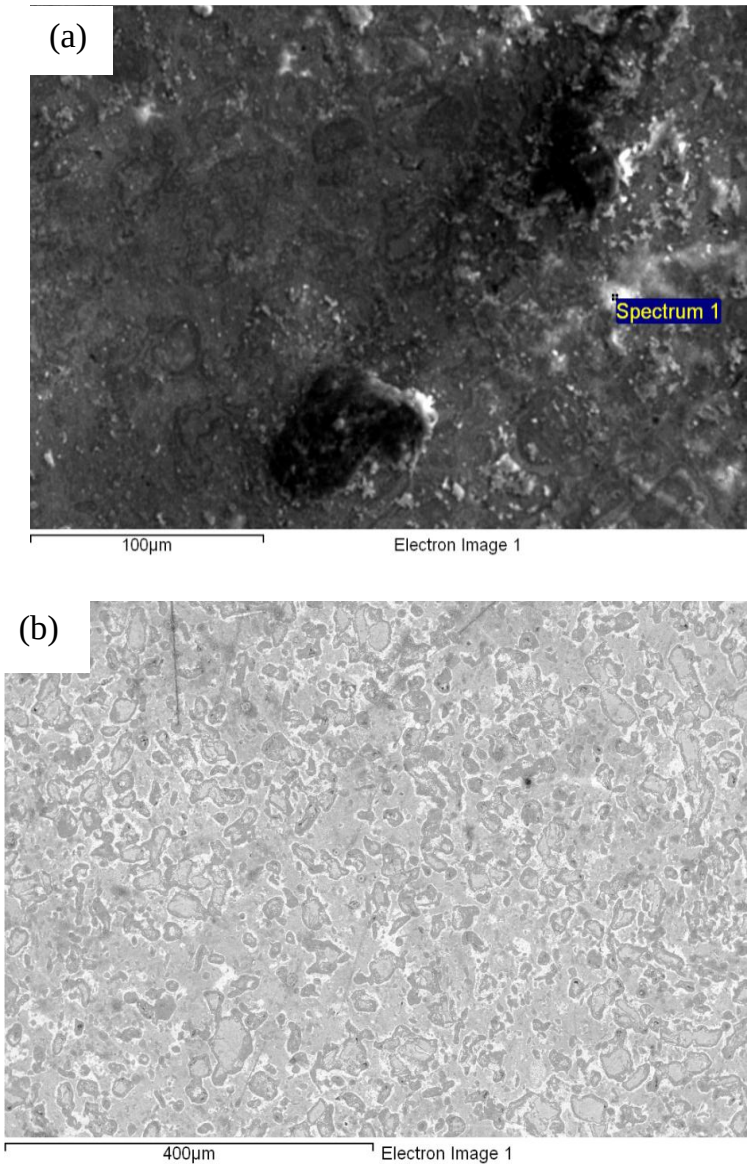

Figure 5.15: microstructure of SPS alloy after leaching studies (a) indicates material present on the surface and (b) backscatter image showing areas of material present indicated by the light regions

With a naturally forming cobalt oxide coating the same principle can be applied, the coating would add hardness to the alloy and reduce the number of ions being released. The cobalt oxide coating can also act to reduce the coefficient of friction by providing a smoother interaction between the two surfaces. The cobalt oxide coating would reduce the contact of the bulk

metallic alloy in contact with one another and ensure the bulk metal substrate is not being worn away, leaving more metal stock available and increasing longevity.

The elemental content release may or may not be of concern. This mainly depends upon the composition and ions being leached out. Some of the ions of Co and Cr are known to produce adverse reactions to the surrounding tissues. Cr ions that undergo slower oxidation release higher oxidative forms of Cr(VI) ions [Langkamer et al. 1992; Merritt and Brown 1996]. These ions are carcinogenic and affect the respiratory tract [Zhitkovich et al. 2005]. A mechanism of the Cr(VI) ions states that the ion enters cells and becomes reduced which produces other Cr ions, Cr(V), Cr(IV) and Cr(III) that combine with amino acids [Levina et al. 2006; Moghaddas et al. 1995]. Co ions have an effect on macrophages and osteoblasts [Cobb &, Schmalzreid 2006; Fleury et al. 2006]. The Co(II) ions causes oxidation and nitration of proteins that contributes to cell damage [Petit 2005; Petit 2006; Kitahara 1996].

5.7 Final Thought

The work conducted in this thesis can be seen as being revolutionary, as it has the potential to change the whole MoM hip replacement industry. This may be a bold statement, but the results presented give the impression so far that significant improvement to the materials are being made for their desired application. The initial work on the hardness measurement shows that the SPS alloy is at least twice as hard as the F75 and F5137 alloys. The tribological performance shows that the wear rate and coefficient of friction are five times lower than the commercial alloys. The elemental leaching of the SPS wear particles show that at least two of the elements are significantly lower than the elemental leaching wear particles generated from the other two alloys.

These results represent a story that promotes positive news for an alternative manufacturing route of cobalt based alloys for orthopaedics. However, much

still needs to be considered before this route can be claimed to be superior. Some of the future work is reported in the next chapter (section 6.2) that needs to be conducted to further the development of this alloy for acceptance. But, here are some stumbling blocks that need to considered.

Powder processing can be an expensive route for manufacturing, as the powders purchased and the equipment used to form an alloy can be costly. When purchasing powder in small quantity the price can be high, however in the larger quantity the price can be reduced significantly to lower the overall cost in the long-term. The Spark Plasma Sintering equipment may be expensive at approximately £250,000 for the machine, however with more products fabricated and the ability to manufacture other alloys, again in the long term it could be profitable.

The SPS machine currently can produce diameters of up to 80mm, this is sufficient for hip replacement devices with the majority of device diameters in the 32-34mm range. The most important factor is the ability for the SPS machine to scaling-up from the production of discs to form the hip replacement device shape. The femoral head and acetabular cup are unique shaped components. There are two ways to form the product, either the shape can be machined from an ingot or a near perfect replica shape of the device is formed and subsequently finished off by polishing. With the alloy being very hard, close to ceramics the chances of machining into shape would be far more difficult that to produce a near perfect shape and finish off. Therefore the machine specifics would need to be altered to accommodate this shape production. The major alteration needed is the shape of the graphite dies, they would need to be designed to ensure that the amount of pressure exerted uniaxially and the process of sintering remains efficient to form a fully dense alloy.

The main stumbling block is the perception that MoM materials should be disregarded due to the current issues regarding metallic ions and high wear rates. The other material used in hip replacement bearing surfaces is ceramics and have been deemed more reliable due to lower wear rates and no metallic ions formed. However, this class of materials are known to be brittle and sufficient long term patient knowledge is available to conclude that ceramics are the future. Metallic materials have been used since the beginning of the hip replacement device and much knowledge is known about the advantages and disadvantages. Therefore, by solving for the disadvantages metallic materials can continue to be the future of hip replacement devices. The SPS manufacturing route of the orthopaedic alloys has gone some way in attempting to solve some of the issues that are currently plighting the MoM materials.

These issues could be considered disadvantages over the existing manufacturing routes, whereby additional costs and expenditure need to be analysed to ensure the product is profitable and also if the SPS manufacturing route is actually the "opportunity cost". However, the initial risk of loss can be outlaid by having a product that has properties that are far more superior compared to the conventional manufacturing routes and could increase longevity for the patient. The increased longevity would enable a higher price for the device to be achieved and the product would be deemed more reliable for patients, surgeons, industry and the public.

Chapter 6
Conclusion and Future Work

6.1 Conclusions

The work conducted has enabled me to gather an increased understanding of cobalt based alloys orthopaedic alloys. This section concludes the work carried out to achieve the objective set out in the beginning of this research project.

6.1.1 Processing, Microstructure and Phase Analysis

6.1.1.1 Current as-cast orthopaedic alloy

An orthopaedic alloy was supplied to investigate the microstructure, compositional analysis and conduct heat treatment analysis to determine its effects. Using an as-cast alloy, I was able to determine that it was the F75 Co-Cr-Mo alloy, the most common commercial used orthopaedic alloy. The melting point was analysed and determined to be in the range of 1375°C to 1400°C which corresponded with literature. The microstructure of the alloy showed a solid Co matrix with secondary phases and carbides present as expected. The XRD analysis on the as-cast sample showed that the secondary phases and carbides were σ and $M_{23}C_6$ & M_6C-$M_{12}C$ phases respectively.

6.1.1.2 Heat treatment

Using two different methods of heat treatment it was possible to show that post processing conditions can affect the microstructure of the cobalt based orthopaedic alloy. In anneal heat treated alloy, the microstructure changed from the room temperature to 1100°C, the carbides increases visually and above 1100°C the number of carbide decreased dramatically. The normalised heat treated alloy showed no significant visual signs of change in the microstructure, apart from in a slight increase in the secondary phases at

1100°C, but it decreases at 1200°C. The observations made upon the microstructures are well complimented with the carbide content of the heat treated alloys. The annealed alloys indicates an increase in the carbide content gradually up to 1100°C and decrease dramatically and the normalised alloy shows no real change in the carbide content, with the level remaining fairly constant. The carbide changes are attributed to carbide dissolution, the temperature of around 1160°C, where the carbides in the microstructure are dissolved into the solid matrix and appear to have vanished. The XRD analysis of the heat treated alloy coincides with the observation of the microstructures. At the temperature of 1000°C the XRD analysis confirmed that the $M_{23}C_6$ carbides remain present in the microstructure. Beyond that, it showed that the only phase present was σ phase indicating a loss of the carbide phases. At the melting point temperature, the only phases present are the σ phase, indicating that no carbides are present and even the FCC Co matrix is not showing up.

6.1.1.3 Novel route to manufacture the F75 alloy

A powder processing route has been attempted to process the F75 composition using nanopowders and spark plasma sintering. The feasibility to produce a dense alloy was successful as indicated by the very low porosity, less than 0.5%. Analysing the resultant microstructure it can be seen that it consists of a cobalt matrix, with chromium, molybdenum and chromium oxide rich phases, and no carbide phases are present which is a vital breakthrough.

6.1.1.4 Mechanism of Chromium oxide formation

The mechanism of chromium oxide formation in the SPS processed alloy demonstrates that no additives are needed to produce the oxide in the microstructure. The oxygen already present in cobalt powder provides the opportunity for oxide formation via the method of sintering in SPS and through a displacement reaction. The SPS system sinters the powder with the pulsed electrical current and the cobalt oxide reacts with the highly oxygen

affinitive chromium to form chromium oxide. This reaction takes place in the graphite chamber without any external interference, as it is a closed system due to the vacuum chamber. The element mapping, line scan and the XRD analysis shows that only chromium oxide is present and no carbides are found in the microstructure.

The oxide compared to carbides has been shown to have more beneficial properties for orthopaedic alloys. The oxide is twice as hard as the carbides, providing more wear resistance to the alloy. Its excellent corrosion resistance and stability in water enables it to withstand attacks from chemicals and remain insoluble. It also can help prevent the compound breaking up and forming detrimental ions for biomolecules to react with, causing damage to the body tissues surrounding the implant and providing protection increasing regeneration of surface oxide layers, reducing metal ion release. The addition of chromium oxide increases the alloys hardness and makes it closer to that of ceramics, therefore lowering wear rates, reducing immunological reactions and longer life span. This oxide has been shown to have no carcinogenic effects, therefore making it more suitable for contact with blood and body fluids.

The content of chromium oxide is measured in the SPS compact against the sintering temperatures. It shows the increasing the temperature causes more chromium oxide to form in the microstructure up to 1075°C. Then the chromium oxide content falls dramatically.

The microstructure and phase analysis of the two commercial used orthopaedic alloys, F75 and F1537 were evaluated. The microstructure indicated the usually FCC Co matrix with σ phases and $M_{23}C_6$ carbides in both alloys.

6.1.2 Properties

6.1.2.1 Heat treatment

In the anneal heat treated alloy, the hardness increased to a maximum of 565HV and then reduced due to carbide dissolution. In the normalised heat treated alloy, the hardness did not show significant changes, probably attributed to the increase in scale. This scale has shown to protect the mechanical properties of the material and prevents changes occurring. Therefore, to increase the mechanical properties of the F75 Co-Cr-Mo alloy for increase wear resistance, the most likely choice is annealing but only to 1100°C. But if you want to provide additional protection to the original properties to prevent loss then normalising is the method that could be used.

6.1.2.2 SPS alloy

The alloy produced via SPS has much smaller grains than conventional manufactured alloys, approximately 1μm, which can enhance strength and toughness. The compacts are also of very high hardness compared to the cast or wrought products despite the absence of carbides in the microstructure. The gain in hardness is because of the presence of oxides and Cr- & Mo- rich phases in the microstructure. Therefore, the SPS route could offer significant advantages over the conventional cast and wrought routes used to prepare this alloy for orthopaedic applications.

The chromium oxide has a major influence on the hardness of the SPS alloy. The trends of the hardness and chromium oxide phase against the sintering temperature are very similar indicating that this phase is very beneficial to the strengths of the alloy, especially for the hip joint application. However, the key to achieving a great alloy is the controlling of the phase, as its ceramic nature can cause sudden fractures if the phase is in high quantity in the microstructure.

6.1.2.3 Tribological Performance

6.1.2.3.1 Microhardness and Nanohardness

The micro- and nano-hardness of the F75, F1537 and SPS compacts were evaluated to determine their strengths before wear testing. The microhardness of the alloys indicated that the SPS alloy is much harder than the two commercial grade alloys and due to the phases present in the microstructure. The HCP cobalt phases, the chromium and molybdenum rich phases and especially the chromium oxide increase hardness, whereas the carbides only contribute to the F75 and F1537. The nanohardness were higher in alloys compared to the microhardness due to the passive layers that form on the surface of these alloys, which usually consists of oxides of cobalt and chromium.

6.1.2.3.2 Wear Testing

The tribological performance of the three alloys has been tested and it can be observed that the SPS alloy has 5-10 times lower wear rate compared to the other two alloys. The friction coefficient of the SPS alloy is lower too giving a smoother motion between the two bearing surfaces. The wear profiles indicate the F75 and F1537 are softer due to the shallower depths of the wear track and the images show some signs of abrasive wear which can accelerate wear rapidly.

6.1.2.3.3 Wear Particles

The wear debris size and size distribution indicate that the wear generated from the SPS alloy is small in size and has a narrower distribution. The shape of the particles indicates that the SPS aspect ratio is closer to 1 indicating a more spherical particle, which can indicate a smaller surface area, compared to a flatter longer particle which has more surface for biological reactions to occur. The metallic elemental content indicates that the SPS alloy releases much less chromium and molybdenum compared to the F75 and F1537, but still has a relatively high cobalt release.

6.1.2.3.4 Metal element leaching

The metal element leaching study conducted indicates that within the first 24 hours in the SPS alloy the amount of cobalt leached out is very high, but the amount of chromium and molybdenum is very low. The F75 and F1537 gradually increase all the elemental contents as the study proceeds, indicating a constant leaching of material out. The post leaching microstructure of the samples, indicate that the F75 and F1537 remain the same, however the SPS alloy forms a films over the surface which consists of cobalt based oxide. As the study continues the high SPS cobalt content decreases, which may show that the cobalt based oxidic layer is preventing elemental content to be leached out.

6.1.3 Overall

The production method of spark plasma sintering has shown much promise over the experiment conducted to evaluate its properties. The significant improvements that have been made indicate that this processing route may be an alternative for long term viability as a hip replacement device material.

Given the recent medical device alert on all MoM hip implants released by the Medicines and Healthcare products Regulatory Agency (MHRA), indicating high revision rates due to soft tissue reaction [MHRA 2010], the SPS fabrication route as suggested in this project may be an alternative way forward to eliminate the adverse issues surrounding MoM devices and assuring the general public of the safety of this type of bearing material in the near future.

6.2 Future Work

The ideal properties of materials used in hip replacement devices need to be biocompatible and have adequate mechanical properties to enable the function to be carried out successfully. Therefore, the material needs to possess high wear resistance and the wear particles generated to not produce any immunological response from the host. This will enable the device to function

effectively for a longer life time. The future scope of the project is detailed below:

6.2.1 Scaling up

The spark plasma sintering process with the use of nanopowders has shown promise in terms of an alternative route to manufacture the F75 alloy composition for orthopaedic applications. The properties of the alloy are significantly improved for its application in a hip replacement device. However, the alloy is currently only produced as a sample. Therefore to produce a full product scaling up is required to either produce a near perfect device or a large enough ingot to be machined or forged into shape. Scaling up process requires more investigation. The same conditions to produce the sample, may not have the same effects on the larger scale and may produce an alloy which is not fully dense. Therefore, processing using the SPS apparatus is needed to be able to produce a scaled up version of the sample, which has a similar microstructure that will exhibit similar properties.

6.2.2 Advanced tribological testing

The current tribological performance test employed in this thesis was a preliminary test to assess the SPS alloy against the conventional manufactured F75 and F1537. Longer tests need to be performed to determine the performance of the SPS alloy in the long term. In the F75 and F1537 usually the running in period is over the first 1,000,000 laps and thereafter steady state wear is adopted, which is when the lowest wear rates are exhibited [Dowson et al. 2004]. Most tests are run for approximately 5,000,000 laps and this determines how the alloy will function in the hip joint [Fisher et al. 2004]. The combination of the pin and the disk can be crucial to the wear test, in this thesis an alumina was used as the ball and the metallic alloys were the discs. This was employed due to the extreme hardness of the SPS alloy compared to the other two conventional manufactured alloys and the alumina ball would have a hardness greater than all the materials being tested, ensuring the

performance could be evaluated. Having dissimilar materials can be a problem during function, as can be seen in the case of the ceramic-on-metal combination that was suggest by Fisher, though it may show promising results in the short term, the long term problems it may cause may not be satisfactory [Fisher et al. 2005]. Therefore, like-for-like materials need to be investigated against one another, i.e. F75 vs. F75, F1537 vs. F1537 and SPS vs. SPS, as it has been known that materials perform more efficiently when paired together [Chiba et al. 2007].

6.2.3 Hip simulator testing

Currently most cobalt based alloys are tested for tribological performance using a hip simulator. A hip simulator is a device that exhibits similar motions and loads that are occur in the region of the hip [Smith et al. 1999]. The hip simulator is meant to give more reliable results than the pin-on-disk wear apparatus, due to the ability to use the appropriate loads and replicate the physiological motion that may occur in the hip [Hung and Wu 2002]. The samples in the hip simulator need to be of the shape of the hip replacement device, therefore the scale up is essential for this part of the study, to form femoral heads and actebular cups components. The hip simulator tests will give a more representative data of performance of the SPS compact as there are now many results of different company products that can be compared with in terms of wear rates [Atkinson et al. 1985; Wang et al. 1996].

6.2.4 Metal ion leaching

The recent MHRA report upon MoM devices used in hip replacement has brought a lot of attention to the materials being used. The metallic cobalt based alloys used in orthopaedics have caused many problems due to the high revision rates from surrounding tissue reactions. It has been known that these reactions are occurring from the metal ions and wear particles released from the alloy during wear. The SPS, F75 and F1537 alloys have been investigated in this thesis for the elements that have leached out. However, some of the

material that may have leached out may not be toxic or carcinogenic. Certain ions of cobalt and chromium are known to be toxic and carcinogenic. Identifying these ions will give an indication of the toxicity of the material leached out. In this thesis, distilled water was used as the medium in the metal elemental leaching study. The use of different mediums such as bovine serum and other blood substitutes will determine how the SPS alloy reacts. In different mediums the leached material may form different compounds where some maybe stable and others unstable. The unstable forms cause the most problems as when biomolecules interact reactions occur.

6.2.5 Biological cell testing for biocompatibility

Biocompatibility of materials is a major issue. Materials that may be introduced in a biological environment need to undergo strict regulations as the example of the ASR device that caused the major recall. Biocompatibility tests of the ISO 10993 regulation enables the material to be evaluated for its genetoxicity, carcinogenicity, reproductive toxicity and cytotoxicity. Some of these testing requires cells to be involved. To test for cell viability, alloys can be subjected to fibroblast cellular cultures, for biocorrosion, artificial physiologic solutions can be used to monitor the material being leached out and for cytoxicity T cells can be introduced to the alloys to determine their effects [Bunea et al. 2003; Faleiro et al. 1996]. Cobalt based alloys have been known to inhibit the activity of T cells and reducing their functionality and causing immunological problems [Treagan 1975; Hartmut et al. 1989].

6.2.6 Other Applications

Cobalt-based alloys have many other functional uses, in dental implants and other joint replacements. Cobalt based dental alloys are used due to their excellent mechanical strengths and corrosion resistance for crowns, bridges and denture bases [Wataha 2000; Bates & Knapton 1977]. However, the same problems occur in the dental alloys as in the hip replacement device, mainly with the release of metallic ions. SPS alloy could be tested for usage as a

dental alloy and scaling up would not be required as the samples are smaller in dimension compared to hip replacement devices. Other joint replacement devices that use cobalt based alloys are knee, ankle and shoulder [Stojilovic et al. 2006; Hermawan et al. 2011; Revell 2008]. Knee replacement devices have been around for a long time, whereas ankle and shoulder are newer joints that are being replaced. With the same cobalt based alloys used, SPS manufacturing could be the alternative fabrication process for these joints. Testing for the criteria for the relevant joints could be investigated to determine if the SPS alloy satisfies the conditions of use.

References

Affatato, S. Spinelli, M. Zavalloni, M. Traina, F. Carmignato, S. Toni, A. Ceramic-On-Metal for Total Hip Replacement: Mixing and Matching Can Lead to High Wear. Artif Organs. 34 (2010) 319-323

Al-Hassani, S.T.S. Consolidation of powder metallurgy bars by direct electrical discharge and rotary swaging, Wire Ind. 46 (1979) 809-816

Alp, T. Al-Hassani, S.T.S. Johnson, W. Electrical discharge compaction of powder: mechanics and material structure, J Eng Mater Technol. 107 (1985) 186-194

Alp, T. Can, M. Al-Hassani, S.T.S. Electroimpact compaction of pm components, Powder Metall. 30 (1987) 29-36

Allen, M.J. Myer, B.J. Millet, P.J. Rushton, N. The effects of particulate cobalt, chromium and cobalt-chromium alloy on human osteoblast-like cells in vitro, J Bone Joint Surg Br. 79 (1997) 475-482

Anselmi-Tamburini, U. Gennari, S. Garay, J.E. Groza, J.R Munir, Z.A. Fundamental investigations on the spark plasma sintering/synthesis process: II. Modeling of current and temperature distributions, Mater Sci Eng A. 394 (2005) 139-148

Archard, J.F. Contact and Rubbing of Flat Surface, J Appl Phys. 24 (1953) 981–988

Armstrong, R.D. Briggs, G. W. D. Charles, E. A. Some effects of the addition of cobalt to the nickel hydroxide electrode, J. Appl. Electrochem. 18 (1988) 215-219

Artola, A. Gurruchaga, M. Vázquez, B. San Román, J. Goñi, I. Elimination of barium sulphate from acrylic bone cements. Use of two iodine-containing monomers, Biomaterials. 24 (2003) 4071-4080

ASTM E92, Standard test method for Vickers hardness of metallic materials, ASTM International, West Conshohocken, PA (2003)

ASTM F1537, Standard Specification for Wrought Cobalt-28Chromium-6Molybdenum Alloys for Surgical Implants, ASTM International, West Conshohocken, PA (2000)

ASTM F732, Standard Test Method for Wear Testing of Polymeric Materials Used in Total Joint Prostheses, ASTM International, West Conshohocken, PA (2006)

ASTM Standard F75 Standard specification for cast cobalt–chromium–molybdenum alloy for surgical implant applications, ASTM International, West Conshohocken, PA (1998)

ASTM Standard G133, Standard test method for linearly reciprocating ball-on-flat sliding wear, ASTM International, West Conshohocken, PA (2002)

Athanasou, N.A. Quinn, J. Bulstrode, C.J.K. Resorption of bone by inflammatory cells derived from the joint capsule of hip arthroplasties, J Bone Joint Surg Br. 74 (1992) 57-62

Athavaley, A. UPDATE: Stryker 4Q Profit Rises 36% As Revenue Strengthens, Dow Jones Newswires (2012)

Atkinson, J.R. Dowson, D. Isaac, J.H. Wroblewski, B.M. Laboratory wear tests and clinical observations of the penetration of femoral heads into acetabular cups in total replacement hip joints ID, Wear. 104 (1985) 225-244

Audi, G. The NUBASE evaluation of nuclear and decay properties, Nucl Phys A. 729 (2003) 3–128

Ball, S.T. LeDuff, M.J. Amstutz, H.C. Early results of conversion of a failed femoral component in hip resurfacing arthroplasty, J Bone Joint Surg Am. 89 (2007) 735-741

Bardos, D.I. High strength Co-Cr-Mo alloy by hot isostatic pressing of powder, Biomater Med Devices Artif Organs. 7 (1979) 73-80

Bates J.F. Knapton, A. G. Metal and alloy in dentistry, Int Met Rev. 22 (1977) 39-60

Becker, B.S. Bolton, J.D. Youseffi, M. Production of porous sintered co-cr-mo alloys for possible surgical implant applications: 1. Compaction, sintering behavior, and properties, Powder Metall. **38** (1995) 201-208

Behl, C. Davis, J.B. Lesley, R. Schuburt, D. Hydrogen peroxide mediates amyloid beta protein toxicity, Cell. 77 (1994) 817-827

Bhatt, H. Goswami, T. Implant wear mechanisms-basic approach. Biomed Mater. 3 (2008) 1-9

Black, J. Biological Performance of Materials, Plenum, New York (1984)

Black, J. Biological Performance of Materials: Fundamentals of Biocompatibility, Marcel Deckker, New York, USA (1992)

Black, J. Metal on Metal Bearings: A Practical Alternative to Metal on Polyethylene Total Joints?, Clin. Orthop Relat Res. 329 (1996) S244-255

Birrell, F. Johnell, O. Silman, A. Projecting the need for hip replacement over the next three decades: influence of changing demography and threshold for surgery, Ann Rheum Dis. 58 (1999) 569-572

Boesel, R.W. Jacobson, M.I. Yoshioka, I.S. Spark sintering tames exotic P-M materials, Mater Eng. 70 (1969) 32-35

Boncoeur, M Palacio, M. Hot Isostatic Pressing. Ind Cream. 775 (1983) 601

Brandes, E.A. Brook, G.B. Smithells metals reference book. 7th ed. London: Butterworth–Heinemann (1992)

Branemark, P.I. Breine, U. Johansson, B. Roylance, P.J. Röckert, H. Yoffey, J.M. Regeneration of bone marrow, Acta Anat. 59 (1964)1–46

Britannica, Encyclopædia Britannica Online. Hip joint,http://www.britannica.com/ EBchecked/ media/66073/Section-through-a-hip-joint (2010)

Brodner W, Bitzan P, Meisinger V. Kaider, A. Gottsauner-Wolf, F. Kotz, R. Elevated serum cobalt with metal-on-metal articulating surfaces, J Bone Joint Surg Br. 79 (1997) 316-321

Bruesch, P. Muller, K. Atrens, A. Neff, H. Corrosion of stainless steels in chloride solution — an XPS investigation of passive films, Appl Phys A. 38 (1985) 1-18

Buckley, D.H. Adhesion, friction and wear of cobalt and cobalt based alloys, Cobalt. 38 (1969) 20-28

Bunea, D. Bojin, D. Zamfir, S. Miculescu, F. Miculescu, M. Experimental researches concerning the Co-Cr-Mo alloys used in implantology. Eur Cells Mater. 5 (2003) S53-54

Campbell, P. McKellop, H. Alim, R. Mirra, J. Nutt, S. Dorr, L. Amustutz, H.C Metal-on-metal hip replacements: Wear performance and Cellular response to wear particles, ASTM International. (1999) 193-209

Carr R, Hole P, Malloy A. Sizing of nanoparticles by visualising and simultaneously tracking the Brownian motion of nanoparticles separately within a suspension. Abstract of the 8th International Congress on Optical Particle Characterisation, 9-13 July 2007, Karl Franzens University, Graz, Austria, p.25

Carr, R.J.G. Hole P, Malloy M. Nanoparticle detection and analysis – tracking nanoparticles in a sample, directly and individually, to give high resolution particle size distributions. Abstract of the International Conference on Nanoparticles for European Industry II, Olympia, London, 2007a

Case, C.P. Langkamer, V.G. James, C. Palmer, M.R. Kemp, A.J. Heap, P.F. Solomon, L. Widespread dissemination of metal debris from implants, J Bone. Joint Surg Br. 76 (1994) 701-712

Catelas, I. Bobyn, D.. Medley, J. B Krygier, J.J. Zukor, D.J. Petit, A. Huk, O.L. Effects of digestion protocols on the isolation and characterization of metal–metal wear particles. I. Analysis of particle size and shape, J Biomed Mater Res. 55 (2001) 320–329

Caudillo, M. Herrera-Trejo, M. Castro, M.R. Ramirez, E. Gonzalez, C.R. Juarez, J.I. On carbide dissolution in an as-cast ASTM F75 alloy, J Biomed Mater Res. 59 (2002)378-385

Cawley, J. Metcalf, J.P. Jones, A.H. Band, T.J. & Skupien, D.S. A tribological study of cobalt chromium molybdenum alloys used in metla-on-metal resurfacing hip arthroplasty, Wear. 255 (2003) 999-1006

Cellard, A. Garnier, V. Fantozzi, G. Baret, G. Fort, P. Wear resistance of chromium oxide nanostructured coatings, Ceram Int. 35 (2009) 913–916

Charnley, J. Anchorage of the femoral head prosthesis to the shaft of the femur, J Bone Joint Surg. 42 (1960) 28–30

Charnley, J. Total prosthetic replacement of the hip, Reconstr Surg. Traumatol. 11 (1969) 9-19

Chiba, A. Kumagai, K. Nomura, N. Satoru, M. Pin-on-disk wear behavior in a like-on-like configuration in a biological environment of high carbon cast and low carbon forged Co–29Cr–6Mo alloys. Acta Materialia. 55 (2007) 1309–1318

Chisea R, Moscatelli M, Giordano C, Siccardi F, Cigada A, Influence of heat treatment on structural, mechanical and wear properties of crosslinked UHMWPE, J Appl Biomater Biomech. 2 (2004) 20-28

Chiesa R, Tanzi MC, Alfonsi S, Paracchini L, Moscatelli M, Cigada A, Enhanced wear performance of highly crosslinked UHMWPE for artificial joints, J Biomed Mater Res. 50 (2000) 381-387

Clarke, I.C. Campbell, P. Kossovsky, N. Debris-mediated osteolysis – a cascade phenomenon involving motion, wear, particulates, macrophages induction and bone lysis. ASTM SEDL. STP 1144 (1992) 7-26

Clarke, I.C. Role of ceramic implants, Clin. Orthop Relat Res. 282 (1992) 19-39

Clemow, A.J.T. Daniell, B.L. Solution Treatment Behavior of Co-Cr-Mo alloy, J Biomed Mater Res. 13 (1979) 265-279

Clyens, S. Al-Hassani, S.T.S. Johnson, W. The compaction of powder metallurgy bars using high voltage electrical discharges, Int. J. Mech. Sci. 18 (1976) 37-40

Cobb, A.G. Schmalzreid, T.P. The clinical significance of metal ion release from cobalt–chromium metal-on-metal hip joint arthroplasty, P. I. Mech. Eng. H. 220 (2006) 385-397

Cocen, U. Onel, K. Ductility and strength of extruded SiCp/aluminium-alloy composites. Compos Sci Technol. 62 (2002) 275-282

Cohen, D. Out of joint: The story of the ASR, BMJ. 342 (2011) 1-9

Considine, G.D. Molybdenum. Van Nostrand's Encyclopedia of Chemistry. New York: Wiley-Interscience. (2005)

Cramer, G.D. Powder metallurgy U.S. Patent 2,355,954, August (1944)

Daniel, J. Pynsent, P.B. McMinn, D.J. Metal-on-metal resufacing of the hip in patients under the age of 55 years with osteoarthritis, J Bone Joint Surg-Br. 86 (2004) 177-184

Darby Jr., J.B. Beck, P.A. Intermediate Phases in the Cr-Mo-Co System of 1300°C, Trans. AIME. 203 (1955) 765-766

Davis, J.R. Handbook of materials for medical devices, Ch. 1. Materials Park, OH: ASM International (2003)

Davis, J.R. ASM Specialty Handbook: Nickel, Cobalt, and Their Alloys, ASM International Handbook Committee (2001)

Davis, J.R. Cast Irons. Ohio: ASM International. (1996) 117

De Groat, G. One-Shot Powder Metal Parts, Am Mach. 109 (1965) 107-109
De Mol van Otterloo, J.L. JDe Hosson, Th.M. Microstructure and abrasive wear of cobalt-based laser coatings, Scripta Mater. 36 (1997) 239-245

Deidar, M.M. Yoon, H.C. Lim, J.K. Mechanical properties of metals for biomedical applications using powder metallurgy process: A review, Met Mater Int. 12 (2006) 193-206

Dennis, J.K. Such, T.E. History of Chromium Plating, Nickel and Chromium Plating. Woodhead Publishing. (1993) 9–12

Deren, J. Haber, J. Podgorecka, A. Burzyk, J. Physicochemical and Catalytic Properties of the System Chromium Oxides-Oxygen-Water, J Catal. 2 (1963) 161-175

Devine, T. M. Wulff, A. Cast vs. wrought cobalt-chromium surgical implant alloys J Biomed Mater Res. 9 (1975) 151-167

Di Bona, K. R. Love, S. Rhodes, N. R. McAdory, D.. Sinha, S. H Kern, N. Kent, J. Strickland, J. Wilson, A. Beaird, J. Ramage, J.. Rasco, J. F. Vincent J. B. Chromium is not an essential trace element for mammals: effects of a low-chromium diet, J Biol Inorg Chem. 16 (2011) 381-390

Disegi, J.A. Kennedy, L. Pilliar, R. Cobalt-Base Alloys for Biomedical Applications. ASTM International (1999)

Dobbs, H.S. Robertson, J.L.M. Heat treatment of cast Co-Cr-Mo for orthopaedic implant use, J Mate Sci. 18 (1983) 391-401

Doorn, P.F. Campbell, P.A. Worrall, J. Benya, P.D. McKellop, H.A. Amstutz, H.C. Metal wear particle characterization from metal-on-metal total hip replacements: transmission electron microscopy study of periprosthetic tissues and isolated particles, J Biomed Mater Res. 42 (1998) 103-111

Donachie, M.J. Superalloys: A Technical Guide. ASM International (2002)

Doshi, N. Mitragotri S. Macrophages Recognize Size and Shape of Their Targets, PLoS One. 5 (2010) e10051

Dourandish, M. Godlinski, D. Simchi, A. Firouzdor, V. Sintering of biocompatible P/M Co-Cr-Mo alloy (F75) for fabrication of porosity-graded composite structures, Mat Sci Eng A. 472 (2008) 338-346

Dowson, D. Hardaker, C. Flett, M. Issac, G.H. A hip joint simulator study of the performance of metal-on-metal joints. Part I: The role of materials, J Arthroplasty. 19 (2004) 118-123

Dowson, G. Powder Metallurgy, The Process And Its Products. A.Hilger (1st ed.) The University of Michigan, USA (1990)

Dumbleton, J.H. Manley, M.T. Metal-on-metal total hip replacement: What does the literature say?, J Arthroplasty. 20 (2005) 174–188

Dusza, J. Blugan, G. Morgiel, J. Kuebler, J. Inam, F. Peijs, T. Reece, M.J. Puchy, V. Hot pressed and spark plasma sintered zirconia / carbon nanofibre composites, J Euro Ceram Soc. 29 (2009) 3177-3184

Duval d'Adrian, A.L. Article of fused metallic oxide and process of producing the same U.S. Patent 1,430,724, October (1922)

Edwards III, C.K. Ghiasuddin, S.M. Schepper, J.M. Yunger, L.M. Kelley, K.W. A newly defined property of somatotropin: priming of macrophages for production of superoxide anion, Science. 239 (1988) 769-771

Eisen, W.B. Metal Hand Book, Powder Metallurgy (10^{th} ed.) Ohio: ASM International, USA (1984)

El Dahshan, M.E. Stringer, J. Whittle, D.P. The oxidation of cobalt-chromium-carbon alloys, Anti-Corros Methods M. 22 (1975) 10-14

Elkabir, G. Rabenberg, L. Persad, C. Marcus, H.L. Microstructural evaluation of a high-energy high-rate p/m processed aluminum alloy, Scripta Metall. 20 (1986) 1411-1416

Emsley, J. Chromium. Nature's Building Blocks: An A-Z Guide to the Elements. Oxford, England, UK: Oxford University Press. (2001) 495–498

Emsley, J. Nature's Building Blocks. Oxford: Oxford University Press. (2001a) 262–266.

Eric, W. Lee, M.D. & Hubert, T.K. Early fatigue failures of cemented, forged, cobalt-chromium femoral stems at the neck–shoulder junction, J Arthroplasty. 16 (2001) 236-238

Ervin, D.R. Bourell, D.L. Persad, C. Rabenberg, L. Structure and properties of high energy, high rate consolidated molybdenum alloy TZM, Mater Sci Eng A. 102 (1988) 25-30

Essner, A. Sutton, K. Wang, A. Hip simulator wear comparison of metal-onmetal, ceramic-on-ceramic and crosslinked UHMWPE bearings, Wear. 259 (2005) 992-995

Evans, E.M. Freeman, M.A.R. Miller, A.J. Metal sensitivity as a cause of bone necrosis and loosening of the prosthesis in total joint replacement, J Bone Joint Surg Br. 56 (1974) 626-642

Faleiro, C. Godinho, I. Reus, U. De Sousa, M. Cobalt-chromium-molybdenum but not titanium-6aluminium-4vanadium alloy discs inhibit T cell activation in vitro, Biometals. 9 (1996) 321-326

FDA. Concerns about metal-on-metal hip implant systems. (2011)

Ferroni, D. Qualini, V. Thermal stabilization of highly crosslinked UHMWPE: A comparative study between annealed and remelted resins, J Appl Biomater Biomech. 8 (2010) 82-88

Fisher, J. Ceramic-on-metal hip implants to undergo trials, Adv Mater Processes. 163 (2005) 60-61

Fisher, J. Dowson, D. Tribology of total artificial joints, P I Mech Eng H. 205 (1991)73-79

Fisher, J. Hu, X.Q. Stewart, T.D. Williams, S. Tipper, J.L. Ingham, E. Stone, M.H. Davies, C. Hatto, P. Bolton, J. Riley, M. Hardaker, C. Issac, G.H. Berry, G. Wear of surface engineered metal-on-metal hip prostheses, J Mater Sci Mater M. 15 (2004) 225-235

Fleck, N.A. On the coldcompaction of powders. J Mech Phys Solids. 43 (1995) 1409-1431

Fleury, C. Petit, A. Mwale, F. Antoniou, J. Zukor, D.J. Tabrizian, M. Effect of cobalt and chromium ions on human MG-63 osteoblasts in vitro: morphology, cytotoxicity, and oxidative stress, Biomaterials. 27 (2006) 3351–3360

Frenk, A. Kurz, W. Microstructural effects on the sliding wear resistance of a cobalt-based alloy, Wear. 174 (1994) 81-91

Friberg, L. Nordberg, G.F. & Vouk, V.B. Handbook on the toxicology of metals. Amsterdam, The Netherlands: Elsevier/North-Holland Biomedical (1979)

Gagnon, S. Molybdenum, Jefferson Science Associates, LLC. (2007)

Gao, L. Wang, H.Z. Hong, J.S. Miyamoto, H. Miyamoto, K. Nishikawa, Y. Torre, S.D.D.L. SiC-ZrO2(3Y)-Al2O3 nanocomposites superfast densified by spark plasma sintering, Nanostruct Mater. 11 (1999) 43-49

German, R.M. Powder Metallurgy Science. Princeton, New Jersey: Metal Powder Industries Federation (1984)

Gilson, E.G. Hard-metal composition and method of making the same, U.S. Patent 1,756,857, April (1930)

Ginebra, M.P. Fernandez, E. De Maeyer, E.A.P. Verbeek, R.M.H. Boltong, M.G. Ginebra, J. Driessens, F.C.M. & Planell, J.A. Setting Reaction and Hardening of an Apatitic Calcium Phosphate Cement, J Dent Res. 76 (1997) 905-912

Ginebra, M.P. Traykova, T. Planell, J.A. Calcium phosphate cements as bone drug delivery systems: a review, J Control Release. 113 (2006) 102-110

Goetzel, C.G. De Marchi V.S. Electrically activated pressure sintering (spark sintering) of titanium aluminum vanadium alloy powders, Powder Metall Int. 3 (1971) 80-134.

Gopalsami, N. Chien, H.T. Goldberger, WMerkle, B. Borton, J. Development of ultrasonic sensor for non-intrusive measurement of temperature in powder materials, Powder Metall. 45 (2002) 271-275

Gradzka-Dahlke, M. Dabrowski, J.R. Dabrowski, B. Modification of mechanical properties of sintered implant materials on the base of Co-Cr-Mo alloy, J Mater Process Tech. 204 (2008) 199-205

Grammatopolous G, Pandit H, Kwon YM, Gundle R, McLardy-Smith P, Beard DJ, et al. Hip resurfacings revised for inflammatory pseudotumour have a poor outcome, J Bone Joint Surg Br. 91 (2009) 1019-1024

Greetham, G. Powder Metallurgy – processing. Materials information Service (2001)

Grigoriev, E.G. Rosliakov, A.V. Electro-discharge compaction of WC-Co and W-Ni-Fe-Co composite materials, J. Mater. Process. Technol. 191 (2007) 182-184

Groza, J.R. Risbud, S.H. Yamanaki, K. Plasma activated sintering of additive-free AlN powders to near-theoretical density in 5 minutes, J. Mater. Res. 7 (1992) 2463-2645

Guertin, J. Jacobs, J.A. Avakian, C.P. Chromium (VI) Handbook. CRC Press. (2005) 7–11

Gupta, K.P. 2005 The Co-Cr-Mo (cobalt-chromium-molydenum) system, J Phase Equilib Diff. 26 (2005) 87-92

Hallab, N. Merritt, K. Jacobs, J.J. Metal sensitivity in patients with orthopaedic implants, J Bone Joint Surg Am. 82 (2001) 428-428

Hamadouche, M. Boutin, P. Daussange, J. Bolander, M.E. Sedel, L. Alumina-on-Alumina Total Hip Arthroplasty : A Minimum 18.5-Year Follow-up Study. J Bone Joint Surg Am. 84 (2002) 69-77

Hanawa, T. Hiromoto, S. Asami, K. Characterization of the surface oxide film of a Co–Cr–Mo alloy after being located in quasi-biological environments using XPS, Appl Surf Sci. 183 (2001) 68–75

Hanawa, T. Metal ion release from metal implants, Mater Sci Eng C. 24 (2004) 745-752

Hansen, K. Mossman, B.T. Generation of superoxide (O_2) from alveolar macrophages exposed to asbestiform and nonfibrous particles, Cancer Res. 47 (1987) 1681-1686

Harris, K. and Sikkenga, S. Investment Cast Cobalt Alloys, 24th BICTA Conference on Investment Casting. 8 (1999) 1-10

Harris, W.H. Osteolysis and particle disease in hip replacement: A review, Acta Orthop. 65 (1994) 113-123

Hartmut, F.H. Veron, C. Martin, P. Cobalt dental alloys and allergic reactions to nickel-chromium, an overview, Biomaterials. 10 (1989) 545-548

Hashimoto, K. Asami, K. Naka, M. Masumoto, T. The role of alloying elements in improving the corrosion resistance of amorphous iron base alloys, Corros Sci. 19 (1979) 857-867

Haute Authorite de Sante. Commision d'evaluation des produits et prestations (2008)

Hawkins, M. Why we need cobalt?, T I Min Metall B. 110 (2001) 66–71

Haynes, D.R. Rogers, S.D. Hay, S. The differences in toxicity and release of bone-resorbing mediators induced by titanium and cobalt-chromium-alloy wear particles, J Bone Joint Surg Am. 75 (1993) 825-834

Hebrard, F. Kalck, P. Cobalt-Catalyzed Hydroformylation of Alkenes: Generation and Recycling of the Carbonyl Species, and Catalytic Cycle, Chem Rev. 109 (2009) 4272–4282

Heimann, P.M. Moseley's Interpretation of X-Ray Spectra, Centaurus. 12 (1968) 261-274

Hench L.L. Ethridge, E.C. Biomaterials-the interfacial problem, Adv Biomed Eng. 5 (1975) 35-150

Hench, L.L. Wilson, J. Introduction to Bioceramics. Singapore: World Scientific (1993)

Hermawan, H. Ramdan, D Djuansjah, J.R.P. Metals for Biomedical Applications. Biomedical Engineering - From Theory to Applications. InTech. (2011)

Hingston, J. Leaching of chromated copper arsenate wood preservatives: a review, Environ Pollut. 111 (2001) 53–66

Hjelm, P.J. Versuche mit Molybdäna, und Reduction der selben Erde". Svenska vetensk. Academ. Handlingar 49 (1788) 268

Hoyt, S.L. Hard metal composition and method of making the same, U.S. Patent 1,843,768, February (1932)

Hull, A.W. A new method of chemical analysis, J Am Chem Soc. 41 (1919) 41 1168-1175

Hung, J.-P. Wu, J.S.-S. A comparative study on wear behavior of hip prosthesis by finite element simulation, Biomed Eng Appl Basis Comm. 14 (2002) 139-148

IARC. Surgical implants and other foreign bodies— composite medical and dental implants. IARC monographs on the evaluation of carcinogenic risks to humans. Lyon (France): International Agency for Research on Cancer (IARC) (1999) 157.

Inam, F. Development of Ceramic – Carbon Nanotube (CNT) Nanocomposites, PhD Thesis, Queen Mary, University of London (2009)

Inam, F. Yan, H. Reece, M.J. Peijs, T. Dimethylformamide: an effective dispersant for making ceramic–carbon nanotube composites, Nanotechnology. 19 (2008) 1-5

Ingham E, Fisher J. Biological reactions to wear debris in total joint replacement, Proc Inst Mech Eng. 214 (2000) 21-37

Inoue, K. Electric-discharge sintering, U.S. Patent 3,241,956, March (1966)

Inoue, K. Apparatus for electrically sintering discrete bodies, U.S. Patent 3,250,892, May (1966a)

Inoue, K. Servocontrol system for discharge sintering, U.S. Patent 3,508,029, April (1970)

ISO 10933-12 Tests for cytotoxicity: in vitro methods. Biological evaluation of medical devices. Geneva, Switzerland: International Organization for Standardization (1992)

Ivankovic, S. Preussmann, R. Absence of toxic and carcinogenic effects after administration of high doses of chromic oxide pigment in subacute and longterm feeding experiments in rats, Fd Cosmet. Toxicol. 13 (1975) 347-351

Jacobs, J.J. Goodman, S.B. Sumner, D.R. Biologic response to orthopaedic implants. In: Buckwalter, J.A. Einhorn, T.A. Simon, S.R. Orthopaedic basic science: biology and biomechanics of the musculoskeletal system. Rosemont (Ill): American Academy of Orthopaedic Surgeons. (2000) 401

Jacobs, J.J. Shanbhag, A. Glant, T.T. Black, J. Galante, J.O. Wear Debris in Total Joint Replacements, J Am Acad Orthop Sur. 2 (1994) 212-220

Jacobs, J.J. Skipor, A.K. Doorn, P.F. Cobalt and chromium concentrations in patients with metalon metal total hip replacements, Clin Orthop. 329 (1996) S256-263

James, P.J. Particle deformation during cold isostatic pressing of metal powders. Powder Metall. 4 (1977) 199-204

Janaki Ram, G.D. Esplin, C.K. Stucker, B.E. Microstructure and wear properties of LENS® deposited medical grade CoCrMo, J Mater Sci Mater Med. 19 (2008) 2105-2111

Jaroszewicz, J. Michalski, A. Preparation of a TiB_2 composite with a nickel matrix by pulse plasma sintering with combustion synthesis, J Eur Ceram Soc. 26 (2006) 2427-2430

Jasty, M. James, S.P. Bragdon, C.R. Goetz, D.D. Lee, K. Hanson, A. Harris, W.H. Patterns and mechanisms of wear in polyethylene acetabular components retrieved at revision surgery, J Bone Joint Surg Am. 79 (1997) 349-358

Jazarawi, L.M. Bogner, E. Della Valle, C.J. Chen, F.S. Pak, K.I. Stuchin, S. Frankel, V.H. Di Cesare, P.E. Wear rates of ceramic-on-ceramic bearing surfaces in total hip implants: A 12-year follow-up study. J Arthoplasty. 14 (1999) 781-787

Johnson, D.L. Microwave and plasma sintering of ceramics, Ceram Int. 17 (1991) 295-300

Johnson, W. Clyens, S. Al-Hassani, S.T.S. Compaction of metal powders using high voltage electrical discharges and rotary swaging, Metall Met Form. 43 (1976) 382-385

Johnsson R. Thorngren, K.G. Function after total hip replacement for primary osteoarthritis, Int Orthop (SICOT) 13 (1989) 221-225

Johnston Jr., R.B.. Godzik, C.A Cohn, Z.A. Increased superoxide anion production by immunologically activated and chemically elicited macrophages, J Exp Med. 148 (1978) 115-127

Jones, W.D. Powder metallurgy, Met Ind. (1940) 69

Joshi, A. Markovic, L. Hardinge, K. Murphy, J. Total hip arthroplasty in ankylosing spondylitis: An analysis of 181 hips, J Arthroplasty. 17 (2002) 427-433

Kalyanaraman, R. Yoo, S. Krupashankara, M.S. Sudarshan, T.S. Dowding, R.J. Synthesis and consolidation of iron nanopowders, Nanostruct Mater. 10 (1998) 1379-1392

Kelly, E.J. Electrochemical behavior of titanium, Mod Aspect Electrochem. 14 (1982) 319-424

Kennard, F. Cold Isostatic Pressing. ASM International, Engineered Materials Handbook. Vol. 4: Ceramics and Glasses (USA) (1991) 147-152

Kim, H.C. Shon, I.J.. Ko, I.Y Yoon, J.K. Doh, J.M. Lee, G.W. Fabrication of ultrafine binderless WC and WC-Ni hard materials by a pulsed current activated sintering method, J Ceram Process Res. 7 (2006) 224-229

Kimura, H. Powder processing and mechanical characteristics of fully dense nano-intermetallics, Nanostruct Mater. 9 (1997) 93-96

Kircher, R.S. Christensen, A.M. Wurth K.W. Electron Beam Melted (EBM) Co-Cr-Mo Alloy for Orthopaedic Implant Applications, SFF Proceedings (2009) 428-436

Kitahara, J. Yamanaka, K. Kato, K. Lee, Y.W. Klein, C.B. Costa, M. Mutagenicity of cobalt and reactive oxygen producers, Mutat Res. 370 (1996) 133–140

Kocijan, A. Milosev, I. Pihlar, B. Cobalt-based alloys for orthopaedic applications studied by electrochemical and XPS analysis, J Mater Sci Mater Med. 15 (2004) 643-650

Konttinen, Y. T. Zhao, D. Beklen, A. Ma, G. Takagi, M. Kivelä-Rajamäki, M. Ashammakhi, N. The Microenvironment around Total Hip Replacement Prostheses. Clin. Orthop. Relat. R. 430 (2005) 28-38

Koseki, H. Shindo, H. Furuichi, I. Baba, K. Carbon ion implantation improves the tribological properties of Co-Cr-Mo alloy against ultra-high molecular weight polyethylene, Surf Interface Anal. 40 (2008) 1278-1283

Kurtz, S.M. The UHMWPE handbook: ultra high molecular weight polyethylene in total joint replacement, Elsevier Academic Press, London (2004)

Kyomoto, M. Miwa, Y. Pezzotti, G. Strain in UHMWPE for orthopaedic use studied by Raman microprobe spectroscopy, J Biomat Sci Polym E. 18 (2007) 165-178

Langkamer, V.G. Case, C.P. Heap, P. Taylor, A. Collins, C. Pearse, M. Systemic distribution of wear debris after hip replacement, A cause for concern? J Bone Joint Surg Br. 74 (1992) 831–839

Langton, D.J. Jameson, S.S. Joyce, T.J. Hallab, N.J. Natu, S. Nargol, A.V. Early failure of metal-on-metal bearings in hip resurfacing and large-diameter

total hip replacement: a consequence of excess wear, J Bone Joint Surg Br. *92* (2010) 38-46

Lavigne, M. Belzile, E.L. Roy, A. Morin, F. Amzica, T. Vendittoli, P.-A. Comparison of whole-blood metal ion levels in four types of metal-on-metal large diameter femoral head total hip arthroplasty: the potential influence of the adapter sleeve, J Bone Joint Surg Am. 93 (2011) 128-136

Lee, B. Alsenz, R. Ignatiev, A. Van Hove, M. Surface structures of the two allotropic phases of cobalt, Phys Rev B. 17 (1978) 1510-1520

Lee, S.H. Brennan, F.R. Jacobs, J.J. Human monocyte/macrophage response to cobalt-chromium corrosion products and titanium particles in patients with total joint replacements, J Orthop Res. 15 (1997) 40-49

Lee, S-.H. Nomura, N. Chiba, A. Microstructure and mechanical properties of biomedical Co-Cr-Mo alloys with combination of N addition and Cr-enrichment, 1st Asian Biomaterials Congress, Tsukuba, Japan (2007)

Lenel, F.V. Resistance sintering under pressure, J Met. 7 (1955) 158-167

Leszek, W. Jan Dabrowskib, R. Zbigniew, O. Porosity structure and mechanical properties of vitalium-type alloy for implants. Mater Charact. 46 (2001) 221-225

Levina, A. Harris, H.H. Lay, P.A. Binding of chromium(VI) to histones: implications for chromium(VI)-induced genotoxicity, J Biol Inorg Chem. 11 (2006) 225–234

Lhotka, C. Szekeres, T. Steffan, I. Four-year study of cobalt and chromium blood levels in patients managed with two different metal-on-metal total hip replacements, J Orthop Res. 21 (2003) 189-195

Long, M. Rack, H.J. Titanium alloys in total joint replacement—a materials science perspective, Biomaterials. 19 (1998) 1621-1639

Lopez, H.F. Saldivar-Garcia, A.G. Martensitic transformation in a cast Co-Cr-Mo-C alloy, Metall Mater Trans A. 39 (2008) 8-18

Ma, Y.H. Akis, B.C. Ayturk, M.E. Guazzone, F. Engwall, E.E. Mardilovich, I.P. Characterization of Intermetallic Diffusion Barrier and Alloy Formation for Pd/Cu and Pd/Ag Porous Stainless Steel Composite Membranes, Ind Eng Chem Res. 43 (2004) 2936–2945

Maloney, W.J. Smith, R.L. Periprosthetic osteolysis in total hip arthroplasty: the role of particulate debris, J Bone Joint Surg. 77 (1995) 1448-1461

Massalski, T.B. Binary Alloy Phase Diagrams, ASM International, Materials Park, Ohio, USA (1990)

Matsugi, K. Ishibashi, N. Hatayama, T. Yanagisawa, O. Microstructure of spark sintered titanium-aluminide compacts, Intermetallics. 4 (1996) 457-467

Maynard, J.A. Pedrini, V.A. Pedrini-Mille, A. Romanus, B. Ohlerking, F. Morphological and biochemical effects of sodium morrhuate on tendons, J Orthop Res. 3 (1985) 236-248

McGee, M.A. Howie, D.W. Costi, K. Haynes, D.R. Wildenauer, C.I. Pearcy, M.J. McLean, J.D. Implant retrieval studies of the wear and loosening of prosthetic joints: a review, Wear. 241 (2000) 158-165

McKee, G.K. Watson-Farrar, J. Replacement of arthritic hips by the McKee-Farrar prosthesis, J Bone Joint Surg Br. 48 (1966) 245-259

Mcminn, D.J.W. Development of metal/metal hip resurfacing, Hip Int. 13 (2003) 41-53

Merritt, K. Brown, S.A. Distribution of cobalt chromium wear and corrosion products and biologic reactions, Clin Orthop Relat Res. 329 (1996) S233–243

Merritt, K. Brown, S.A. Effect of proteins and pH on fretting corrosion and metal ion release, J Biomed Mater Res. 22 (1988) 111-20

MHRA. Minutes of the committee on the safety of devices meeting 19 July 2001. www.mhra.gov.uk/home/groups/escb/documents/committeedocument /con003574.pdf.

Michalski, A. Jaroszewicz, J. Rosinski, M. The Synthesis of NiAl Using the Pulse Plasma Method with the Participation of the SHS Reaction, Int J Self-propag High-temp Synth. 12 (2003) 237-246

Michalski, A. Jaroszewicz, J. Rosinski, M. Siemiaszko, D. NiAl-Al_2O_3 composites produced by pulse plasma sintering with the participation of the SHS reaction, Intermetallics. 14 (2006) 603-606

Michalski, A. Siemiaszko, D. Nanocrystalline cemented carbides sintered by the pulse plasma method, Int J Refract Met Hard Mater. 25 (2007) 153-158

Michel, R. Noite, M. Reich, M. Loer, F. Systemic effects of implanted prostheses made of cobalt-chromium alloys, Arch Orthop Trauma Surg. 110 (1991) 61-74

Milogev, I. PiSot, V. Campbell, P. Serum levels of cobalt and chromium in patients with Sikomet metal-metal total hip replacements, J Orthop Res. 23 (2005) 526-535

Mineta, S. Namba, S. Yoneda, T. Ueda, K. Narushima, T. Carbide Formation and Dissolution in Biomedical Co-Cr-Mo Alloys with Different Carbon Contents during Solution Treatment, Metall Mater Trans A. 41 (2010) 2129-2138

Moghaddas, S. Gelerinter, E. Bose, R.N. Mechanisms of formation and decomposition of hypervalent chromium metabolites in the glutathione–chromium(VI) reaction, J Inorg Biochem. 57 (1995) 135–146

Montero-Ocampo, C. Juarez, R. Salinas-Rodriguez, A. Effect of Fcc-Hcp phase transformation produced by isothermal aging on the corrosion resistance of a Co-27Cr-5Mo-0.05C Alloy, Metall Mater Trans A. 33 (2002) 2229-2235

Montero-Ocampo, C. Talavera, M. Lopez, H. Effect of alloy preheating on the mechanical properties of as-cast Co-Cr-Mo-C alloys, Metall Mater Trans A. 30 (1999) 611-620

Morral, F. R. Cobalt alloys as implants in humans, J Mater. 1 (1966)384–412.

Mont, M.A. Jones, L.C. Hungerford, D.S. Current Concept Review: Non Traumatic Osteonecrosis of the Femoral Head, J Bone Joint Surg Am. 88 (2006) 1117-1132

Muirhead-Allwood SK. Lessons of a hip failure, BMJ 316 (1998) 644-650

Munir, Z.A. Anselmi-Tamburini, U. Ohyanagi, M. The effect of electric field and pressure on the synthesis and consolidification of materials: a review of the spark plasma sintering method, J Mater Sci. 41 (2006) 763-777

Munir, Z.A. Quach, D.V. Electric Current Activation of Sintering: A Review of the Pulsed Electric Current Sintering Process, J Am Ceram Soc. 94 (2011) 1–19

Murray, D.W. Carr, A.J. Bulstrode, C.J. Which primary total hip replacement? J Bone Joint Surg Br.77 (1995) 520-527

Murray, D.W. Rushton, N. Macrophages stimulate bone resorption when they phagocytose particles, J Bone Joint Surg. 72 (1990) 988–992

Naal, F-D. Maffiuletti, N.A. Munzinger, U. Hersche, O. Sports After Hip Resurfacing Arthroplasty, Am J Sport Med. 35 (2007) 705-711

Nanosight, The LM10 and LM20 Nanoparticle Analysis Instruments. www.nanosight.com 2011

Navarro, M. Michiardi, A. Biomaterials in Orthopeadics, J R Soc Interface. 5 (2008) 1137-1158

Nasser, S. Campbell, P.A. Kilgus, D. Kossovsky, N. Amstutz, H.C. Cementless total joint arthroplasty with titanium alloy articular surfaces, Clin Orthhop Related Res. 261 (1990) 171-185

NJR (National Joint Registry of England and Wales), 8th Annual report, M & M Communication Ltd, National Joint Centre (2011)

North, N. Owens, M. Pearson, C. Thermal stability of cast and wrought marine iron, Studies in conversation. 21 (1976) 192-197

Okazaki, K. Electro-discharge consolidation applied to nanocrystalline and RSP/MA powders, Mater Sci Eng A. 287 (2000) 189-197

Oliver, W.C. Pharr, G.M. An improved technique for determining hardness and elastic modulus using load and displacement sensing indentation experiments, Mater Res. 7 (1992) 1564-1583

Omori, M. Okubo, A. Gilhwan, K. Hirai, T. Consolidation of thermosetting polyimide by the spark plasma system, J Mater Synth Process. 5 (1997) 279-282

Orru, R. Licheri, R. Locci, A.M. Cincotti, A., Cao, G. Consolidation/synthesis of materials by electric current activated/assisted sintering, Mat Sci Eng R. 63 (2009) 127-287

Papp, J.F Lipin, B.R. Chromite: Industrial Minerals & Rocks: Commodities, Markets, and Uses (7th ed.) SME (2006)

Pang, M. Eakins, D.E Norton, M.G. Bahr, D.F. Structural and Mechanical Characteristics of Anodic Oxide Films on Titanium, Corrosion. 57 (2001) 523-531

Pardo, A. Merino, M.C. Coy, A.E. Viejo, F. Carboneras, M. Arrabal, R. Influence of Ti, C and N concentration on the intergranular corrosion behaviour of AISI 316Ti and 321 stainless steels, Acta Mater. 55 (2007) 2239-2251

Park, Y.S. Hwang, S.K. Choy, W.S. Kim, Y.S. Moon, Y.W. Lim, S.J. Ceramic failure after total hip arthroplasty with an alumina-on-alumina bearing. J Bone Joint Surg Am. 88 (2006) 780-787

Patel, B. Inam, F. Reece, M.J. Edirisinghe, M. Bonfield, W. Huang, J. Angadji, A. A novel route for processing cobalt-chromium-molybdenum orthopaedic alloys, J R Soc Interface. 7 (2010) 1641-1645

Pazzaglia, U. E. DellOrbo, C. Wilkinson, M. J. The foreign body reaction in total hip arthroplasties: a corre-lated light-microscopy, SEM and TEM study, Arch Orthop Traum Su. 106 (1985) 209–219

Peissl, S. Mori, G. Leitner, H. Ebner R. Eglsaer, S. Influence of chromium, molybdenum and cobalt on the corrosion behaviour of high carbon steels in dependence of heat treatment, Mater. Corros. 57 (2006) 759-765

Persad, C. Peterson, D.R. Zowarka, R.C. Composite solid armature consolidation by pulse power processing: A novel homopolar generator application in EML technology, IEEE Trans Magn. 25 (1989) 429-432

Petit, A. Mwale, F. Tkaczyk, C. Antoniou, J. Zukor, D.J. Huk, O.L. Induction of protein oxidation by cobalt and chromium ions in human U937 macrophages, Biomaterials 26 (2005) 4416–4422

Petit, A. Mwale, F. Tkaczyk, C. Antoniou, J. Zukor, D.J. Huk, O.L Cobalt and chromium ions induce nitration of proteins in human U937 macrophages in vitro, J Biomed Mater Res Part A. 79 (2006) 599–605

Petit, C. Taleb, A. Pileni, M.P. Cobalt nanosized particles organized in a 2d superlattice: synthesis, characterization, and magnetic properties, J Phys Chem B. 103 (1999) 1805-1810

Philipson, M.R. Westwood, M.J. Geoghegan, J.M. Henry1, A.P.J. Jefferiss, C.D. Shortcomings of the National Joint Registry: a survey of consultants' views, Ann R Coll Surg Engl. 87 (2005) 109-112

Private Healthcare UK, Private hip replacement costs in the UK and abroad. Intuition Communication Ltd (2011)

Que, L.D.L. Topoleski, T. Third-body wear of cobalt-chromium-molybdenum implant alloys initiated by bone and poly(methylmethacrylate) particles, J Biomed Mater Res. 50 (2000) 322–330

Ragan, K. An electron microscopy study of phases transformations an room temperature strengthening mechanisms in a Co-Cr-Mo-C alloy, University of Toronto (1974)

Raghunathan, S.K. Persad, C. Bourell, D.L. Marcus, H.L. High-energy, high-rate consolidation of tungsten and tungsten-based composite powders, Mater Sci Eng A. 131 (1991) 243-253

Rajagopalan, P.K. Desai, S.V. Kalghatgi, R.S. Krishnan, T.S. Bose, D.K. Studies on the electric discharge compaction of metal powders, Mater Sci Eng A. 280 (2000) 289-293

Ramirez, L.E Castro, M. Mendez, M. Lacaze, J. Herrera, M. Lesoult, G. Precipitation path of secondary phases during solidification of the Co–25.5%Cr–5.5%Mo–0.26%C alloy, Scripta Mater. 47 (2002) 811-816

Ratner, B. D. Bankman, I. Biomedical Engineering Desk Reference, Academic Press, Oxford (2009)

Ratner, B.D. Hoffman, A.S. Frederick, J.S. & Jack, E.L. Biomaterials Science: An Introduction to Materials in Medicine. Academic Press (2004)

Restrepo, C. Parvizi, J. Kurtz, S. Sharkey, P. Hozack, W. Rothman, R. The Noisy Ceramic Hip: Is Component Malpositioning the Cause? J Arthoplasty. 23 (2008) 643-649

Revell, P.A. Joint Replacement technology Woodhead Publishing Limited, Cambridge, England (2008)

Rideout, S. Manly, W.D. Kamen, E.L. Lement, B.S. Beek, P.A. Intermediate Phases in Ternary Alloy Systems of Transition Elements, Trans AIME. 191 (1951) 872-876

Ring, PA. Replacement of the hip joint, Ann R Coll Surg Engl. 48 (1971) 344-55

Riu, D.H Kong, Y.M. Kim, H.E. Effect of Cr2O3 addition on microstructural evolution and mechanical properties of Al2O3, J Eur Ceram Soc. 20 (2000) 1475-1481

Reed, T.B. Free energy of formation of binary compounds. Cambridge: MIT Press (1971)

Rosenthal, R. Cardoso, B.R. Bott, I.S. Paranhos, R.P.R. Carvalho, E.A. Phase characterisation in as-cast F75 Co-Cr-Mo-C alloy, J Mater Sci. 45 (2010) 4021-4028

Ross, W.F. Method and apparatus for making solid objects from metal powder, U.S. Patent 2,372,605, March (1945)

Saito, S. Sawaoka, A. Fast Sintering of Metal Powders Under Pressure, Powder Metall Int. 5 (1973) 70-75

Saldivar-Garcia, A.J. Lopez, H.F. Microstructural effects on the wear resistance of wrought and as-cast Co-Cr-Mo-C implant alloys, J Biomed Mater Res. 74 (2005) 269-274

Salinas-Rodriguez, A. Rodriguez-Galicia, J.L. Deformation behavior of low-carbon Co-Cr-Mo alloys for low-friction implant applications, J Biomed Mater Res. 31 (1996) 409-419

Sastry, K.Y. Froyen, L. Vleugels, J. Van der Biest, O. Schattevoy, R. Hennicke, J. Mechanical milling and field assisted sintering consolidation of nanocrystalline Al-Si-Fe-X alloy powder, Rev Adv Mater Sci. 8 (2004) 27-32

Scales, J.T. Examination of implants removed from patients. J Bone Joint Surg-Br. 53 (1971) 344–346

Schaffer, A.W. Pilger, A. Engelhardt, C.Increased blood cobalt and chromium after total hip replacement, Clin Toxicol. 37 (1999) 839-844

Scheele, C.W.K. Versuche mit Wasserbley;Molybdaena, Svenska vetensk. Academ Handlingar. 40 (1779) 238

Schmalzried, T.P. Kwong, L.M. Jasty M, Sedlacek, R C. Haire, T.C. Connor, D. Bragdon, C.R. Kabo, J.M. Malcolm, A.J. Harris, W.H. The mechanism of loosening of cemented acetabular components in total hip arthroplasty. Analysis of specimens retrieved at autopsy, Clin Orthop 274 (1992) 60-78

Schmalzried, T.P. Szuszczewicz, E.S. Peterson, T.D. Eliminating polyethylene will not put an end to osteolysis. Study of metal-metal hip implants finds resorption despite the lack of polyethylene debris, Orthop Int. 5 (1999) 308-310

Schmiedberg, S.K. Chang, D.H. Frondoza, C.G. Valdevit, A.D.C. Kostuik, J.P. Isolation and characterization of metallic wear debris from a dynamic intervertebral disc prosthesis, J Biomed Mater Res. 28 (1994) 1277-1288

Shakery, M. Al-Hassani, S.T.S. Davies, T. Electrical discharge powder compaction, J Powder Metall Int. 11 (1979) 120-124

Shanbhag, A.S. Jacobs, J.J. Black, J. Galante, J.O. Glant, T.T. Macrophage/particle interactions: Effect of size, composition and surface area, J Biomed Mat Res. 28 (1994) 81-90

Sheeja, D. Tay, B.K. Lau, S.P. Nung, L.N. Tribological characterisation of diamond-like carbon coatings on Co–Cr–Mo alloy for orthopaedic applications, Surf Coat Tech. 146-147 (2001) 410-416

Shen, Z. Peng, H. and Nygren, M. Formidable increase in the superplasticity of ceramics in the presence of an electric field, Adv Mater. 15 (2003) 1006–1009

Shimmin, A.J. Back, D. Femoral neck fractures following Birmingham hip resurfacing: a national review of 50 cases, J Bone Joint Surg Br. 87 (2005) 463-464

Sidhu, T.S. Prakash, S. Agrawal, R.D. Hot corrosion performance of a NiCr coated Ni-based alloy, Scripta Materialia. 55 (2006) 179-182

Sieber, H.P. Rieker, C.B. Ko¨ttig, P. Analysis of 118 second generation metal-on-metal retrieved hip implants, J Bone Joint Surg Br. 81 (1999) 46–50

Sims, C.T. A comptemporary view of cobalt-base alloys, J Met. 21 (1969) 27-42

Sims, C.T. Stoloff, N.S. Hagel. W.C. The Superalloys, Wiley, New York, USA (1972)

Singh, P. Birks, N. The Attack of Co-Cr Alloys by Ar-SO2 Atmospheres, Oxid Met. 13 (1979) 457–474

Skinner, H. Ceramic Bearing Surfaces. Clin Orthop Relat Res.369 (1999) 83-91

Smith, D.C. Pilliar, R.M. Metson, J.B. McIntyre, N.S. Dental implant materials. II. Preparative procedures and surface spectroscopic studies, J Biomed Mater Res. 25 (1991) 1069-1084

Smith, S.L. Burgess, I.C. Unsworth, A. Evaluation of a hip simulator, Proc Instn Mech Eng H. 213 (1999) 469-473

Snider, A.M.Jr, X-ray techniques for coatings analysis, Analysis of Paints and related materials: Current techniques for solving coatings problems, ASTM International, Philadelphia (1992) 82-104

Song, Z. Kishimoto, S. Shinya, N. A novel pulse-current-assisted sintering method for fabrication of metallic cellular structures, Adv Eng Mater. 6 (2004) 211-214

Spriano, S. Verne, E. Faga, M.G. Bugliosi, S. Maina, G. Surface treatment on an implant cobalt alloy for high biocompatibility and wear resistance, Wear. 259 (2005) 919-925

St. John, K.R. Zardiackas, L.D. Poggie, R.A. Wear Evaluation of Cobalt-Chromium alloy for use in a Metal-on-Metal Hip prosthesis, J Biomed Mater Res B. 68 (2004) 1-14

Stephen, R.J.B. Della Rocca, G. Prather, J.H. Curry, M. Maloney, W.J. Clohisy, J.C. Clinical Presentation of patients with tears of acetabular labrum, J Bone Joint Surg Am. 88 (2006) 1448 -1457

Stojilovic, N. Ehrman, J.D Bender, E.T. Tokash, J.C. Ramsier, R.D. Kovacik, M.W. Analysis of prosthetic knee wear debris extracted from synovial fluid, Appl Surf Sci. 252 (2006) 3760–3766

Storp, S. Holm, R. ESCA investigation of oxide layers on some Cr- containing alloys, Surf Sci. 68 (1977) 10-19

Streicher, R.M. Semlitsch, M. Schon, R. Weber, H. Reiker, C. Metal-On-Metal Articulation for Artificial Hip Joints: Laboratory Study and Clinical Results, P I Mech Eng H. 210 (1996) 223-232

Sullivan, C.P. Donachie, M.J. Morral, F.R. Cobalt-Base SuperAlloys 1970: a critical survey of cobalt base development with emphasis on the relationship of mechanical properties to microstructure, Centre d'Information du Cobalt, Brussels (1970)

Sumita, M. Hanawa T. Teoh**,** S.H. Development of nitrogen-containing nickel-free austenitic stainless steels for metallic biomaterials—review, Mat Sci Eng C. 24 (2004) 753-760

Sun, Y. Liang, J. Xu, Z.-H. Wang, G. Li, X. Nanoindentation for measuring individual phase mechanical properties of lead free solder alloy, J Mater Sci Mater El. 19 (2008) 514-521

Sundfeldt, M. Carlsson, L.V. Johansson, C.B. Thomsen, P. Gretzer, C. Aseptic loosening, not only a question of wear: a review of different theories, Acta Orthop. 77 (2006) 177-197

Sutula, L.C. Impact of gamma sterilization on clinical performance of polyethylene in the hip, Clin Orthop. 319 (1995) 28-40

Sweeney, H.J. Arthroscopy of the hip: Anatomy and portals, Clin Sports Med. 20 (2001) 697–702

Takagi, S. Chow, L.C. Ishikawa, K. Formation of hydroxyapatite in new calcium phosphate cements, Biomaterials. 19 (1998) 1593-1599

Takahashi, Y. Yamamoto, M. & Tabata, Y. Osteogenic differentiation of mesenchymal stem cells in biodegradable sponges composed of gelatin and b-tricalcium phosphate, Biomaterials. 26 (2005) 3587-3596

Tall, P. D. Ndiaye, S. Beye, A. C. Zong, Z. Soboyejo, W.O. Lee, H.-J. Ramirez, A.G. Rajan, K. Nanoindentation of Ni–Ti Thin Films, Mater Manuf Process. 22 (2007) 175–179

Tang, C.F. Pan, F. Qu, X.H. Jia, C.C. Duan, B.H. He, X.B. Spark plasma sintering cobalt base superalloy strengthened by Y–Cr–O compound through high energy Spark plasma sintering cobalt base superalloy strengthened by Y–Cr–O compound through high-energy milling, J Mater Process Technol. 204 (2008) 111–116

Tang, L. Eaton, J.W. Fibrin(ogen) mediates acute inflammatory responses to biomaterials, J Exp Med. 178 (1993) 2147-56

Taylor, G.F. Apparatus for making hard metal compositions, U.S. Patent 1,896,854, February (1933)

Taylor and Francis, Handbook of Biomaterials Evaluation, Scientific, Technical and Clinical Testing of Implant Materials. (Ed. Von Recum) (2nd ed.) PA, USA (1999)

Tharani, R. Dorey, F.J. Schmalzreid, T.P. The risk of cancer following total hip or knee arthroplasty, J Bone Joint Surg Am. 83 (2001) 774-780

Thomas, P.S. Paul, C.P. Brian, T.M. Charles, R.B. William, H.H. Long-duration metal-on-metal total hip arthroplasties with low wear of the articulating surfaces, J. Arthroplasty. 11 (1996) 322-31

Thompson, G. J. and Puleo, D.A. Ti-6Al-4V ion solution inhibition of osteogenic cell phenotype as a function of differentiation time course in vitro, Biomaterials. 17 (1996) 1949-1954

Tipton, C.M. Matthes, R.D. Bedford, T.G. Maynard, J.A. & Walmer, H.C. An In Situ Study of the Influence of a Sclerosing Solution in Rabbit Medical Colateral Ligaments and its Junction Strength, Connect Tissue Res. 2 (1983) 95-102

Tokita, M. Trends in Advanced SPS Spark Plasma Sintering Systems and Technology. J Soc Powder Tech Jpn. 30 (1993) 790-804

Treagan, I. Metals and the immune resonse. An overview, Res Common Chem Pathol Pharmacol. 12 (1975) 189-220

Tyurin, A.G. Thermodynamic assessment of the effect of chromium and molybdenum on the passivability of nickel-base alloys, Prot Met+. 39 (2003) 568–574

Urban, R.M. Jacobs, J.J. Gilbert, J.L. Migration of corrosion products from modular hip prostheses. Particle microanalysis and histopathological findings, J Bone Joint Surg Am. 75 (1994) 1345-1359

Urban, R.M. Jacobs, J.J. Tomlinson, M.J. Dissemination of wear particles to the liver, spleen, and abdominal lymph nodes of patients with hip or knee replacement, J Bone Joint Surg Am. 82 (2000) 457-457

Van der Krogt, P. Molybdenum. Elementymology & Elements Multidict. (2007)

Vandamme, N.S. Wayman, B.H. Topoleski, L.D.T. Wear behaviour of carbide coated Co-Cr-Mo implant alloy, J Mater Sci Mater M. 14 (2003) 47-53

Vanmeensel, K. Laptev, A. Hennicke, J. Vleugels, J. Van der Biest, O. Modelling of the temperature distribution during field assisted sintering, Acta Mater. 53 (2005) 4379-4388

Varan, R. Bobyn, J. D. Medley, J .B. Yue, S. The effect of microstructure on the wear of cobalt-based alloys used in metal-on-metal hip implants, P I Mech Eng H. 220 (2006) 145-159

Vauquelin, L.N. Memoir on a New Metallic Acid which exists in the Red Lead of Sibiria, J Nat Phil Chem Arts. 3 (1798) 146

Villermaux, F. Zirconia–alumina as the new generation of ceramic–ceramic THP: wear performance evaluation including extreme life conditions. In Transactions of the Sixth World Biomaterials Congress, Society for Biomaterials. (2000)

Visuri T. Long-term results and survivorship of the McKee-Farrar total hip prosthesis. Arch Orthop Trauma Surg. 106 (1987) 368-374

Visuri, T. Pukkala, E. Paavalolainen, P. Cancer risk after metal on metal and polyethylene on metal total hip arthroplasty. Clin Orthop. 329 (1996) S280-289

Wang, A. Stark, C. Dumbleton, J.H. Mechanistic and morphological origins of ultra-high molecular weight polyethylene wear debris in total joint replacement prosthesis, Proc Inst Mech Eng H. 210 (1996) 141-155

Ward, P.A. Duque, R.E. Sulavik, M.C. Johnson, K.J. In vitro and in vivo stimulation of rat neutrophils and alveolar macrophages by immune complexes. Production of O-2 and H2O2, Am J Pathol 110 (1983) 297-309

Wang, S. Cobalt—Its recovery, recycling, and application, J Miner Met Mater Soc. 58 (2006) 47-50

Wataha, J.C. Biocompatibility of dental casting alloys: A review, J Prosthet Dent. 83 (2000) 223-234

Weeton J.W. Signorelli, R.A. Effect of Heat Treatment Upon Microstructures, Microconstituents, and Hardness of a Wrought Cobalt Base Alloy, Trans ASM. 47 (1955) 815-852

Weissler, G.A. Resistance measurements on copper powder using high dc currents, J Powder Bulk Solids Technol. 2 (1978) 38-40

Whittle, D.P. Stringer, J. Improvement in properties: additives in oxidation resistance by additions of reactive elements or oxide dispersions, Phil Trans R Soc Lond A. 295 (1980) 309-329

Widmer, R. Hot Isostatic Pressing. Cast Eng Foundry World. 14 (1982) 44-45

Wilches, L.V. Uribe, J.A Toro, A. Wear of materials used for artificial joints in total hip replacements, Wear. 265 (2008) 143-149
Wiles, P. The surgery of the osteo-arthritic hip, Br J Surg. 45 (1957) 488-497

Willert, H.G. Buchhorn, G.H. Fayyazi, A. Metal-on-Metal Bearings and Hypersensitivity in Patients with Artificial Hip Joints: A Clinical and Histomorphological Study, J Bone Joint Surg. 87 (2005) 28-36

Williams, D.F. Definitions in Biomaterials: Proceedings of a Consensus Conference of the European Society for Biomaterials, Elsevier, New York or Amsterdam (1987)

Williams, D.J. Clyens, S. Compaction of metal powders using high voltage electrical discharges, Metall Met Form. 44 (1977) 125-127

Williams, D.J. Johnson, W. Neck formation and growth in high-voltage discharge forming of metal powders, Powder Metall. 25 (1982) 85-89

Williams, R.L. Brown, S.A Merritt, K. 19 Electrochemical studies on the influence of proteins on the corrosion of implant alloys, Biomaterials 9 (1988) 181-186

Willmann, G. Ceramics for total hip replacement--what a surgeon should know, Orthopaedics 21 (1998) 173-177

Wu, X.Y. Guo, J.D. Effect of liquid phase on densification in electric-discharge compaction, J Mater Sci. 42 (2007) 7787-7793

Wu, X.Y. Zhang, W. Li, D.X. Guo, J.D. Microstructure of WC in WC-Co cemented carbides consolidated by electric discharge, Mater Sci Technol. 23 (2007) 627-629

Xie, G.Q. Ohashi, O. Chiba, K. Yamaguchi, N. Song, M. Furuya, K. Noda, T. Frequency effect on pulse electric current sintering process of pure aluminium powder, Mater Sci Eng A. 359 (2003) 384-390

Yan, Y. Neville, A. Dowson, D. Williams, S. Fisher, J. Tribo-corrosion analysis of wear and metal ion release interactions from metal-on-metal and ceramic-on-metal contacts for the application in artificial hip prostheses, Proc. IMechE. 222 (2008) 483–492

Yan, H. Zhang, H. Ubic, R. Reece, M.J. Liu, J. Shen, Z. Zhang, Z. A lead-free high-curie-point ferroelectric ceramic, CaBi2Nb2O9, Adv Mater. 17 (2005) 1261-1265

Yang, F.M. Sun, X.F. Zhang, W. Kang, Y.P. Guan, H.R. Hu, Z.Q. 2001 Secondary M_6C precipitation in K40S cobalt-base alloy, Mater Lett. 49 (2001) 160–164

Yen, S.K. Hsu, S.W. Electrolytic Al_2O_3 coating on Co-Cr-Mo implant alloys of hip prosthesis, J Biomed Mater Res 54 (2001) 412-418

Yoritoshi, M. Yuichiro, K. Nobuhiro, T. Microstructures and mechanical properties of bulk nanocrystalline Fe–Al–C alloys made by mechanically alloying with subsequent spark plasma sintering, Sci Technol Adv Mater. 5 (2005) 133-143

Youdelis, W.V. Kwon, O. Carbide phases in cobalt base superalloy: role of nucleation entropy in refinement, Met Sci. 17 (1983) 379-384

Young, J.A. Cobalt (II) oxide. J Chem Educ. 78 (2001) 1328

Yue, H. Wei, W. Yue, Z. Lv, P. Wang, L. Ma, G. Su, Z. Particle size affects the cellular response in macrophages, Eur J Pharm Sci 41 (2010) 650-657

Zavodov, N.N. Kozlov, A.V. Luzganov, S.N. Polishchuk, V.P. Shurupov, A.V. Sintering of metal powders by a series of heavy current pulses, High Temp. 37 (1999) 130-135

Zhan, C. Kaczmarek, R. Loyo-Berrios, N. Sangl, J. Bright, R.A. Incidence and short-term outcomes of primary and revision hip replacement in the United States, J Bone Joint Surg Am. 89 (2007) 526-533

Zhang, J. Zavaliangos, A. Groza J.R. The current state of E-Learning under implementation: A survey of distance learners, Powder Metall Sci Technol Briefs. 9 (2003) 5-12

Zhang, P. Recovery of metal values from spent nickel–metal hydride rechargeable batteries, J Power Sources. 77 (1999) 116-122

Zhitkovich A, Peterson-Roth E, Reynolds M. Killing of chromium-damaged cells by mismatch repair and its relevance to carcinogenesis, Cell Cycle 8 (2005) 1050–1052

Zhou, Z.J. Kwon, Y.S. W-Cu composite by resistance sintering under ultra-high pressure, J Mater Process Technol. 168 (2005) 107-111

Zhuang, L.Z. Langer, E.W. Effects of cooling rate control during the solidification process on the microstructure and mechanical properties of cast Co-Cr-Mo alloy used for surgical implants, J Mater Sci. 24 (1989) 381-388

Zimmer, Inc. Understanding alternative bearing surfaces in total hip replacement, 97-2100-69 40ML, USA (2003)

Zimmermann, J. Ciacchi, L.C Origin of the selective Cr oxidation in CoCr alloy surfaces, J Phys Chem Lett. 1 (2010) 2343–2348

Zum Gahr**,** K.H. Wear by hard particles, Tribol Int. 31 (1998) 587-596